Chapter 1: Organic dyes for dye-sensitized solar cells

This chapter is devoted to the study of organic dyes employed in dye-sensitized solar cells (DSSCs). In section 1 a survey of DSSCs is given, with special attention to the main features related to molecular sensitizers. This is followed by the general objectives in section 2. Section 3 is dedicated to the computational modeling of the dyes, paying particular attention to the charge transfer character of the optical state. The results are given in sections 4-7 and general conclusions are outlined in section 8.

1. Overview of dye-sensitized solar cells

1.1 Semiconductor

The choice of a semiconductor with a nanostructured morphology was a key point for the success of DSSCs.[1] The use of mesoporous TiO_2 provides a high internal surface to accommodate a dye monolayer. DSSCs based on a TiO_2 photoanode are known as n-type cells, due to photoinduced electron injection into the semiconductor's band. This is by far the most frequent DSSC design,[2] although there are also examples of p-type sensitization,[3] usually with NiO,[4] where holes are injected into the valence band of a semiconductor. In this thesis, dyes for n-type sensitization have been investigated.

In order to overpass the Shockley-Queisser limit efficiency,[5] tandem cells wih n- and p-type semiconductors have been proposed.[6] In the tandem scheme, a broader part of the solar spectrum may be covered. This can be achieved by having dyes that absorb high energy photons on the n-type photoanode while low energy photons are absorbed by dye molecules on the p-type photoanode.

1.2 Molecular sensitizer

As it was emphasized previously, the sensitizer is one of the key components in DSSCs, responsible for the primary step of sunlight absorption. To achieve high photoconversion efficiencies, the sensitizer should absorb as much of the incoming light as possible. Namely, the absorption should be intense and ideally cover the whole solar spectrum. Of course, this is a difficult task, and in order to optimize the light harvesting properties of the sensitizers, panchromatic engineering[7-14] for DSSCs has become very popular in recent years.

1.2.1. Metal complexes

A wide range of sensitizers have been investigated in the past recent years to improve the performance of DSSCs. Metal complexes based on Ru(II) were intensively investigated in the early years of DSSCs because of their broad absorption in the visible region of the spectrum due to the metal to ligand charge transfer (MLCT) singlet state.[15] Chemical substitutions on the ancillary ligands, typically bipyridine, allowed easy tuning of the photophysical and electrochemical properties,[2] optimizing the electron injection process to the semiconductor. The N3 dye (Figure 1.1), a distorted octahedral complex of Ru(II) with two thiocyanato ligands and two bipyridyl ligands substituted with carboxylic acid groups, is one of the most famous Ru(II) sensitizers together with the black dye.[2] Efficiencies of ~10% were obtained with the N3 dye,[16] mainly ascribed to the binding ability of the four COOH groups, which lead to strong adsorption on the semiconductor surface, enhancing the electron injection process. The popular black dye shown in Figure 1.1, also known as N749 dye, was employed by Grätzel and co-workers[17] to harvest light from the visible to the near-IR region of the solar spectrum in modular solar cells. This complex consists in a Ru(II) metal center with a distorted octahedral coordination environment with three thiocyanato ligands and one terpyridine ligand substituted with three carboxyl groups. The combination of these ligands leads to a stabilization of the π^*-type orbital of the terpyridine ligand and a destabilization of the t_{2g} orbital of the Ru involved in the MLCT state.[17] The result is a red-shift in the MLCT absorption band compared to Ru complexes with two terpyridine ligands,[18] and a conversion of the incident light into electrical energy over the whole visible and near-IR part of the spectrum, with an efficiency of 10.4 %.[17]

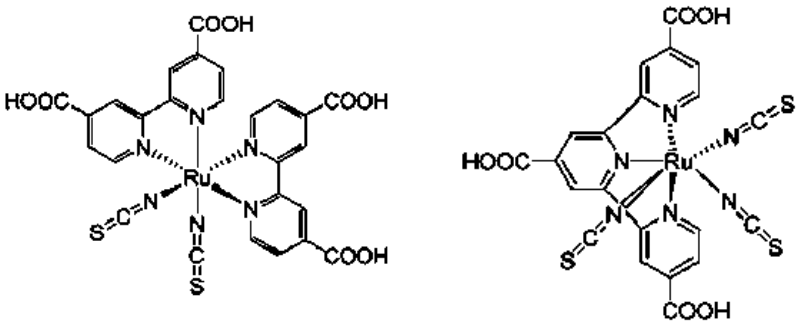

Figure 1.1 N3 dye (left) and black dye N749 (right) taken from reference 2.

Apart from Ru metal complexes, other metal complexes have also been investigated, mainly based on Os[19] among others,[2] but they haven't been able to improve the good performance of the N3 dye or the closely related black dye. Other systems such as Zn

porphyrins,[20,21] phthalocyanines[22,23] and their free base analogues have also been tested[24] as sensitizers in DSSCs due to their improved optical response in the near-IR region of the spectrum. It is important to notice that one of the main inconveniences and a limiting factor for high conversion efficiencies is the tendency of molecular sensitizers to aggregate on the semiconductor's surface.[25] This problem can be circumvented by the introduction of peripheral bulky chains or the use of coadsorbents.[2]

1.2.2. Organic dyes

The use of sensitizers including a metal, however, is far from the original low-cost and environmentally friendly spirit of DSSCs. In this regard, organic dyes present several advantages compared to metal complexes based on Ru. In general, their molar extinction coefficients are larger, and their photophysical and electrochemical properties may be easily tuned by appropriate molecular design and straightforward synthesis.[26,27] The common structure of these organic dyes is that of a donor and an acceptor group connected by a conjugated π-bridge (D-π-A).[8] The acceptor moiety usually has functional groups with the ability to anchor on the semiconductor's surface either by covalent bonding, electrostatic or noncovalent interactions, or hydrogen bonding.[2,28] Photoinduced CT takes place in these dyes, since the HOMO is mainly located on the donor group and the LUMO over the acceptor. The spatial orientation of the dye with respect to the semiconductor surface favors charge separation for efficient electron injection and also minimizes recombination between injected electrons and the oxidized dye, since after photoabsorption, the hole is located on the donor group. The D-π-A arrangement offers many opportunities in terms of design, since different characteristics may be optimized, such as the matching of the HOMO and LUMO levels with the energy levels of the semiconductor and redox mediator.[13]Also, by suitable combination of the three units, charge separation may be optimized for efficient electron injection to the semiconductor, and the optical response may also be extended to longer wavelengths by judicious chemical modifications or by the combination of sensitizers with complementary absorption characteristics.[29]

Representative electron rich units that serve as donor groups in D-π-A type dyes are coumarins, triarylamines, indolines or carbazoles, among many others.[27] In particular, triarylamines[30,31] have been the most widely used groups due to their electron donating ability along with good hole transport properties. Acceptor groups have not been so

extensively studied as donor groups,[2] and cyanoacrilic acid[28] is the most widely used unit, because of its electron withdrawing capability and the presence of the COOH anchoring group, which has several possible binding modes onto the metal oxide surface. The π-bridge linking the donor and acceptor groups is usually based on one or more conjugated rings such as: thiophene, benzene, cyclopentadithiophene, ethylenedioxythiophene, and any combination of these that one can imagine.[2,26,27]

(a) Requirements of the dye

There are several characteristics the sensitizer should have in order for the DSSC to achieve a good performance. Ideally, the dye should absorb over the whole visible range and if possible, over part of the near-IR region, with a large molar extinction coefficient, in order to harvest as much of the incoming sunlight as possible. In relation to the structure of the dye, it should have anchoring groups, such as carboxylic groups for instance, for the dye to strongly bind on the semiconductor surface, establishing a direct contact for electron injection. Moreover, for an optimal driving force of the electron injection process, the LUMO of the dye should be located over the anchoring group and lie energetically above the conduction band edge (CBE) of TiO_2.

As shown in Figure 5 (Introduction, section 1.1.1), there are several recombination processes that should be avoided (or minimized) in order to obtain high photo-to-current efficiencies, namely, recombination of the electrons in the conduction band of TiO_2 with the oxidized dye or with the redox couple.[2] Naturally, regeneration of the dye by the redox couple should be faster than recombination of the injected electrons in the semiconductor with the oxidized sensitizer. Optimal dye regeneration may be achieved by suitable choice of the dye, who's HOMO should lie below the energy level of the redox couple, so that electrons can be accepted by the oxidized molecule. Also, to minimize the competing process of charge recombination between the oxidized dye and the injected electrons, the hole on the dye created after electron injection should be located as far as possible from the semiconductor surface. Another process which should be avoided is non-radiative decay of the excited state of the dye back to the ground state, since it competes with the charge injection process. This may be partially achieved by avoiding the formation of dye aggregates on the surface of the semiconductor.

(b) Direct vs indirect injection

Apart from the light-harvesting role, the sensitizer also governs the mechanism of charge injection towards the semiconductor. Dyes may be categorized as indirect or direct,[32,33] depending on how the the electrons are transferred to the semiconductor. With indirect dyes, an excited electronic state, with the promoted electron mainly located on the acceptor moiety, is populated after photoexcitation, followed by electron injection from the sensitizer to the semiconductor. DSSCs operating with such a two stepwise mechanism are known as Type I,[2] and the indirect injection process may be inferred from the overlap of the DSSC device absorption spectrum to that of the free dye. In Type II DSCCs,[34-36] a direct type dye is used, in which electron injection takes place directly from the HOMO of the sensitizer to the conduction band of the semiconductor upon photoabsorption. Although both classes of dyes have their pros and cons regarding the efficiency of electron transfer to the semiconductor or unwanted processes,[32] such as back electron transfer to the oxidized dye, in this thesis only indirect type dyes have been studied.

2. General objectives

In this chapter, the characteristics of several D-π-A dyes with triarylamine as donor group and cyanoacrylic acid as acceptor group were investigated. Special attention was paid to the role of the π-linker in the photophysical properties of the dye. Several closely related π-spacers based on the thiophene unit were investigated to understand how small chemical modifications may influence the absorption wavelength, the probability of the electronic transition and the electron/hole separation. In particular, the geometric characteristics imposed by the linker, such as its length, the planarity, and the linearity were considered. Their effect on the π-conjugation along the dye, the energy of the frontier molecular orbitals involved in the optical state, and the intramolecular charge transfer character of the electronic transition were studied. Modification on the triarylamine donor group was also explored and the effect on the optical properties rationalized.

Apart from the chemical nature of the π-bridge, its length has an effect on the charge transfer character of the absorbing state. Moreover, the alignment between the sensitizer's ground and excited state oxidation potentials with the redox potential of the redox couple and the conduction band edge of the semiconductor can also be influenced by the nature and length of the conjugated π-linker. An adequate matching between these levels is essential so that efficient electron injection can take place as well as dye regeneration.

Towards this end, ground and excited state potentials of D-π-A dyes with different lengths of the π-bridge were also studied.

The influence of the solvent on the absorption band of a quinoidal D-π-A dye was also investigated. By considering explicit solvent molecules, the specific solute-solvent interactions responsible for the observed solvatochromic shift of the absorption band were explored.

3. Computational modeling

3.1 Model systems

The search for sensitizers with suitable light-harvesting characteristics is crucial in order to obtain highly efficient DSSCs. Even in the case where the main interest focuses on the absorption properties of indirect dyes, it is clear that the covalent linkage of the molecular sensitizer on the semiconductor surface will affect the energetics of the photoabsorbing states, and it even might modify their electronic structure. Hence, in order to take into account these interactions at the interface, it would be ideal to treat the dye-semiconductor tandem simultaneously. On the other hand, the computational study of the entire system presents important difficulties, both due to methodological reasons and computational cost limitations. Fortunately, in our studies there are several points that justify the computational investigation of the pristine dyes in solution, completely avoiding the presence of semiconductor models in the calculations. Namely:

(i) Our studies focus on the properties related to the donor moiety and the conjugated bridges, but not to the acceptor (anchoring) group, for which the presence of the semiconductor is expected to play a larger role.

(ii) In all our investigations we were interested in relative trends within a molecular family of sensitizers holding the same acceptor group.

(iii) In a first stage, the absorption properties of the sensitizer are experimentally recorded in organic solvents, without the presence of the semiconductor. Hence, computations of the dyes in solution can be compared with these results and could even eventually replace this first experimental screening.

(iv) Study of the properties of the dyes in solution can lead to clear strategic rules for design of new sensitizers with improved properties, which can then be combined with different semiconductors.

Such strong simplification of the studied system allowed us to focus on the detailed study of the photophysical characteristics of the dye itself, and in particular, on the CT process between the donor and acceptor groups that takes place upon absorption.

A chemical strategy commonly employed to prevent dye aggregation at the surface of the metal oxide is the use of sterically hindering substituents. These are bulky groups that typically consist on hydrophobic long alkyl or alkoxy chains, which are incorporated in the periphery of the donor group or in the π-conjugated linker. Due to the presence of these bulky chains, the dye molecules are further spaced out when adsorbed on the surface of the semiconductor, and thus dye aggregation is suppressed because the efficiency of π-stacking interactions between neighbors is reduced. On the other hand, this also reduces the surface coverage of the semiconductor. Some of the dyes studied in this chapter were synthesized by experimental groups and contained long alkoxyl chains in the donor group and alkyl chains in the π-bridge. These chains however, are not involved in the optical S_1 state since they do not participate in the π-conjugation along the molecule. Therefore, the dyes have been modeled by replacing the alkoxy and alkyl chains with methoxy groups and hydrogen atoms, respectively. Since the role of these chains is merely mechanical, with any impact on the photophysical properties of the dye, for the sake of computational simplification we have systematically neglected their presence in our calculations.

3.2 Electronic structure methods

3.2.1 Wave function based methods

There is a wide variety of wave function based quantum chemistry methods for the calculation of electronic excited states, depending on the chosen reference and how electron correlation effects are introduced.[37] The configuration interaction singles (CIS) method[38] is the simplest excited state method. One might argue that certain static correlation effects of the excited state are included within this method since the CIS wave function is a linear combination of singly excited slater determinants. However, the lack of dynamic correlation in CIS can result in errors of up to 1 eV in the computed excitation energies.[39] A way to improve CIS is to include dynamical correlation analogously to the MP2 method for the ground state. This may be done by the CIS(D) approach,[40,41] which is a perturbative correction to CIS that introduces double excitation effects for the excited states. The excitation energies with CIS(D) are improved relative to those calculated with

CIS, and can still be applied to relatively large molecules by the use of the resolution of the identity (RI) approximation,[42,43] in which the use of auxiliary basis expansions reduces considerably the computational cost. A further approximation may be done to improve the accuracy of CIS(D) calculations and reduce computational costs by semi-empirically scaling the opposite-spin components of the CIS(D) expression in what is known as SOS-CIS(D).[44] The SOS-CIS(D) method has been applied to calculate D-π-A dyes and good results have been obtained.[11]

Other single reference accurate methods for single electron excitation energies are the equation-of-motion coupled cluster (EOM-CC) method[45-49] and the algebraic diagrammatic construction (ADC) method.[50] An attractive feature of the EOM-CC approach is that a variety of multiconfigurational wave functions can be described within a single reference formalism. In the ADC(n) family of methods, for each n-th order of ADC, the excited state is treated at an equivalent level to the Møller–Plesset perturbation expansion of the same order. Several techniques have recently allowed to reduce the computational cost of the ADC family by the use of approximations such as the already mentioned RI[42,43] or the SOS approach.[51] These two methods however are still rather expensive and limited to small-medium sized molecules.

Regarding multiconfigurational-based methods, the complete active space self-consistent field (CASSCF)[52] method and its second order perturbative correction (CASPT2)[53] are amongst the most used. Other standard methodologies are the multireference configuration interaction (MRCI)[54] and multireference coupled-cluster (MRCC) approaches.[55,56] The drawback of all the aforementioned methods however is that electron correlation is recovered at the expense of high computational cost, limiting its use to relatively small molecules.

It is needless to say that a correct description of the ground state electronic structure of a molecule is fundamental prior to the calculation of its excited states. Herein we were interested in the vertical absorption of organic dyes from their ground state equilibrium geometry. The ground state in these systems is of closed-shell nature, as in the vast majority of organic molecules, and since there is no symmetry present, near degeneracies of frontier MOs are avoided. Therefore, a single-reference wave function is appropriate for the ground state description of D-π-A dyes.

3.2.2 Time-dependent density functional theory

Time-dependent density functional theory (TDDFT) theory[57] is a sensible choice to compute excited states due to the size of the molecular systems studied in this chapter. In recent years, the application of this methodology to calculate valence-excited states of large molecules has grown tremendously[58] due to the compromise between computational effort and chemical accuracy. Compared to wave function approximations, TDDFT accounts for dynamic correlation in the description of excited states with a much reduced computational cost. The calculation of vertical excitation energies with TDDFT has become a routine task and the agreement with experimental data frequently lies on the range of 0.1-0.5 eV.[39]

(a) General overview

Although the scope of this section is not to rewrite the formulation of TDDFT already available in very pedagogical papers and books,[59-61] it will be presented in a nutshell just to illustrate the essence of the method. The formal foundations of TDDFT rely on the Runge-Gross theorems,[62] which in a sense are analogous to the Hohenenberg-Kohn theorems for ground state DFT.[63] The latter state that the energy is a unique functional of the electron density and also provide a variational principle to calculate the ground state energy. The first Runge-Gross theorem yields a unique one-to-one mapping between the time-dependent electron density and the time-dependent external potential of an N-electron system. The second theorem provides a least action principle thanks to which the time-dependent density may be obtained from the time-dependent Schrödinger equation. In practice, this may be achieved via the popular Kohn-Sham (KS) approach.[64,65] Excitation energies and other properties may then be obtained by solving the time-dependent KS equation[60] via two different strategies. One is to propagate the KS wave function in real time via what is commonly known as real-time TDDFT,[57] appropriate for intense fields. The other strategy, which is the one usually implemented in the majority of standard quantum chemistry packages, is linear response TDDFT (LR-TDDFT).[66] Within this approach, the time-dependent KS equation is solved perturbatively to first order in the frequency domain. This is appropriate for many practical situations in spectroscopy, in which the spectral response of a system to a weak probe is determined.

Within the LR-TDDFT framework, the excitation energies (ω) are obtained by solving a non-Hermitian eigenvalue equation named after Casida,[66] that for real KS orbitals takes the form

$$\begin{bmatrix} \boldsymbol{A} & \boldsymbol{B} \\ \boldsymbol{B} & \boldsymbol{A} \end{bmatrix} \begin{pmatrix} \boldsymbol{X} \\ \boldsymbol{Y} \end{pmatrix} = \omega \begin{bmatrix} 1 & 0 \\ 0 & -1 \end{bmatrix} \begin{pmatrix} \boldsymbol{X} \\ \boldsymbol{Y} \end{pmatrix} \tag{1.1}$$

In case a hybrid exchange-correlation (xc) functional is used (incorporating a portion of exact exchange from Hartree-Fock theory), the elements of matrices **A** and **B** take the following form[67] in a canonical basis

$$\begin{aligned} A_{ia\sigma,jb\tau} = {} & \delta_{\sigma\tau}\delta_{ij}\delta_{ab}(\varepsilon_{a\sigma} - \varepsilon_{i\tau}) + \left(i_\sigma a_\sigma \middle| j_\tau b_\tau\right) \\ & - \delta_{\sigma\tau} c_{HF} \left(i_\sigma j_\sigma \middle| a_\tau b_\tau\right) + (1 - c_{HF}) \left(i_\sigma a_\sigma \middle| f_{\sigma\tau} \middle| j_\tau b_\tau\right) \end{aligned} \tag{1.2}$$

$$B_{ia\sigma,jb\tau} = \left(i_\sigma a_\sigma \middle| b_\tau j_\tau\right) - \delta_{\sigma\tau} c_{HF} \left(i_\sigma b_\sigma \middle| a_\tau j_\tau\right) + (1 - c_{HF}) \left(i_\sigma a_\sigma \middle| f_{\sigma\tau} \middle| b_\tau j_\tau\right) \tag{1.3}$$

where indices *i,j* correspond to ground state occupied orbitals while *a,b* are for virtual orbitals and σ,τ represent spin variables. In these equations c_{HF} is the coefficient of the HF exchange in the hybrid functional and ε is a ground state orbital energy. The four index integrals expressed in Mulliken notation are

$$\left(i_\sigma a_\sigma \middle| j_\tau b_\tau\right) = \iint \phi_i(r_1)\phi_a(r_1) r_{12}^{-1} \phi_j(r_2)\phi_b(r_2) dr_1 dr_2 \tag{1.4}$$

$$\left(i_\sigma a_\sigma \middle| f_{\sigma\tau} \middle| j_\tau b_\tau\right) = \iint \phi_i(r_1)\phi_a(r_1) f_{\sigma\tau} \phi_j(r_2)\phi_b(r_2) dr_1 dr_2 \tag{1.5}$$

where $f_{\sigma,\tau}$ is the time-independent non-local xc-kernel in the adiabatic approximation, who's form will depend on the chosen xc-functional.

A further approximation to Casida's equation, known as the Tamm-Dancoff approximation (TDA),[68] may be introduced which consists in setting **B=0** in equation 1.1. This means that all contributions to the excitation energies coming from de-excitation of the correlated ground state are neglected. Then, a hermitian eigenvalue equation with half the dimensions of the original equation is obtained.

$$\boldsymbol{AX} = \omega \boldsymbol{X} \tag{1.6}$$

The good point of the TDA is that it is a computationally simple method, which yields excitation energies of the same quality as TDDFT, or even improved in some cases,[68] and that the working equation resembles very much the one of the CIS method, but with the **A** matrix depending on the xc functional. This is because the TDA to time-dependent

Hartree-Fock (TDHF), also known as random-phase approximation (RPA) in the physicists community,[69,70] is precisely the CIS method.[39] Therefore, an advantage of working with the TDA is that one may think in terms of wave functions, which is what we always aim to do when describing excited states. In practice, ground state approximate xc density functionals are used in TDDFT calculations, in the so-called adiabatic approximation, with the assumption that the electronic density varies slowly with time.[57,61]

(b) Charge transfer states

Despite the proven success of LR-TDDFT to calculate low-lying valence excited states, it has severe problems describing Rydberg states and CT excitations,[67,71-74] which are the ones we are particularly interested in this chapter. For CT states calculated with standard density functionals, excitation energies are seriously underestimated[71] and the computed potential energy curves do not follow the correct 1/R dependence,[71] where R corresponds to the separation between the positive and negative charges of the CT state. This asymptotic behavior of the energy along the CT separation can be grasped by considering a donor system and an acceptor system separated by a distance R. To remove an electron from the donor, we must supply at least the energy corresponding to its ionization potential (I_d), and when the electron is transferred to the acceptor, there will be an energy gain of the order of the acceptor's electron affinity (A_a). Once the hole is created in the donor, it will feel an electrostatic attraction with the electron at the acceptor, resulting in a Coulombic energetic gain of -1/R. The energy required to create the CT state is then given by:

$$E(R) = I_d - A_a - \frac{1}{R} \qquad (1.7)$$

Fom this simple model we should expect the excitation energy of a CT state to increase along the charge separation coordinate R. Dreuw et. al showed,[71] however, that this is not the case when pure xc functionals, i.e with no Hatree-Fock exchange, are used.

Let us now consider a CT state arising from electron transfer from an occupied orbital *i* on a donor molecule A to a virtual orbital *a* on an acceptor molecule B, and for simplicity, with no overlap between these two orbitals.[67] In such an extreme situation, the only terms of matrix **A** (from equation 1.2) that survive are the first and the third, corresponding to the energy difference between the donor and acceptor orbitals, and the non-local HF exchange contributions. This last term is not zero since orbitals *i* and *j* are located on the same molecule A while orbitals *a* and *b* are located on molecule B. The importance of this term is that it contains the Coulombic electrostatic interaction between the holes created in

orbitals *i* and *j* with the electrons transferred to orbitals *a* and *b*. This term is thus essential for the correct 1/R asymptotic behavior of the potential energy curve along intermolecular separation of the donor and acceptor units, and thus the presence of exact exchange is crucial. On the other hand, the elements of matrix **B** (equation 1.3) are all zero when the two orbitals involved in the CT state do not overlap.

With these simple arguments, it is straightforward to understand that pure xc functionals underestimate dramatically excitation energies of CT states because these are obtained as energy differences of the donor and acceptor MOs, and it is well known that the self-interaction error in density functional theory (DFT) leads to artificial underestimation of the HOMO-LUMO gap.[75] In the popular paper by Dreuw and Head-Gordon,[67] they gave an additional interpretation to the incorrect asymptotic energy profile of CT states computed with standard density functionals. They related this failure to an electron transfer self-interaction, because the energy of the accepting orbital falsely includes its Coulomb repulsion with the donating orbital, and showed that this can only be cancelled by the presence of exact exchange.

One solution to the CT problem within TDDFT is the use of "range-separated hybrid" or "long range corrected" (LRC) functionals.[76-81] This approach has been quite successful for the calculation of CT states of diverse systems because of the smooth inclusion of long-range Hartree-Fock (HF) exchange.[11,82,83] The basic idea is the partition of the Coulomb operator into short-range and long-range components, which may be achieved by the use of the error function:

$$\frac{1}{r_{12}} = \frac{1 - erf(\omega r_{12})}{r_{12}} + \frac{erf(\omega r_{12})}{r_{12}} \qquad (1.8)$$

The first term on the right is the short-range component and on a length scale of ~1/ω it decays to zero, while the second term consists of a long-range background component. The ω parameter thus controls the relative significance of both terms and its value is usually determined empirically or by physical arguments, and the most common used values are in the 0.2-0.4 $bohr^{-1}$ range.[78] The range-separated functional then includes short-range exchange from a density functional approximation such as LDA, GGA or hybrid, while the long-range part consists of exact exchange. The success of this kind of functionals for the description of CT states is that one takes profit of the correct short-range behavior of

standard DFT xc functionals, while its incorrect long-range asymptotic behavior due to the self-interaction error is replaced by the correct Hartree-Fock one.

3.2.3 Importance of the basis set

A good choice of the basis set is very important for the calculation of electronically excited states. Polarization functions are mandatory when dealing with excited states and the use of diffuse functions can, in many occasions, sensibly improve the computed transition energies and excited state properties. For instance, in the calculation of excitation energies of D-π-A dyes, the vertical energies to the S_1 CT state are reduced in the order of 0.1 eV when the 6-31+G(d) basis set is used in comparison with the 6-31G one.[11] From the dependence of the excitation energy on the basis set plotted in Figure 1.2, the inclusion of diffuse functions certainly has an impact on the calculated values. The use of polarization functions on hydrogen atoms or moving to a triple-ζ basis set has a minor effect. The excitation energies are numerically converged with the 6-31+G(2d,p) basis.

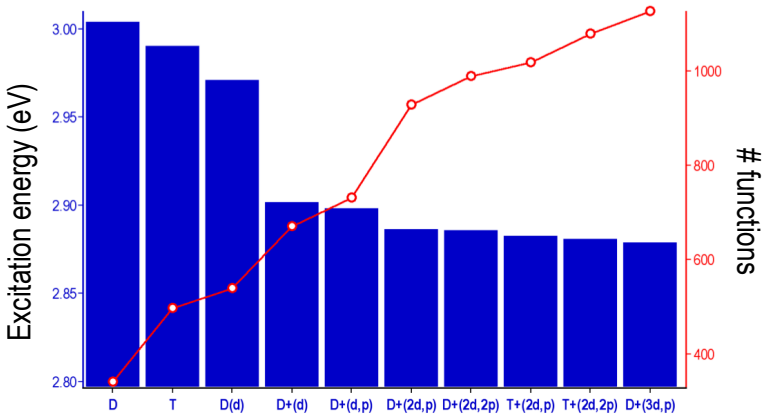

Figure 1.2 Dependence on the excitation energy with the basis set for the S_1 CT state of a representative D-π-A dye. The number of functions per basis set is also shown. Calculations were done with Pople basis sets, where D stands for 6-31G and T for 6-311G.

3.2.4 Chosen methods

Considering the properties of the methods and basis sets commented above, together with the type of electronic transitions of organic dyes we want to study (π,π*-type with CT character), we include herein a short rationalized explanation of the chosen methods within this chapter.

For the calculation of vertical excitation energies, TDDFT has been used and in most cases, within the TDA. The range separated hybrid functional LRC-ωPBEh[79] has been systematically employed, since good results have been obtained for the calculation of strong CT states of organic systems.[84] Alternatively, the CAM-B3LYP functional[85] was used in one of the studied dyes. The 6-311+G(2d,2p) basis set was used in general. For one of the studies, the size of the dyes limited the use of very large basis sets and 6-31G(d) was used. For another study, the 6-31+G(d,p) basis set was considered, which already gives reasonable results (Figure 1.2).[86-89]

For the optimization of the ground state geometries, the same functional employed for the excited states was used, LRC-ωPBEh. With the exception of one of the studies in which the excited states were computed with CAM-B3LYP, for which the ground state was optimized using the B3LYP functional.[90,91] Ground state geometries have been optimized with different basis sets: 6-31G(d), 6-31+G(d) or 6-31+G(d,p).[86-89]

3.3 Solvent effects

The inclusion of solvent effects in electronic structure calculations has progressed considerably in the past decade. Realistic models including explicit solvent molecules[92-94] are now affordable due to the boost in computational efficiency. Within this explicit scheme, one may calculate the desired properties with different approaches such as molecular mechanics (MM), quantum mechanics (QM), or the hybrid QM/MM approach, depending on the effects one is interested and, in particular, the size of the model.[95-99] Molecular dynamics simulations can also be very useful in order to determine how solvent molecules distribute around a particular solute.[92,93] This approach was used in section 7 to determine which were the relevant solvent-solute interactions responsible for the differences observed in the absorption spectrum of a D-π-A dye recorded with different solvents.

When specific solute-solvent interactions (e.g. hydrogen bonds, non-covalent interactions...) are not relevant, one way to model the electrostatic interaction between solute and solvent is with implicit solvation models.[100] These are also usually known as self-consistent reaction field (SCRF) models, because the presence of a continuum solvent introduces additional terms in the molecular solute's Hamiltonian that precisely depend on

the solute electron density, thus establishing a reaction field. Therefore, an iterative procedure has to be performed until the wave function of the solute is converged.

There are many different flavors of implicit solvation models, depending on the degree of sophistication one is interested in. The most popular though among standard quantum chemistry packages are polarizable continuum models (PCM),[101-104] also known as dielectric continuum models or "apparent surface charge" SCRF models, in which the quantum chemical description of a molecular system is coupled to a continuum description of the environment. Among this family, the most common implemented versions are the conductor-like model (C-PCM),[105,106] which is sometimes referred to as PCM leading to certain confusion in the literature, and the "integral equation formalism"[107,108] one (IEF-PCM). This latter one is equivalent to the "surface and simulation of volume polarization for electrostatics" (SS(V)PE) model,[109] which was developed parallel to IEF-PCM. In these models, a solute-shaped cavity of merged atom-centered spheres is constructed which simulates the solvent as a continuum dielectric surface characterized by its dielectric constant (ε). The basic idea behind these models is that the electronic density of the solute polarizes the dielectric solvent, and thus an induced surface charge density emerges on the cavity. In practice, the induced surface charge is discretized into point charges, and these are determined self-consistently from the solute's electrostatic potential at the cavity surface, by solving a set of linear equations. Broadly speaking, what these models do is to determine the total electrostatic potential arising from the given charge distribution by solving the classical electrostatic Poisson equation with several approximations. The total potential consists of the solvent's potential and the continuum's solvent one, the latter one being a reaction-field potential arising from polarization of the solvent medium.

In principle, the IEF-PCM model offers a more sophisticated treatment of the electrostatic interactions between the continuum solvent and the solute as compared to C-PCM. Within the IEF-PCM model, surface polarization is treated exactly and volume polarization is also included in an approximate manner. In the limit of $\varepsilon \rightarrow \infty$, C-PCM converges to IEF-PCM and since C-PCM is less computationally demanding, it is usually used for solvents with high dielectric constants.

Solvent effects in excited state calculations may be introduced via two different approaches,[110] depending on whether the response of the solvent to the solute's excitation

is split or not among its different degrees of freedom. Upon a change in the electronic state of the solute, the solvent can respond in two different ways. One response is the polarization of the solvent's electronic density, which will be a fast process. In contrast, the response of the nuclei in terms of reorientation of solvent molecules will be a much slower process. These two kinds of response of the solvent to the change in electronic state of the solute are treated differently in two extreme time regimes. In the non-equilibrium regime, the fast degree of freedom, that is, the electronic polarization of the solvent, is treated in equilibrium with the solute's excited state electronic density, while the slow degrees of freedom remain in equilibrium with the ground state electron density. In the equilibrium regime, all the degrees of freedom, i.e. electronic and nuclear, are considered equilibrated with the electron density of the electronic state of interest of the solute. In practice, PCM models deal with these two situations by considering two different dielectric constants in the working equations.[110] When dealing with non-equilibrium solvation, the dynamic (optical) dielectric constant of the solvent is used, which is related to the square of the solvent refractive index n. For equilibrium solvation, the static (zero-frequency) dielectric constant is considered. The recommendation is to use non-equilibrium solvation when calculating vertical excited states, since the absorption or emission processes are considered to be fast enough so that solvent molecules won't have time to reorientate responding to the solute's new situation. When carrying out geometry optimizations, non-equilibrium solvation is a more sensible choice since its time scale is of the same order as that of the solvents molecular motion.

There are two different approaches for describing non-equilibrium solvation, namely, the linear response (LR)[111,112] or the state-specific (SS)[113-116] one. In the LR framework, the excitation energies are determined from the solvated ground state with no explicit calculation of the solvated excited state wave functions. That is, the SCRF is included in the conventional excited state calculation, by adding the necessary terms to the excited state method equations. On the other hand, with the SS approach, a single excited state is modeled and its energy is determined by making the electrostatic potential generated by the excited state density self consistent with the solvent reaction field. Thus, in the SS approach, the excitation energies are calculated from the difference in the energy of each state, for which each electronic density is solved self consistently with the solvent reaction field. Basically, the SS approach considers the capability of part of the solvent degrees of freedom to instantaneously respond to changes in the solute wave function upon excitation,

an effect that the LR approach does not account for. In this thesis, the LR approach has always been applied since it allows an easier interpretation and comparison of the excitation energies among a set of molecules.

3.4 Computational tools for excited state characterization

In this section several computational tools used to characterize the optical state of the investigated D-π-A dyes will be discussed. From an excited state calculation with TDDFT one can nowadays routinely obtain the transition dipole moment as well as the oscillator strength corresponding to transitions from the ground to excited singlet states. These parameters give us information about the intensity of the transition and also provide insight into the nature of the absorbing state. In this chapter we are interested in the CT state of organic dyes, which in the case of the investigated molecules, corresponds always to the lowest excited singlet (S_1). Electronic structure calculations can provide other quantities which may be used to characterize the nature of an excited state, as for instance, Mulliken charges.[117] The Λ test introduced by Peach and collaborators[118] in 2008 will be used to quantify the spatial overlap between the ground and CT states. These tools employed to analyze the results will be discussed in the following lines, together with other not so standard strategies used to characterize the optical CT state. In particular, tools involving interaction energies as a CT measure have also been explored, as for instance, the first excited singlet-triplet gap. This gap can be related to the exchange integral between the orbitals involved in the transition, and depends on the overlap between the frontier orbitals, thus being a suitable parameter to characterize CT. We have also taken advantage of the difference in the excitation energy calculated by CIS and TDHF, which can be related to the CT character, as it will be discussed in the following lines.

Moreover, for efficient electron injection into the semiconductor conduction band and dye regeneration, an appropriate alignment between the energy levels of the sensitizer, semiconductor and redox couple is required. Herein we will discuss how the ground and excited state oxidation potentials of the dye are determined from electronic structure calculations.

3.4.1 Basic concepts

Before going into the details of the computational tools, I would like to briefly contextualize in a few lines how we chemists treat the interaction of photons with

molecules and how the transition dipole moment naturally appears in the development of the theory. When dealing with the interaction between light and matter, one needs to resort to time-dependent perturbation theory to describe transitions between the unperturbed energy states.[119] As always happens in science, approximations must be done under meaningful assumptions, so that simple models and manageable expressions can help to describe the problem of interest and knowledge can be easily extracted. The first approximation consists in treating light as a classical electromagnetic field while matter is treated with quantum mechanics, within the framework of the semiclassical theory of light-matter interactions. Then, the most popular approximation in the physics community is imposed, that is: first order truncation of the perturbation operator, which is expressed as a multipolar expansion of the electric field. This approach is known as the electric dipole approximation,[119] and it is valid under the assumption that the wavelength of the electromagnetic radiation inducing the transition is much larger than the typical size of the considered molecule interacting with the photons, which is a reasonable presumption when considering the UV/Visible range of the electromagnetic spectrum.

Because of the coupling between the oscillating electric field of the radiation and the electron density of the molecule, a radiative transition may occur. Within the electric dipole approximation, the probability of a transition between two electronic states (ψ_i and ψ_f) is proportional to the square of the transition dipole moment μ, which in the basis of adiabatic states (stationary states of the electronic hamiltonian within the Born-Oppenheimer approximation) is defined as follows

$$\boldsymbol{\mu} = \langle \psi_i | q\boldsymbol{r} | \psi_f \rangle \tag{1.9}$$

and represents the effective electric dipole moment of the molecule when making a transition between two electronic states. We have considered μ to be independent of the nuclear coordinates, truncating the Taylor series of μ about the equilibrium geometry of the final state to first order, in what is commonly known as the Franck-Condon[120] approximation.

The transition dipole moment is in turn related to the oscillator strength f, by

$$f = \left(\frac{8\pi^2 m_e \nu}{3he^2} \right) |\boldsymbol{\mu}|^2 \tag{1.10}$$

where ν corresponds to the excitation frequency.

The oscillator strength, which is a dimensionless quantity, can also be related to the intensity of an electronic transition by the area under an absorption band[120]

$$f = 4.315 \cdot 10^{-9} \int \varepsilon(\bar{\nu}) d\bar{\nu} \qquad (1.11)$$

where ε is the molar extinction coefficient measured experimentally when recording an absorption spectrum and the numerical prefactor is in units of cm^{-1}. Therefore, the oscillator strength links the experimental intensities measured in a macroscopic world to a quantum mechanical observable, which accounts for the electronic structure of the absorbing molecules.

In principle, oscillator strengths should obey the Thomas-Reiche-Kuhn sum rule,[61] which states that the sum of the oscillator strengths from the transition of one state, *i*, to all the other states, *j*, must be equal to the total number of electrons in the system. When oscillator strengths are calculated with TDDFT, this rule is satisfied, but the TDA does not obey it.[39] However, this sum rule is only strictly valid in the limit of a complete basis set, something which we are always far from when calculating excited states of realistic systems. Moreover, experience has shown that meaningful results for electronic transitions can be obtained with TDA calculations. Also, if one is not interested in absolute values but rather in relative ones for comparison, as it is the case in this thesis, the TDA seems an adequate choice.

In this chapter we are interested in the radiative transition from S_0 to S_1 of organic dyes, and by analyzing expressions 2.9 and 2.10 we can understand when the probability of this electronic excitation will be large. In a TDA calculation, one can think of an excited state wave function, analogous to the one in a CIS calculation, that is, a linear combination of single excitations from the reference ground state Slater determinant. If S_1 corresponds mainly to an HOMO-to-LUMO excitation, then due to the one-electron nature of the dipole moment operator in expression 2.9, the integral will only depend on these orbitals. Therefore, in this single-excitation picture, the HOMO and LUMO should overlap to some extent, but because of the position operator, the larger the separation between hole and electron, the larger the transition dipole moment will be. The structure of the D-π-A dyes is thus ideal to obtain large oscillator strengths, since the HOMO and LUMO are spatially separated while the π-conjugated bridge guarantees spatial overlap between them.

3.4.2 Charge transfer characterization

(a) Electronic distribution

Although partial atomic charges are not physical observables, they may be estimated by Mulliken population analysis from the density matrix.[117] One of the major drawbacks this technique presents is that it depends strongly on the basis set, since charges on atomic centers are assigned on the basis of the total electron density in basis functions located on that center. Probably due to its simplicity, it has remained very popular for qualitative interpretations despite recent developments of new partitioning schemes. In the context of excited states, Mulliken charges associated to an electronic transition can be estimated from hole and particle transition density matrices. This is a straightforward manner to measure the CT extent of an excited state, since the difference between the charge at the initial and final states, i.e. the transition charge, quantifies the amount of electrons relocated within the molecule due to the excitation.

Another route to quantify the CT magnitude is to calculate the Λ parameter,[118] which is a measure of the degree of spatial overlap between the occupied and virtual orbitals involved in the electronic excitation. This measure (Λ) is defined as the sum of overlap integrals between moduli occupied (φ_i) and virtual orbital (φ_a) pairs weighted by the associated transition amplitudes (c_{ia})

$$\Lambda = \frac{\sum_{ia} c_{ia}^2 \left\langle |\varphi_i| \middle| |\varphi_a| \right\rangle}{\sum_{ia} c_{ia}^2} \tag{1.12}$$

The Λ parameter takes values between 0 and 1. Large overlap between states results in high Λ values indicating low CT character and vice versa. In their study,[118] the authors that proposed this method explored a large set of molecular systems with CT electronic transitions and concluded that this kind of excitations covers a wide range of Λ values, i.e. $0.06 < \Lambda < 0.72$ (with the PBE functional). Despite this wide range of values, the Λ parameter is suitable as a qualitative diagnostic test of CT excitation, since it captures the essential physics of the problem.

(b) Interaction energies

In this chapter interaction energies have been employed as CT measures taking advantage of how excitation energies indirectly depend on the overlap between the electronic states as

well as the electron-hole separation. First, we will discuss a measure based on the gap between the first excited singlet and triplet states as a measure of CT.

In the CIS method, the absolute energy of an electronic state can be expressed as[38]

$$E_{CIS} = E_{HF} + \sum_{ia} (c_{ia})^2 (\varepsilon_a - \varepsilon_i) + \sum_{ia,jb} c_{ia} c_{jb} \left(ia \middle|\middle| jb\right) \qquad (1.13)$$

where E_{HF} is the Hartree–Fock reference energy, i, j and a, b correspond to occupied and virtual spin–orbitals, c_{ia} is the i to a excitation amplitude, ε_p the one-electron p-orbital energy and ($ia||jb$) the antisymmetrized two-electron integrals. In a simple two electrons in two orbitals model, the lowest excited singlet and triplet states correspond to the ‘‘+’’ and ‘‘-‘‘ combinations of the spin-α and spin-β HOMO-to-LUMO electronic promotions, respectively. Following this model, the energy difference between the two states with different spin multiplicity is given by the exchange integral between the HOMO and LUMO (φ_H and φ_L in equation 1.14)[121]

$$\Delta E_{ST} = E(S_1) - E(T_1) \approx 2K_{HL} = 2\int \frac{\varphi_H^*(1)\varphi_L^*(1)\varphi_H(2)\varphi_L(2)}{r_{12}} d\boldsymbol{r}_1 d\boldsymbol{r}_2 \qquad (1.14)$$

Expression 2.14 explicitly reveals that the exchange integral K_{HL} depends on the separation between the two electrons (r_{12}) and the overlap between the two frontier orbitals. Larger overlaps and smaller interelectronic distances result in larger K_{HL} and vice versa. It is well known that the exchange integral between π and π* orbitals decreases with the conjugation length in organic molecules.[122,123] Also, the singlet–triplet gap becomes small for electronic transitions between separated spatial regions.[120,124] Hence, it seems plausible to use the ΔE_{ST} as an alternative interaction measure of the CT degree.

We have used another interaction-like measure for the CT degree of the excitation based on the role of the removed terms in the TDA[69,70] to the TDHF methodology. Recalling that the linear response TDHF equations are analogous to those of TDDFT in equation 1.1, with $c_{HF} = 1$ in equations 2.2 and 2.3, then the matrix elements of **A** and **B** are compactly expressed as

$$\begin{aligned} A_{ia,jb} &= \delta_{ij}\delta_{ab}(\varepsilon_a - \varepsilon_i) + \left(ia \middle|\middle| jb\right) \\ B_{ia,jb} &= \left(ia \middle|\middle| bj\right) \end{aligned} \qquad (1.15)$$

As mentioned previously, the TDA sets the terms of the **B** matrix to zero, and TDHF reduces to the CIS approach.

When an excited state is obtained as a result of an electronic transition with a pure CT character, that is, with no spatial overlap between the occupied *i*, *j*,... and virtual *a*, *b*,... orbitals involved in the transition, **B=0** (equation 1.15), which has been previously[67,71,74,125] noticed. Therefore, the weight of these terms can be related to the CT character of the transition. It is expected that a small separation between interacting electrons and large occupied-virtual overlaps will result in sizable values of the antisymmetrized integrals in **B**. As a simple approach to estimate the collective magnitude of the $B_{ia,jb}$ terms, the difference between CIS and TDHF excitation energies to the excited singlet state (ΔE_{TDA}) have been computed.

3.5 Oxidation potentials

The ground and excited state oxidation potentials (GSOP and ESOP)[126] of a set of organic dyes have also been calculated. These photoelectrochemical parameters are crucial to know if electron transfer to the semiconductor is possible, as well as if a particular redox couple is capable of regenerating the oxidized dye. The driving force of these processes is the relative value of the ESOP vs. the CBE of the semiconductor, as well as the GSOP vs. the redox potential of the redox mediator. For efficient electron injection and dye regeneration, the GSOP and ESOP should lie at least 0.2 eV higher (more negative) and lower (more positive) respectively than the CBE of TiO_2 and the I^-/I_3^- redox potential.[127] The GSOP and ESOP are the Gibbs free energy difference between the neutral and oxidized species in the ground $(G^0\text{-}G^+)_{GS}$ and excited state $(G_0\text{-}G^+)_{ES}$. There are different approaches to evaluate these values from a computational viewpoint.[126,127] The simplest one would be to approximate the GSOP by the negative of the HOMO energy, $-\varepsilon_H$, by virtue of Koopmans' theorem,[121] and then subtract the vertical excitation energy to calculate the ESOP. Within this approach however, the geometry reorganization in the excited state is neglected. Herein we have used a more rigorous approach[127] to estimate these parameters. The GSOP has been calculated as the Gibbs free energy difference between the neutral and oxidized dye in the ground state. This has been obtained including translational, rotational and vibrational enthalpies and entropies within the harmonic approximation. The ESOP has then been approximated by the following expression:

$$(G^0 - G^+)_{ES} \approx (G^0 - G^+)_{GS} - E_{0-0} \qquad (1.16)$$

subtracting the adiabatic transition energy ($E_{0\text{-}0}$) to the lowest singlet state from the estimated GSOP. In the computation of the adiabatic transition energy we assume equal zero-point energy corrections in the ground and excited states, thus $E_{0\text{-}0}$ is obtained as the energy gap between the two states in their equilibrium geometries.

4. Role of the linker in D-π-A dyes

4.1 Introduction

The thiophene unit is probably the most popular building block[128] for materials used in organic electronics. Its electronic properties may be readily tuned by structural modifications thanks to well-established synthetic routes. Moreover, the stabilization of the conjugated chain in polythiophenes, thanks to the polarizability of the sulfur atom, grants superb charge transport properties. In the context of D-π-A dyes for DSSCs, the thiophene π-spacer has the appropriate electronic properties to enable photoinduced CT in the sensitizer, and the optical properties may be enhanced by subtle chemical variations.[2] In this sense, the cyclopentadithiophene linker is a paradigm of how to improve the performance of DSSCs.[129-131]

In our work, several dyes were considered to study the influence of the π-bridge and other subtle chemical modifications on their photophysical properties. These dyes are shown in Figure 1.3 and they all have a D-π-A architecture, with bis(4-methoxyphenylamino)phenyl (D_B) as the donor group and cyanoacrylic acid as the acceptor (A). Within this scheme, we wanted to compare the widely used cyclopentadithiophene (*cpdt*) and bithiophene (*bt*) linkers,[2,26,31] with the closely related benzodithiophene (*bdt*) and dithientothiophene (*dtt*) units. In all these π-bridges, two thiophene units are present and the difference remains in how they are connected, either bonded directly (in *bt*) or by means of an additional fused ring, which may be cyclopentadiene (in *cpdt*), benzene (in *bdt*), or thiophene (in *dtt*). Apart from the effect that different linkers may have in the photophysical properties of the dyes, other structural modifications were also considered. For instance, the inclusion of an ethylene unit (*e*) between the donor group and the linker, since this strategy is commonly used by experimentalists to tune the absorption wavelength of the dye. In this case, an *e* is added to the linker label to represent the presence of the ethylene unit. Moreover, for the dye with the *cpdt* linker, the D_B donor group was also compared to bis(4-methoxyphenylamino)thienyl (D_T), where the phenyl ring bonded to the π-bridge is replaced by a thiophene unit.

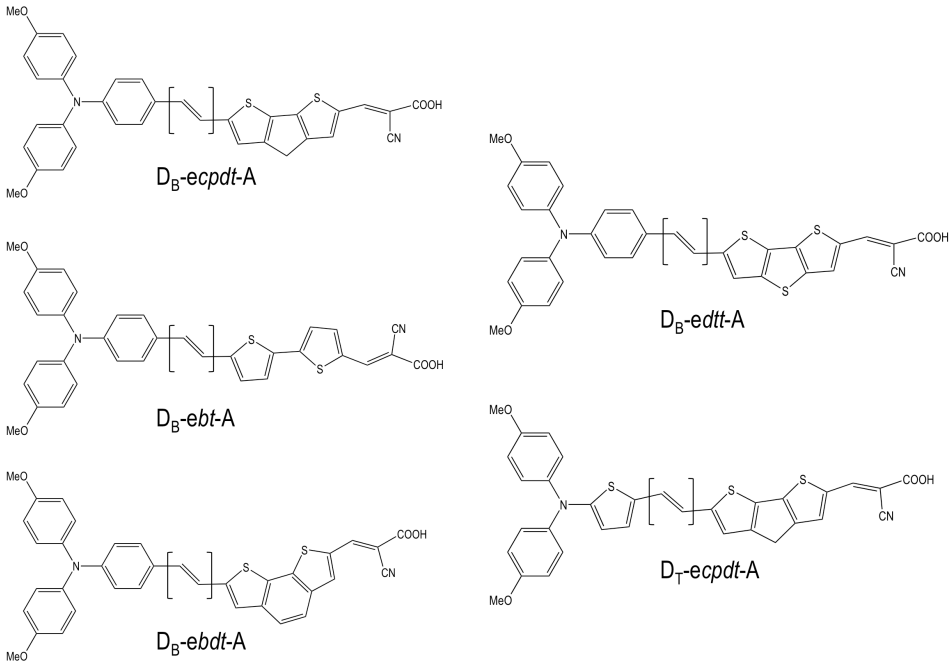

Figure 1.3 Studied D-π-A organic dyes with bis(4-methoxyphenyl-amino)phenyl (D_B) or bis(4-methoxyphenyl-amino)thienyl (D_T) as donor groups, the cyclopentadithiophene (*cpdt*), bithiophene (*bt*), benzodithiobphene (*bdt*), dithienothiophene (*dtt*) units as linkers, and the cyanoacrylic acid (A) as the electronic acceptor. The parentheses indicate two different possibilities, i.e. with (*e* prefix in the bridge acronym) and without the ethylene unit.

4.2 Ground state geometries

Before studying the absorption properties of the considered dyes in solution, the ground state molecular structure was characterized. Rotation about single bonds in these molecules leads to different conformations. We considered the isomerism regarding the relative *cis* (C) or *trans* (T) conformation of three pairs of double bonds between: (i) ethylene-linker, (ii) linker-acceptor, (iii) C=C and C=O in the acceptor. The different conformers are labeled with a three-letter string, as shown in Figure 1.4. When the ethylene unit is not present, this is indicated by the letter *n* at the first string position.

Although for all the dyes investigated in this chapter there are two possible isomers of the COOH group, only the most stable one was considered, in which the O-H bond is in a *cis* conformation relative to the C=O bond. Likewise, when referring to the *bt* linker, the energetically preferred *trans* disposition between the two thiophene rings was the only one considered.

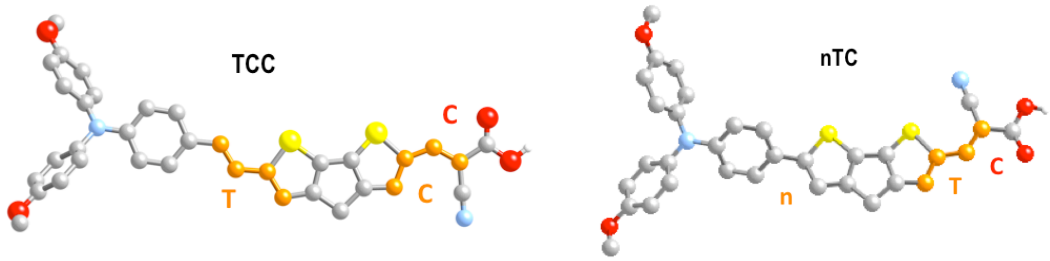

Figure 1.4 Nomenclature employed in this work to distinguish between molecular conformers.

As it has been shown in multiple occasions, structural characteristics of the organic dyes can have a substantial influence on their electronic structure, thus playing a crucial role regarding their photoabsorption ability.[7,82,132-134] Here we focus on how the different π-bridges and conformations affect the donor-acceptor spatial separation, the planarity along the molecule, and the linearity, by using the parameters shown in Figure 1.5 to describe the geometric characteristics of the dyes.

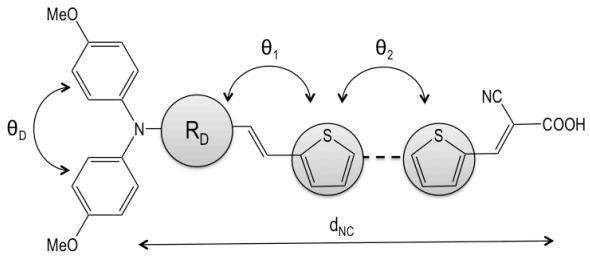

Figure 1.5 General molecular pattern of the studied organic dyes with measured geometrical parameters: donor to acceptor separation (d_{NC} in Å), and dihedral angles between the two methoxyphenyl rings of the donor (θ_D), the adjacent rings between donor and linker (θ_1) and the two thiophenes in the the π-bridge (θ_2).

As a first approximation, the donor–acceptor spatial separation induced by the linker, measured for instance as the distance between the nitrogen atom in the donor unit and the carboxylic carbon atom of the acceptor group (d_{NC} in Figure 1.5), can be associated to the hole/particle separation distance generated by the optical transition. Apart from the size of the linker, it is also important to take into account differences between molecular conformations. On average, the dyes with the *ecpdt*, *ebt* and *edtt* linkers present very similar donor to acceptor distances (d_{NC} ~18.0 Å), which are ~0.5 Å longer than the separation with *ebdt*. The donor-acceptor separation in D_T-*ecpdt*-A decreases by 0.5 Å with respect to D_B-*ecpdt*-A (Table 1.1). Evidently, the presence of the ethylene unit increases the separation. The N–C distance in molecular dyes with ethylene is between 16.8 and 18.3 Å, while it is 2.0 to 2.5 Å shorter without ethylene ($15.0 \leq d_{NC} \leq 15.8$ Å).

Table 1.1 Average structural parameters (d_{NC} in Å and all dihedrals in degrees) of the studied organic dyes optimized geometries[a].

bridge	d_{NC}	θ_1	θ_2	θ_D
ethylene				
ecpdt	18.0	4.9	0.1	60.4
ebt	18.0	7.1	6.8	60.8
ebdt	17.4	10.9	0.1	61.0
edtt	17.9	7.3	0.0	61.1
ecpdt[b]	17.4	6.0	0.0	69.5
no ethylene				
cpdt	15.7	26.9	0.1	62.3
bt	15.7	26.7	10.7	59.5
bdt	15.2	25.8	0.1	62.1
dtt	15.6	30.3	0.0	60.5
cpdt[b]	15.3	19.6	0.3	66.7

[a]Averaged values between all conformers of each molecule. [b]D_T donor group.

Apart from the nature of the bridge, different conformations of the molecular dyes also lead to different donor-acceptor separations. In general, it is expected that *cis* stereoisomerism of double bond pairs results in larger molecular linearity. As a consequence, the separation distance between the D and A fragments (d_{NC}) induced by the linker is larger for the *cis* forms of the donor-linker and linker-acceptor fragments with respect to the *trans* cases (Table 1.2). Taking the dye with the *cpdt* linker as an example, among the different conformers, d_{NC} can vary up to 0.6 Å and 0.2 Å in the D_B-*ecpdt*-A and D_B-*cpdt*-A families, respectively (Table 1.2). For the *cxx* conformers, i.e. when the donor group and the π-linker are in a *cis* disposition with respect to the ethylene unit, the donor-acceptor separation is 0.3-0.4 Å longer than for the *txx* conformers. The relative disposition of the π-linker and acceptor group also affects the N-C separation. When the double bond of the thiophene unit in *ecpdt* is oriented in *cis* with respect to the C=C bond of the acceptor unit, i.e. in the *xcx* conformers, d_{NC} is 0.2-0.3 Å longer than when it is in *trans*, i.e. in the *xtx* conformers. Finally, the relative orientation of the C=C and C=O bonds in the acceptor unit, i.e. *xxc* vs *xxt* conformers, does not have a significant effect on the donor-acceptor separation. In summary, the trend followed by d_{NC} among the different conformations is *ccx* > *ctx* > *tcx* > *ttx* and *ncx* > *ntx* and holds for the remaining investigated linkers (Appendix, Table A1.1). Although the largest variation of d_{NC} among the conformations of the dyes including the *bt* and *dtt* units is similar to that of *cpdt*, due to the size of the *bdt* fragment, d_{NC} has a larger variation up to 1.2 Å and 0.5 Å between the different conformations of the D_B-*ebdt*-A and D_B-*bdt*-A families, respectively. From these

results we can conclude that for those conformations with a *cis* disposition between donor-linker and linker-acceptor, i.e. *ccx* and *ncx*, a subtle increase in the charge separation associated to the electronic excitation process is expected, as well as an increase in the transition probability.

Table 1.2 Structural parameters (d_{NC} in Å and θ_1 in degrees) and relative energies (kcal/mol) with respect to the most stable conformation for the studied conformers of D_B-ecpdt-A and D_B-cpdt-A optimized organic dyes.

conformer	d_{NC}	θ_1	ΔE
ethylene			
CCC	18.21	1.1	1.33
CCT	18.25	2.8	1.90
CTC	18.06	2.3	0.78
CTT	18.07	8.4	1.32
TCC	17.90	3.1	0.78
TCT	17.96	3.3	1.34
TTC	17.63	8.6	0.00
TTT	17.63	9.7	0.56
no ethylene			
nCC	15.77	26.8	0.73
nCT	15.82	26.8	1.26
nTC	15.59	26.5	0.00
nTT	15.60	27.4	0.50

The energy differences between structural conformers are rather small i.e. < 1.9 kcal/mol for the D_B-*ecpdt*-A family and <3.0 kcal/mol for all the other cases (Appendix, Table A1.1). The results indicate that the energetic cost of the *trans* to *cis* isomerization around the ethylene unit between the donor and the π-bridge is 0.5–0.8 kcal/mol, while the linker-acceptor *trans* conformation is 0.6–0.8 kcal/mol more stable than the *cis* form. The *cis* configuration between the two double bonds in the acceptor group is slightly more stable (0.5–0.6 kcal/mol) than in the *trans* case. Hence, the TTC is the most stable conformer of the D_B-*ecpdt*-A family in acetonitrile (ACN) solution. The trends of the geometrical parameters and relative energies in Table 1.2 are not exclusive for the *cpdt* linker, and very similar behaviors are obtained for the other studied molecules (Appendix, Table A1.1), with small shifts in the absolute values already indicated by the differences in the averaged values of Table 1.1.

The molecular planarity of the studied chromophores is a key geometrical element, which controls the electronic properties of the dye. Naturally, the degree of coplanarity between

the donor and the linker must have a great impact on the donor–acceptor electronic coupling through the π-system of the bridge. In other words, the dihedral angle θ_1 in Figure 1.5 will determine to a large extent the conjugation of the molecule and the overlap between the π-system of the two ends. The ethylene unit connecting donor and linker groups relaxes the geometrical tension between rings, resulting in rather small θ_1 angles (< 10º on average). These angles however can vary up to ~15º within different conformations of a dye with the same linker. In general, *trans* stereoisomerism between the donor group and the linker yields smaller θ_1 angles with respect to the *cis* case, with the exception of the *ecpdt* linker, which does not follow this trend. When the olefinic unit is not present, the molecular planarity is severely lost, and θ_1 increases by about 20° and 15° for the D_B and D_T donors, respectively.

In addition to the disposition between the donor and the conjugated bridge measured by θ_1, it is also important to consider the planarity of the linker itself, i.e. the dihedral angle between the two thiophene rings (θ_2). For all the linkers where the two thiophenes cannot freely rotate, i.e. *cpdt*, *dtt* and *bdt*, the bridge is perfectly planar ($\theta_2 < 0.4$º) and this rigidity imposes the linker's fragments to virtually lie on the same plane. On the contrary, when the rotation between the two thiophene rings is not constrained, i.e. for *bt*, the linker prefers to break its planarity ($0.0 < \theta_2 < 16.1$º) in order to avoid steric hindrance between rings, which reduces the π-conjugation of the molecule.

As for the geometrical characteristics of the donor group, the two methoxyphenyl rings are oriented out of the molecular plane defined by the linker and acceptor fragments, with no major differences in the dihedral angles between both rings (θ_D in Figure 1.5) for the investigated linkers with the D_B donor group. Therefore, this parameter is not expected to have a major influence on the relative photophysical properties of the dyes. The θ_D angle ranges from 56° to 65º for all the cases with the D_B donor group, and becomes a bit larger when the phenyl ring in D_B is replaced by a thiophene unit in D_T, with $\theta_D \leq 75.2$º. The presence or absence of the ethylene fragment between the donor and the linker has almost no influence on θ_D.

4.3 Vertical transition

For all the studied dyes, the optical transition mainly corresponds to the electronic promotion from the HOMO, mostly located on the D_B (or D_T) group, to the LUMO,

centered at the cyanoacrylic acid (A), with both orbitals partially delocalized over the conjugated π-bridge. The next most important contributions in the first excited singlet wave function come from the HOMO-1 to LUMO and HOMO to LUMO+1 configurations (Figure 1.6), with the HOMO-1 delocalized all over the molecule and the LUMO+1 delocalized on the acceptor, π-bridge, and partially on the donor group.

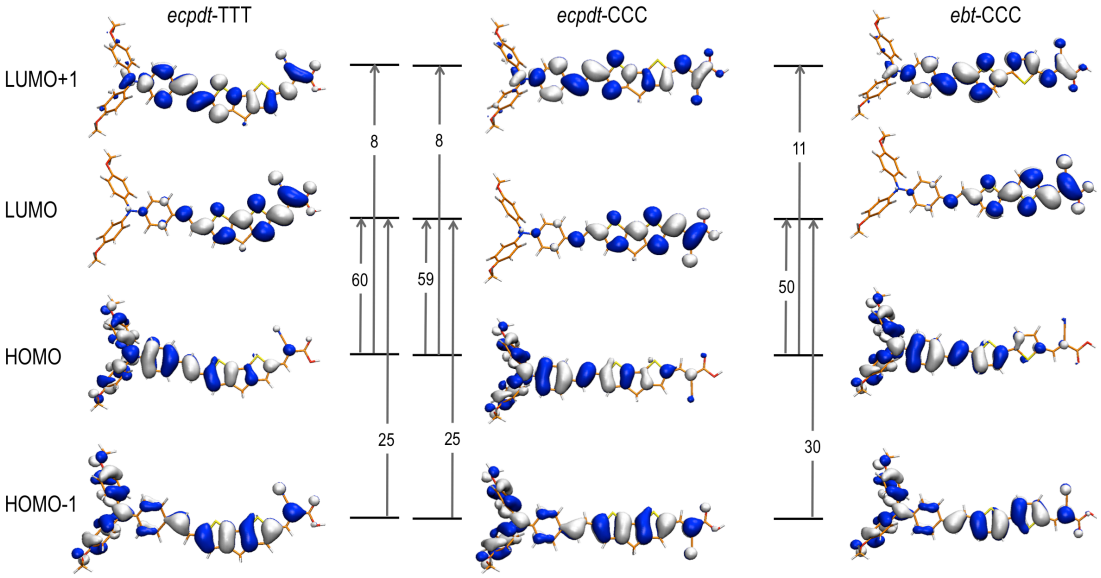

Figure 1.6 Frontier MOs of the all *trans* (TTT) and all *cis* (CCC) D_B-*ecpdt*-A conformers and the all *cis* D_B-*ebt*-A dyes. Vertical arrows indicate the main contributions (in %) of the S_0 to S_1 transition.

The average vertical transition energy of the D_B-*ecpdt*-A dye in acetonitrile is computed to be 2.79 eV while with the *ebt* linker it is 2.85 eV. The frontier MOs of the *ebt* family are stabilized with respect to the *ecpdt* counterparts, but since the HOMO and LUMO stabilize by the same amount in *ebt* (0.05 eV), this cannot explain the difference in the vertical transition energy. However, the LUMO+1 and specially the HOMO-1 are more involved in the S_0 to S_1 transition (Figure 1.6). The larger participation of these higher energy contributions accounts for the small blue shift of the energy gap (0.04–0.09 eV) in *ebt* dyes with respect to *ecpdt* ones.

On average, excitation energies with the *ebdt* and *edtt* linkers are 0.27 and 0.12 eV, respectively, larger than the *ecpdt* energies (Table 1.3). The chemical change of the *ecpdt* π-bridge by *ebdt* or *edtt* has a minor effect on the HOMO and the LUMO energies. The reason for this increase must be assigned to the HOMO-1 stabilization with the *ebdt* and *edtt* linkers with respect to *ecpdt* (Appendix, Table A1.2), which has a substantial

participation in the transition (25–30%) and is markedly located on the linker fragment. This stabilization of the HOMO-1 is related to the increase in conjugation with the *edbt* linker and the presence of the sulfur atom in *edtt*.

Table 1.3 Average ground to first excited singlet vertical transition energies ΔE (in eV), oscillator strengths *f,* and charge increment at the donor and acceptor fragments ΔQ (in electrons) of the D_B-bridge-A organic dyes[a].

bridge	ΔE	*f*	ΔQ	
			Donor	Acceptor
ethylene				
ecpdt	2.79	2.55	0.13	–0.15
ebt	2.85	2.29	0.15	–0.16
ebdt	3.06	2.09	0.18	–0.20
edtt	2.91	2.46	0.16	–0.17
ecpdtb	2.68	2.43	0.17	–0.13
no ethylene				
cpdt	2.95	2.12	0.16	–0.18
bt	3.01	1.87	0.20	–0.20
bdt	3.21	1.61	0.23	–0.26
dtt	3.11	1.97	0.20	–0.22
cpdtb	2.79	1.99	0.21	–0.16

[a]Averaged values between all conformers of each molecule. [b]D_T donor group

The substitution of benzene by thiophene in the donor group systematically reduces the excitation energy by 0.09–0.15 eV. This mutation mainly affects the HOMO, which becomes energetically higher with the five-member ring (D_T), while the LUMO is basically unaffected and the LUMO+1 is stabilized. Thus, the HOMO-LUMO (and LUMO +1) gap decreases.

Transition energies for the dyes without the ethylene unit follow the same trends, although the loss of conjugation in all molecules with respect to the cases with ethylene systematically increases the electronic excitation energies by 0.1–0.2 eV. As shown in Table 1.4 for the *ecpdt* and *cpdt* linkers, the excitation energies remain constant for all molecular conformations. This behavior is also obtained for the conformers of the other dyes (Appendix, Table A1.3).

Table 1.4 Average ground to first excited singlet transition energies ΔE (in eV), oscillator strengths *f,* and charge increment at the donor and acceptor fragments ΔQ (in electrons) for the different conformers of the D_B-*ecpdt*-A and D_B-*cpdt*-A dyes.

conformer	ΔE	*f*	ΔQ	
			Donor	Acceptor
ethylene				
CCC	2.79	2.70	0.12	–0.16
CCT	2.80	2.72	0.13	–0.16
CTC	2.79	2.57	0.12	–0.15
CTT	2.80	2.58	0.13	–0.15
TCC	2.79	2.55	0.13	–0.15
TCT	2.79	2.58	0.13	–0.15
TTC	2.78	2.34	0.13	–0.15
TTT	2.78	2.34	0.13	–0.15
no ethylene				
nCC	2.95	2.19	0.16	–0.19
nCT	2.96	2.21	0.16	–0.19
nTC	2.94	2.04	0.16	–0.18
nTT	2.95	2.05	0.16	–0.18

The intensity of the optical transition can be revealed by means of the TDDFT dimensionless computed oscillator strengths *f* from the ground state to the lowest excited singlet. In average, the *ecpdt* linker triggers the largest transition probabilities (Table 1.3). The D_B-*edtt*-A and D_T-*ecpdt*-A give rise to very similar values, which are just a little bit lower than in the D_B-*ecpdt*-A case. The presence of the *ebt* and *ebdt* linkers significantly lowers the oscillator strengths with respect to *ecpdt*, especially the latter one. To trace back the differences between π-linkers in the computed strengths it is important to bear in mind that *f* is proportional to the square of the dipole moment integral between the ground and excited states. This integral directly depends on the charge separation created by the electronic transition; hence, it must be proportional to d_{NC}. This dependence becomes evident when comparing the values between conformers of the same dye (Tables 2.2 and 2.4).

In addition, in order to obtain significant transition moments it is necessary to have a non-zero spatial overlap between the two states. In other words, the extension of the overlap between the MOs involved in the transition will also tune the magnitude of the oscillator strengths. In this sense, the planarity of the molecule (related to the θ_1 and θ_2 dihedral angles) is expected to improve this overlap and increase *f*. For example, the transition

probability is systematically reduced for the dyes without the ethylene fragment because of the shorter molecular length and the loss of planarity along the molecules

The overlap between the MOs involved in the transition is not only ruled by the planarity, but will also be affected by the linearity. This overlap is expected to be larger for linear molecules than for those cases with curved geometries. Also, more linear geometries are accompanied by a larger donor-acceptor separations, which also favors larger *f* values. In order to quantify the molecular linearity of the investigated dyes, a linear coefficient (LC) may be defined as in Figure 1.7, which is related to angles between the donor, π-bridge, and acceptor units. The similar oscillator strengths computed for the D_B-*ecpdt*-A and D_B-*edtt*-A families can be ascribed to the similar degrees of linearity and planarity imposed by the linker and the donor group. Although the *edbt* linker is planar, it induces less linear geometries compared to the *ecpdt* case because of the "bulkier" fused ring, therefore, lower oscillator strengths are obtained.

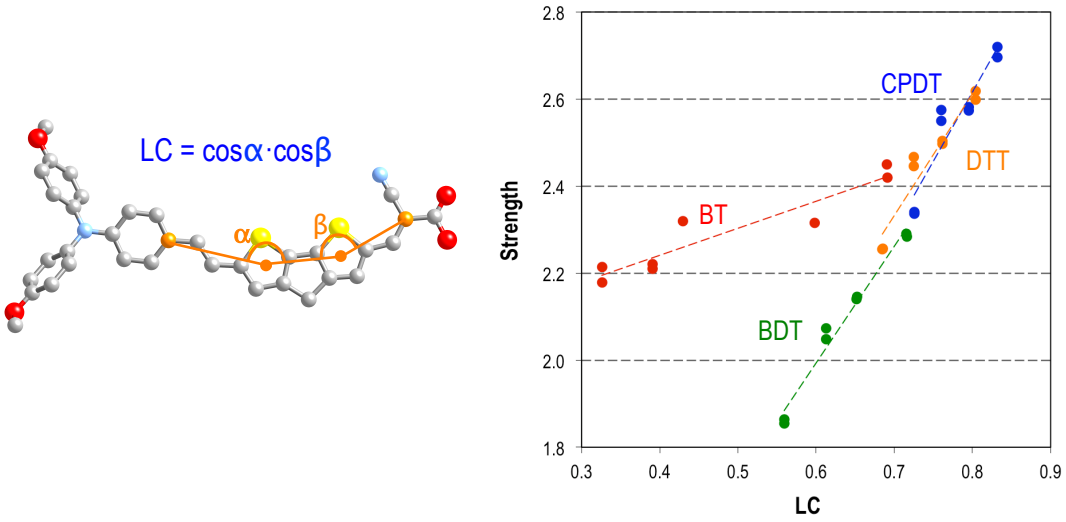

Figure 1.7 Definition of linearity coefficient (LC) from the α and β angles (left). Plot of the oscillator strength vs LC for all the conformers of the dyes with the ethylene unit (right).

For the *ebt* linker, both factors, planarity and linearity, are responsible for the lower transition probabilities. This is clearly seen when comparing the dye with the *ecpdt* linker, with analogous molecules with the *ebt* linker where the thiophenes are oriented in *cis* or in *trans* (Figure 1.8). The *ecpdt* linker is planar and induces linear geometries, hence, the value of *f* is the largest compared to the other two molecules. With *trans-ebt*, planarity is still preserved but linearity is severely lost, as the value of LC indicates, leading to lower *f*

values. With *cis-ebt* planarity is lost and linearity is still reduced compared to *ecpdt*, thus leading to the lowest transition probability.

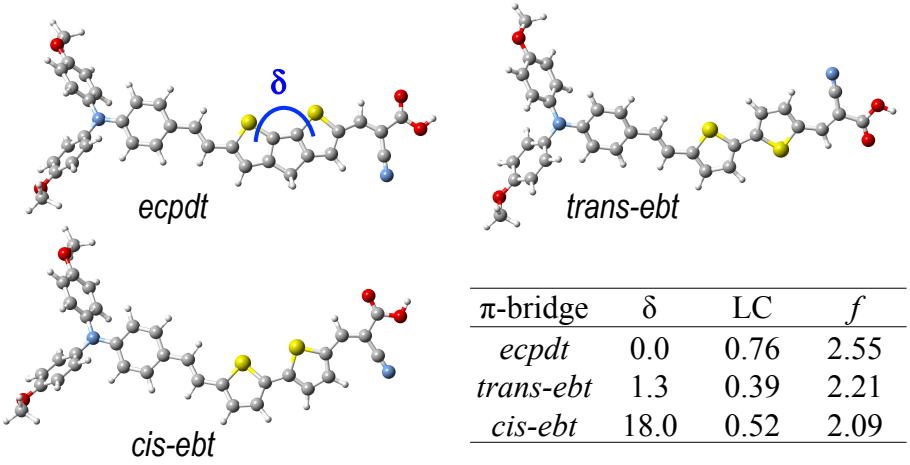

π-bridge	δ	LC	*f*
ecpdt	0.0	0.76	2.55
trans-ebt	1.3	0.39	2.21
cis-ebt	18.0	0.52	2.09

Figure 1.8 Comparison between the linker's planarity (δ) and the dye's linearity (LC) with the computed oscillator strengths (*f*) for three representative dyes (in their TCC conformation).

In general, the transition Mulliken charges at the donor and the cyanoacrylic acid acceptor groups, ΔQ in Table 1.3, are of the same order of magnitude for all molecules. The slight differences between dyes can be understood by how well localized the HOMOs and LUMOs (involved in the electronic transition) are in the donor and acceptor groups, respectively. Larger localizations will result in larger overall negative charge transferred to the cyanoacrylic acid. Similarly, molecules without the ethylene unit present a systematic increase of ΔQ. This behavior is qualitatively revealed by the slightly different spatial localization of the HOMO and LUMO orbitals for the D_T-*ecpdt*-A and D_B-*bdt*-A and related dyes without the ethylene unit, respectively (Figure 1.9). There are basically no differences in the computed ΔQ values between conformers of the same dye (Table 1.4).

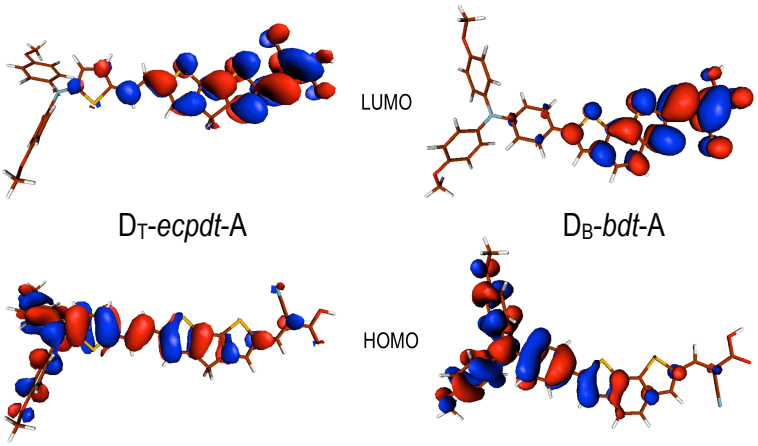

Figure 1.9 HOMO (down) and LUMO (up) of D_T-*ecpdt*-A (left) and D_B-*bdt*-A (right) dyes.

4.4 Conclusions

The photophysical properties of a set of D-π-A organic dyes have been explored. The study focuses on the cyclopentadithiophene (*cpdt*) unit as a conjugated bridge and how it influences the characteristics of the optical transition in comparison to other similar linkers. The differences in the calculated excitation energies and oscillator strengths of the studied dyes have been plainly rationalized by means of geometrical parameters related to the linearity and planarity of the molecules, which affect the relative energies of frontier MOs and the electronic interaction between donor and acceptor π-systems. The results point to the reasons why *cpdt* yields, in general, larger extinction coefficients. The presence of an ethylene unit between the donor and linker fragments increases the number of π-electrons, the donor–acceptor separation, and the molecular planarity, leading to systematically red shifted excitation energies and larger oscillator strengths, independently of the employed π-bridge.

4.5 Computational details

Geometry optimizations for all studied organic sensitizers in the ground state have been performed with no symmetry restrictions within the DFT methodology, with the LRC-ωPBEh density functional[79] and the 6-31+G(d) atomic basis set. The solvent effects in acetonitrile were taken into account by the C-PCM method.[106] The vertical excitation energies were calculated at these geometries by the same density functional with the TDDFT methodology within the TDA[68] and the 6-311+G(2d,2p) basis set. The Q-Chem program[135] has been employed in all calculations.

4.6 Appendix

Table A1.1 Structural parameters (d_{NC} in Å and θ_1 in degrees) and relative energies (kcal/mol) with respect to the most stable conformation for the optimized organic dyes.

dye	conformer	d_{NC}	θ_1	ΔE	dye	conformer	d_{NC}	θ_1	ΔE
D_B-*ebt*-A	CCC	18.2	9.4	1.49	D_B-*edtt*-A	CCC	18.2	11.2	1.75
	CCT	18.3	7.4	2.02		CCT	18.2	11.6	2.29
	CTC	18.0	9.7	0.57		CTC	18.0	11.1	0.86
	CTT	18.1	11.4	1.08		CTT	18.0	12.2	1.39
	TCC	17.9	7.3	0.81		TCC	17.8	2.9	0.88
	TCT	17.9	7.1	1.35		TCT	17.9	4.2	1.42
	TTC	17.8	1.7	0.00		TTC	17.5	2.8	0.00
	TTT	17.9	3.1	0.52		TTT	17.5	2.5	0.51
D_B-*bt*-A	nCC	15.8	25.4	0.90	D_B-*dtt*-A	nCC	15.7	30.6	0.88
	nCT	15.8	25.7	1.43		nCT	15.8	30.5	1.40
	nTC	15.7	28.3	0.00		nTC	15.5	30.0	0.00
	nTT	15.7	27.2	0.53		nTT	15.5	30.1	0.51
D_B-*ebdt*-A	CCC	17.9	6.7	2.37	D_T-*ecpdt*-A	CCCC	17.8	8.8	2.72
	CCT	18.0	14.6	2.90		CCTC	17.7	12.0	2.02
	CTC	17.6	20.4	1.23		CTCC	17.3	10.0	2.03
	CTT	17.6	18.0	1.72		CTTC	17.0	15.4	1.36
	TCC	17.2	7.9	1.13		TCCC	17.4	0.3	1.22
	TCT	17.3	4.3	1.64		TCTC	17.2	0.4	0.56
	TTC	16.8	7.5	0.00		TTCC	17.5	0.0	0.70
	TTT	16.8	7.6	0.52		TTTC	17.3	1.1	0.00
D_B-*bdt*-A	nCC	15.4	26.4	1.03	D_T-*cpdt*-A	TCC	15.4	20.2	0.64
	nCT	15.5	25.9	1.60		TCT	15.4	20.5	1.20
	nTC	15.1	25.3	0.00		TTC	15.3	18.1	0.00
	nTT	15.0	25.4	0.47		TTT	15.3	19.6	0.53

Table A1.2 Average molecular energies of frontier orbitals (in eV) for the studied organic dyes.

bridge	H-1	H	L	L+1
ethylene				
ecpdt	-7.48	-6.67	-1.47	-0.08
ebt	-7.59	-6.72	-1.52	-0.24
ebdt	-7.73	-6.78	-1.52	-0.24
edtt	-7.62	-6.75	-1.52	-0.16
ecpdt[a]	-7.46	-6.56	-1.50	-0.16
no ethylene				
cpdt	-7.65	-6.78	-1.41	0.30
bt	-7.81	-6.83	-1.47	0.08
bdt	-7.95	-6.86	-1.50	0.14
dtt	-7.81	-6.86	-1.47	0.24
cpdt[a]	-7.65	-6.67	-1.44	0.14

[a]D_T donor group.

Table A1.3 Ground to first excited singlet transition energies ΔE (in eV) and oscillator strengths *f* for the studied organic dyes.

dye	conformer	ΔE	*f*	*dye*	*conformer*	Δ*E*	*f*
D_B-*ebt*-A	CCC	2.88	2.42	D_B-*edtt*-A	CCC	2.91	2.60
	CCT	2.87	2.45		CCT	2.92	2.62
	CTC	2.87	2.32		CTC	2.92	2.50
	CTT	2.87	2.32		CTT	2.93	2.50
	TCC	2.83	2.21		TCC	2.90	2.45
	TCT	2.84	2.22		TCT	2.90	2.47
	TTC	2.85	2.18		TTC	2.90	2.26
	TTT	2.83	2.21		TTT	2.91	2.26
D_B-*bt*-A	nCC	3.02	1.90	D_B-*dtt*-A	nCC	3.10	2.02
	nCT	3.03	1.92		nCT	3.11	2.04
	nTC	3.00	1.84		nTC	3.11	1.91
	nTT	2.99	1.84		nTT	3.12	1.91
D_B-*ebdt*-A	CCC	3.05	2.28	D_T-*ecpdt*-A	CCCC	2.70	2.58
	CCT	3.06	2.29		CCTC	2.70	2.50
	CTC	3.09	2.14		CTCC	2.68	2.41
	CTT	3.08	2.15		CTTC	2.69	2.19
	TCC	3.04	2.05		TCCC	2.67	2.55
	TCT	3.04	2.07		TCTC	2.67	2.41
	TTC	3.05	1.86		TTCC	2.67	2.47
	TTT	3.06	1.86		TTTC	2.66	2.31
D_B-*bdt*-A	nCC	3.20	1.66	D_T-*cpdt*-A	TCC	2.79	2.04
	nCT	3.20	1.68		TCT	2.80	2.05
	nTC	3.22	1.55		TTC	2.78	1.95
	nTT	3.23	1.55		TTT	2.79	1.95

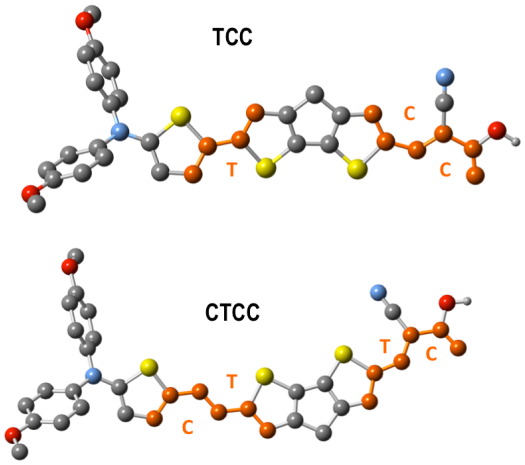

Figure A1.1 Nomenclature employed to distinguish between D_T-*cpdt*-A (top) and D_T-*ecpdt*-A (bottom) conformers.

5. Influence of the length of the bridge of D-π-A dyes on the CT state

5.1 Introduction

As it has been discussed in section 3.2.2(b) of this chapter, the calculation of CT states with TDDFT methods is problematic if the xc functional that is used is not adequate. To obtain sensible physical results, the use of at least hybrid functionals, and more desirably, long range corrected ones is mandatory. It is therefore always interesting to have some means to characterize the degree of CT in a transition as a diagnosis of such character and also for a qualitative measurement for comparison between similar systems one may be interested. The D-π-A structure of the investigated dyes (Figure 1.10) offers a great opportunity in this sense because of the strong CT character of the S_1 state in these compounds

The main objectives of this work pointed towards two complementary directions. In the first place, our efforts aimed to expose a detailed analysis of the fundamental structural and electronic characteristics of our target molecular dyes, that is D-π-A dyes with the (bis(4-methoxypheny)amino)phenyl group and cyanoacrylic acid as the donor and acceptor moieties respectively, and the polythiophene (Tn) and polycyclopentadithiophene (Cn) series as the π-spacers (Figure 1.10). We were specially interested on how the length of the π-bridge influences the electronic structure of the Cn and Tn series. Simultaneously, we were also interested on the development and application of simple computational tools for the analysis of the electronic structure of the organic dyes. In this work, special emphasis was placed on the use of standard and novel computational strategies for the study of the CT nature of electronic transitions. In particular, the CT nature of the transition was characterized by standard computational tools, as well as by new ones, taking advantage of how the expressions of the excitation energies within different methodologies are affected by having zero overlap between the donor and acceptor units. In relation to the LRC functionals used to compute CT states, the adequacy of the empirical ω parameter that dictates how the long range non-local exchange is introduced was also assessed.

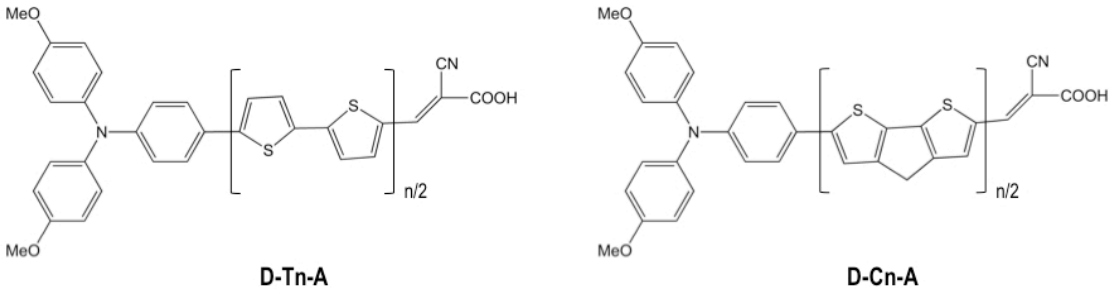

Figure 1.10 Studied D-π-A dyes with polythiophene (Tn) and polycyclopentadithiophene (Cn) linkers.

5.2 Molecular geometries

Before studying the photophysical properties of the organic dyes, we will analyze in detail their geometrical characteristics (Figure 1.11), paying special attention to the differences between them (Table 1.5).

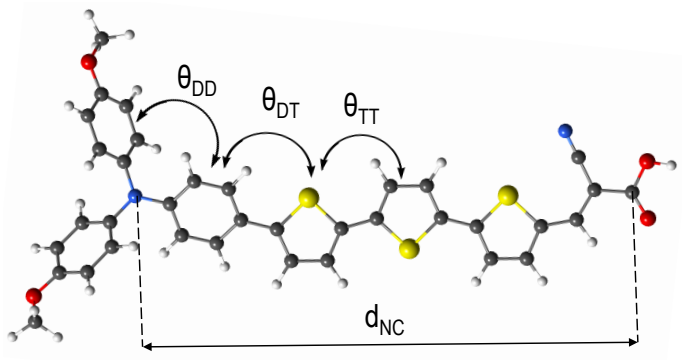

Figure 1.11 Molecular structure of the D-T3-A dye with the description of the d_{NC}, θ_{DD}, θ_{DT} and θ_{TT} geometrical parameters of Table 1.5.

Obviously, amongst the polythiophene linkers, T1 gives rise to the shortest donor–acceptor spatial separation (d_{NC} = 11.60 Å). The distance between the nitrogen atom in the (bis(4-methoxyphenyl)amino)phenyl fragment (D) and the carboxylic group at the other end of the molecule is approximately 4 Å longer for each additional thiophene ring in the Tn or Cn spacers. The geometry of the triarylamine moiety is practically invariant with the length and type of the linker (Tn or Cn). The optimized dihedral angles between the phenyl ring connected to the conjugated bridge and the two end methoxyphenyl rings (θ_{DD}) are ~30°, rather close to the values experimentally observed in triphenylamine.[136]

The geometry stabilization obtained via electronic conjugation is not enough to overcome the steric hindrance between hydrogen atoms in the phenyl-thiophene junction and the θ_{DT} torsion angles computed with the LRC-ωPBEh functional are ~30° in all cases. The rest of

the molecular structure, that is, the π-spacers and the cyanoacrylic acid moiety, exhibit a considerable degree of planarity. In particular, the rigidity of the Cn linkers imposes the Cn-A fragment to virtually lie on the same plane. On the other hand, the angular torsion between thiophene rings in Tn dyes strongly depends on the computational method employed to optimize the geometries. As a result of the self-interaction error, the B3LYP functional favors electronic delocalization and systematically increases coplanarity between contiguous conjugated rings. That is, smaller θ_{DT} and θ_{TT} torsion angles with respect to LRC-ωPBEh and MP2 geometries. This effect is especially notorious for the θ_{TT} angles in the D-Tn-A dyes. The LRC-ωPBEh and MP2 methods produce qualitatively similar structures. Both approaches tend to break planarity along the Tn linkers (θ_{TT}). In general, the loss of molecular planarity (θ_{DT} and θ_{TT}) is more severe in MP2 than in LRC-ωPBEh calculations. The excited state calculations presented in the following section will be performed on the LRC-ωPBEh optimized geometries.

Table 1.5 Geometrical parameters (see Figure 1.11) for the gas phase optimized ground state of the D-Tn-A and D-Cn-A dyes. Dihedral angles θ_{DD} and θ_{TT} (for n=3,4) correspond to average values. Here ωPBEh refers to LRC-ωPBEh.

Linker	d_{NC}	θ_{DD}	θ_{DT}			θ_{TT}		
	ωPBEh	ωPBEh	B3LYP	ωPBEh	MP2	B3LYP	ωPBEh	MP2
T1	11.60	27.7	19.1	27.5	33.5	-	-	-
T2	15.64	29.5	23.2	29.5	34.8	0.1	17.7	26.8
T3	19.40	29.3	24.5	31.0	34.6	1.8	17.4	27.9
T4	23.24	30.7	23.0	29.7	34.6	4.5	22.1	28.4
C2	15.58	29.2	20.9	30.6	35.2	0.1	0.1	0.1
C3	19.52	30.1	22.0	30.7	35.0	0.1	0.1	0.1
C4	23.42	30.8	22.1	30.8	35.0	0.1	0.0	1.8

5.3 Frontier molecular orbitals

The spatial characteristics of the frontier MOs and their energies provide a simple picture to rationalize the properties of the optical transition in molecular dyes. The linker fragment connects the donor and acceptor groups, establishing a spatial separation and electronic coupling between them, facilitating the electron–hole detachment and, as a consequence, reducing the probability of electron–hole recombination. For a favorable electric dipole assisted electronic transition, the conjugated system of the bridge must interact with both, the HOMO of the donor and the LUMO of the acceptor.

In this sense, the molecular orbital energy diagram of the donor, linker and acceptor fragments is useful to illustrate the adequacy of the Tn and Cn linkers in D-π-A type sensitizers (Figure 1.12). The HOMO and LUMO of the Tn and Cn bridges correspond to π-bonding and π-antibonding combinations of the CC double bonds in thiophene, with smaller contributions from the sulfur atoms. The increase of the conjugation length in the linker with respect to the shortest T1 bridge destabilizes and stabilizes the bonding and antibonding orbitals, respectively. Thus, longer linkers have smaller HOMO–LUMO gaps. The orbital diagram in Figure 1.12 also indicates that, due to the geometry constraints imposed in the Cn family, the two frontier orbitals are slightly higher in energy than their Tn counterparts. In all cases, the π-like HOMO of the donor group is fairly close in energy to the linkers' HOMOs, and the LUMO of the cyanoacrylic acid acceptor group is within the energy range of the LUMOs of the linkers. The appropriate energy matching between these frontier orbitals allows efficient CT upon sunlight absorption.

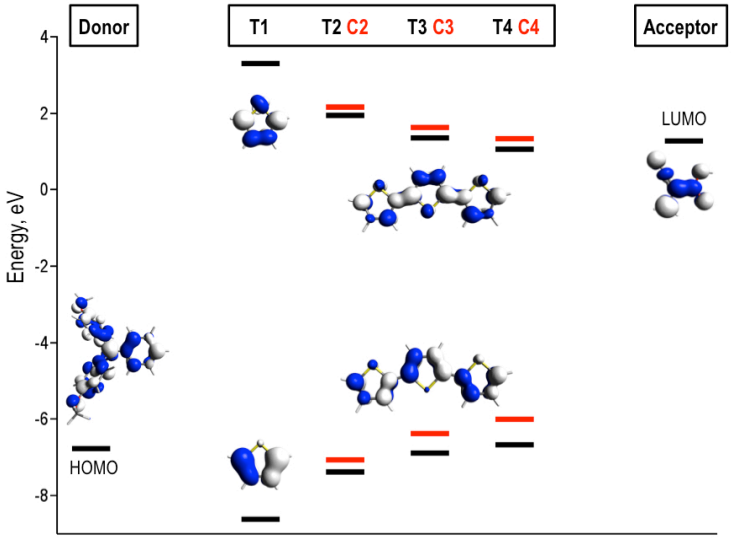

Figure 1.12 MO diagram of the donor and acceptor groups (HOMO and LUMO respectively) and the Tn (n=1–4) and Cn (n=2–4 red markers) conjugated linkers (HOMO and LUMO). For the sake of simplicity, only the representations of MOs for the T1 and T3 linkers are shown.

The frontier MOs for all Tn and Cn dyes are basically obtained as the result of combining the fragment orbitals in Figure 1.12. The energy diagram of the HOMO-1, HOMO and LUMO for the two sets of dyes is shown in Figure 1.13. The HOMO and HOMO-1 orbitals are different combinations between the HOMOs from the donor and linker moieties. The dye's HOMO is mainly located over the donor group with important delocalization towards the π-bridge. The main contribution to the HOMO-1 comes from the linker's HOMO with some contribution from the two methoxy-phenyl rings of the donor group and

a minor participation of the acceptor's π-system. The LUMO results from the bonding interaction between the LUMOs in the linker and acceptor moieties. Coplanarity between linker and acceptor groups facilitates the electron delocalization of the LUMO. Orbital energy differences between dyes are the direct consequence of the HOMO and LUMO energies of the Tn and Cn linkers discussed previously (Figure 1.12).

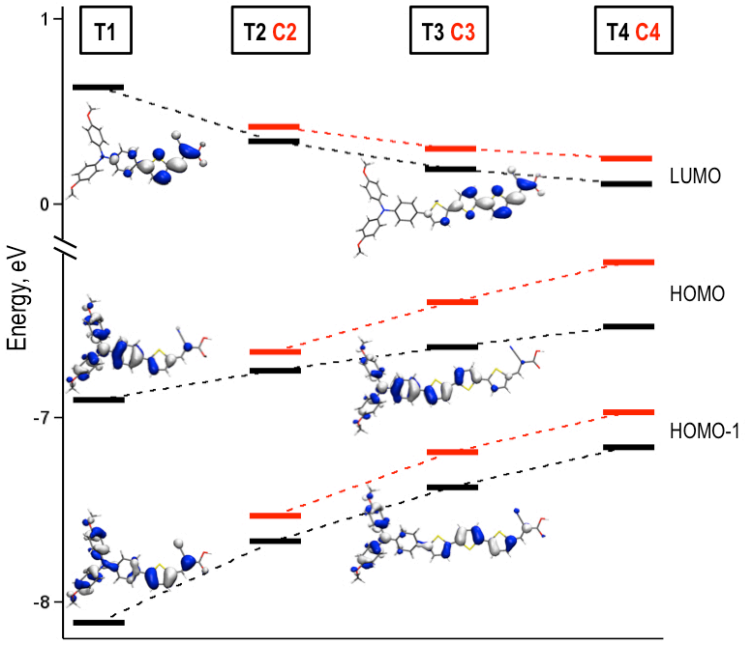

Figure 1.13 MO diagram for the Tn (n = 1–4, black markers) and Cn (n = 2–4, red markers) dyes. For the sake of simplicity, only the representations of MOs for the T1 and T3 dyes are shown.

It is important to notice that the structural dissimilarities between the D-Tn-A and D-Cn-A dyes can have important consequences in their electronic structure properties. The molecular structure at the acceptor side of the chromophores, that is, the cyanoacrylic acid plus the connected thiophene ring, is almost identical for all molecules. The most important geometrical differences between the Cn and Tn dyes appear along the rest of the polythiophene linker and the phenyl ring bonded to it. Thus, those orbitals located in this region, such as the HOMO and HOMO-1, are susceptible to present larger contrast, as it is observed in the energy diagram of Figure 1.13. The large degree of molecular planarity and the *cis* disposition of the carbon–carbon double bonds in the Cn family favor the delocalization of the π-type frontier orbitals. The D-Cn-A HOMOs are more delocalized towards the linker than in the D-Tn-A dyes, a feature that becomes clear when comparing the orbitals of the longest D-T4-A and D-C4-A pair (Figure 1.14). As a result, the Cn bridges are expected to induce better donor–acceptor electronic couplings than the Tn ones.

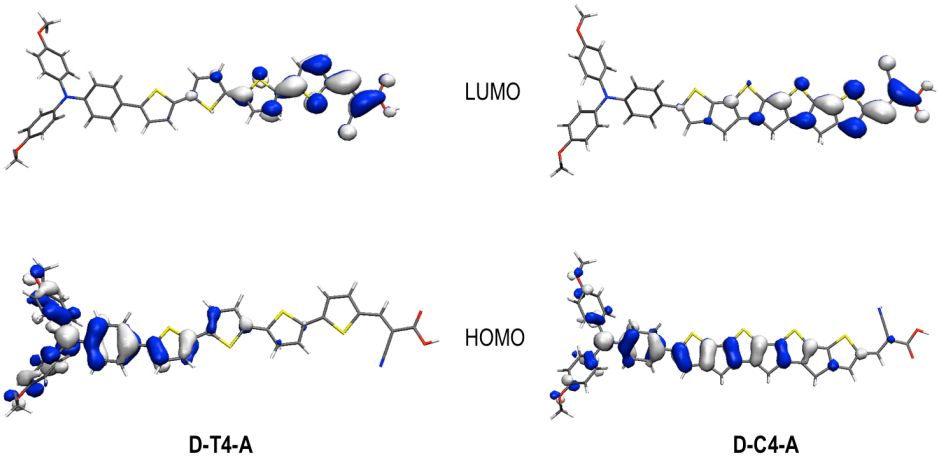

Figure 1.14 Isodensity representation of the HOMO (bottom) and LUMO (top) of D-T4-A (left) and D-C4-A (right) dyes.

5.4 S_0 to S_1 vertical transition

As a first approximation, vertical excitations to the low-lying states can be rationalized by the energy separation between frontier MOs. The excitation energy for the shortest D-T1-A dye is computed at 3.32 eV. The reduction of the energy gap between occupied and virtual frontier orbitals (Figure 1.13) results in lower transition energies as the length of the linker increases (Figure 1.15 and Appendix, Table A1.4), which has been experimentally measured for the Tn series.[7,137] Computed energies for D-Cn-A dyes are lower than for D-Tn-A ones with the same number of thiophene rings (n), in agreement with experimental observations.[129] Electronic excitations to S_1 in D-T2-A and D-C2-A are close to each other (3.20 and 3.14 eV), but due to the larger HOMO destabilization in D-Cn-A compared to that in D-Tn-A when the number of rings is increased, the optical gap in the D-Cn-A family decreases more rapidly with the molecular degree of conjugation (3.09 and 2.81 eV for n = 4).

Computed oscillator strengths to the optical state increase linearly with the donor–acceptor separation, that is d_{NC}. The Cn linkers present larger transition probabilities, which must be attributed to the imposed planarity (Table 1.5) and linearity (Figure 1.14) in the ground state geometry, which favors the dipole interaction between initial and final states.

The HOMO-to-LUMO contribution to the transition remains constant within the D-Cn-A dyes (~50%). On the other hand, the lack of planarity at the donor-linker junction and along the conjugated bridge induces the participation from other frontier MOs, e.g. HOMO-1 or LUMO+1, which becomes more significant as the molecular length increases (Appendix, Table A1.4).

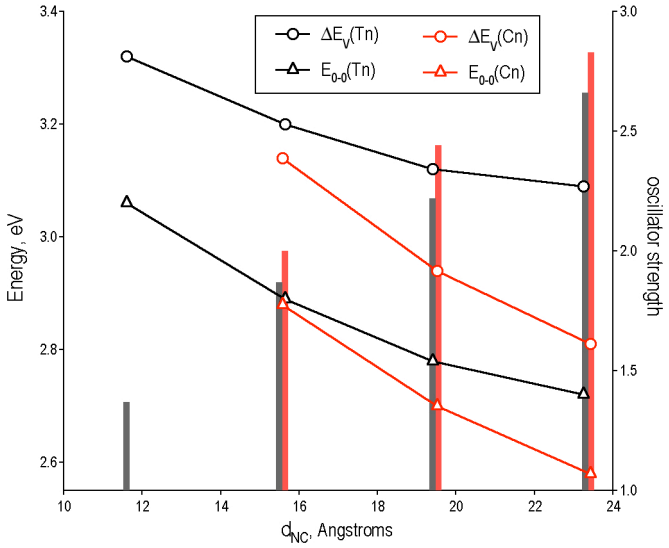

Figure 1.15 Oscillator strengths (grey and red bars for Tn and Cn dyes, respectively) and vertical (circles) and adiabatic (triangles) excitation energies for the S_0 to S_1 transition computed at the LRC-ωPBEh/6-31G(d) level.

5.5 Excited state relaxation

The main structural changes upon excited state geometry optimization of D-Tn-A and D-Cn-A dyes are shown in Table 1.6, which also contains ground state parameters to facilitate their analysis. Compared to the ground state, excited state relaxed geometries tend to favor molecular planarity. The phenyl-thiophene (θ_{DT}) dihedral angle in both families is notably reduced from ~30° in the ground state to 2°–13° in the CT state. Likewise, the planarity along the polythiophene rings (θ_{TT}) in Tn linkers evolves from an average θ_{TT} close to 20° to become virtually planar. This is also true for the Cn linkers in the S_0 and S_1 states. On the other hand, there is practically no variation in other structural parameters, such as the molecular length (d_{NC}) or the θ_{DD} dihedral angles.

The trends found for the adiabatic transition energies are very similar to the ones obtained for the vertical values (Figure 1.15). The structural flexibility in the Tn series allows for larger relaxation of the molecular geometries at the ground and excited singlet states. More concretely, dihedral angles between thiophene rings can vary to a greater extent, while in the Cn set the structure of the bridge is rather rigid. This mostly affects the stabilization of the ground state, which prefers a non-planar disposition between rings (Table 1.6). As a consequence, the average distortion energy, i.e. the difference between the adiabatic energy and the vertical energy at the excited state optimized geometry, is larger in the D-Tn-A series than in the D-Cn-A one, about 0.05 eV per thiophene ring.

Table 1.6 Comparison between geometrical parameters (see Figure 1.11) for the S_0 and S_1 optimized structures of D-Tn-A and D-Cn-A dyes computed with the LRC-ωPBEh functional. Dihedral angles θ_{DD} and θ_{DT} (for n=3, 4) correspond to average values.

Linker	θ_{DT}		θ_{TT}	
	S_0	S_1	S_0	S_1
T1	27.5	2.3	-	-
T2	29.5	4.6	17.7	0.6
T3	31.0	7.4	17.4	0.2
T4	29.7	12.4	22.1	0.6
C2	30.6	2.3	0.1	0.0
C3	30.7	9.2	0.1	0.1
C4	30.8	13.1	0.0	0.0

5.6 Absorption and emission spectra

Electronic structure calculations of the studied dyes in the ground and excited state geometries can be combined to simulate their absorption and emission spectra (Figure 1.16). As commented above, the electronic transition to the lowest singlet gives by far the largest absorption peak at the low energy range and represents the major feature of the absorption spectrum in this type of molecules. Due to the fact that structural differences between D-Tn-A and D-Cn-A dyes are more pronounced for the ground state geometries, these are more noticeable in the absorption spectra. Compared to the D-Tn-A family, D-Cn-A dyes account for a larger red-shift of the absorption maximum as the number of thiophene rings increases. On the other hand, the gap between the absorption and emission peaks is larger for the Tn linkers due to their molecular flexibility, which allows for a larger geometrical relaxation.

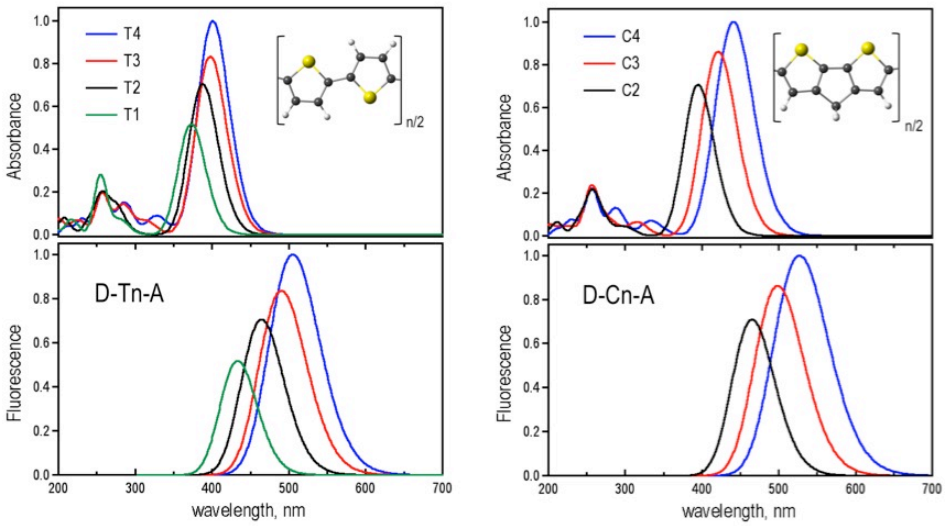

Figure 1.16 Simulated optical absorption and emission spectra for the D-Tn-A (left) and D-Cn-A (right) dyes normalized to the T4 and C4 peaks, respectively.

5.7 Charge transfer character

One of the major strengths of organic D-π-A type sensitizers is the effective electron–hole separation originated from the intramolecular electronic excitation to a CT state upon sunlight absorption. This phenomenon accounts for their capacity to produce high photocurrent conversion efficiencies,[2] since the rapid electron–hole recombination is avoided and the excited electron is effectively transferred to TiO_2. Beside the analysis of our target molecules, in this section we attempt to exemplify how electronic structure calculations can provide a variety of tools to measure the CT magnitude of the electronic transitions. Here we will try to quantify the degree of CT of the excitation with traditional and nonconventional schemes.

We first analyze the CT character of the S_1 bright state of the investigated dyes with a population analysis of the transition density matrix. The Mulliken analysis for the D-T1-A dye indicates that ~0.15 electrons are transferred to the acceptor moiety through the electronic excitation (|ΔQ| in Table 1.7). The amount of displaced electrons decreases with the length of the molecule, indicating that the role of the conjugated bridge in the transition increases with the number of thiophene rings. The D-Cn-A dyes follow exactly the same trend.

Likewise, the length of the transition dipole moment can be related to the CT character of the excitation, and it can be seen as a combined measure of charge-separation upon light absorption.[138-140] The dipole moment for the case of two classical point charges $+q$ and $-q$ is expressed as the product qr, where r is the displacement vector. Considering small modifications in the S_0/S_1 overlap, the magnitude of the computed S_0 to S_1 transition dipoles for the D-Tn-A and D-Cn-A series is driven by the donor–acceptor separation, with longer dyes leading to larger transition dipoles, as it has already been discussed for the computed oscillator strengths (Figure 1.15). Following the classical dipole analogy, the amount of displaced charge from the donor to the acceptor can be roughly approached as the quotient between the modulus of the computed dipole (μ) and the length of the molecule (d_{NC}). The μ/d_{NC} values in Table 1.7 are linearly correlated to the |ΔQ| results obtained from the Mulliken population analysis, with almost no difference between D-Tn-A and D-Cn-A dyes with equal n.

The overlap degree between the ground and excited state wave functions can be quantified with the Λ parameter, as it has been previously discussed. This Λ test has been recently employed in the study of triarylamine-type organic dyes, with Λ values in the 0.45–0.60 range.[12,82,83] In the present study, the computed Λ values also fall within the same narrow range (Table 1.7). The Λ values in the D-Cn-A set are systematically larger than in the D-Tn-A dyes with the same number of thiophene rings. These differences must be traced back to the geometrical restrictions imposed by Cn linkers, i.e. molecular planarity and linearity of the π-system, which induce larger overlaps. In general, longer bridges induce larger spatial separations between the ground and excited state, hence the Λ overlaps decrease with n, indicating an increase of CT character. This trend is not perfectly followed in the D-Tn-A set, and it might be attributed (again) to geometrical factors, such as the lack of molecular planarity between adjacent thiophene rings.

Table 1.7 Computed parameters related to the CT character of the S_0 to S_1 transition discussed in the text: $|\Delta Q|$, μ and μ/d_{NC} (in a.u.), ΔE_{TDA}, ΔE_{ST} and $2K_{HL}$ (in eV).

Dye	$\|\Delta Q\|$	μ/d_{NC}	μ	Λ	ΔE_{TDA}	ΔE_{ST}	$2K_{HL}$
T1	0.147	0.176	3.86	0.54	0.212	1.78	0.43
T2	0.106	0.151	4.46	0.57	0.210	1.72	0.28
T3	0.081	0.133	4.89	0.48	0.205	1.68	0.18
T4	0.065	0.122	5.36	0.48	0.201	1.65	0.10
C2	0.102	0.156	4.58	0.61	0.226	1.68	0.49
C3	0.078	0.141	5.22	0.55	0.223	1.58	0.54
C4	0.061	0.131	5.78	0.48	0.220	1.52	0.47

5.8 Interaction measures of charge transfer

Now we would like to turn our attention to other rather different procedures for analyzing the CT nature of the transition. Here we apply and rationalize three interaction-energy based techniques to complement the more traditional approaches previously discussed. The first one consists in the calculation of ΔE_{ST} and K_{HL} with the CIS method. As mentioned above, these two quantities are related by equation 1.14, and for larger HOMO-LUMO overlaps and smaller electron-hole separations, i.e. decreased CT character, the larger the ΔE_{ST} and K_{HL} terms will be.

The computed CIS ΔE_{ST} energies for the D-Tn-A and D-Cn-A dyes are in the 1.5–1.8 eV range (Table 1.7), and are comparable to the gap obtained between the $^3\pi\pi^*$ and $^1\pi\pi^*$ states of typical organic molecules,[141-144] indicating important interaction through exchange. The computed ΔE_{ST} energy correlates with the length of the molecule in agreement with the

other metrics discussed in this section (Table 1.7). Longer dyes present smaller singlet–triplet CIS energy gaps, which can be associated to lower overlaps and larger electronic separations (equation 1.14). On the other hand, the excited singlet and triplet states of the studied molecules are far to be simply described by the single occupation of the HOMO and LUMO. Therefore, equation 1.14 represents a severe approximation, and should be only taken into account in a qualitative manner. The CIS ΔE_{ST} value is much larger than the $2K_{HL}$ one (Table 1.7), a direct consequence of the important participation of other frontier orbitals located at the linker. Moreover, the weight of the HOMO-to-LUMO determinant varies depending on the linker and the spin multiplicity (Appendix, Table A1.4). This diversity in the form of the singlet and triplet wave functions makes it difficult to rationalize the differences between the two series, at least using simple arguments.

Now we would like to employ another interaction-like measure for the CT degree of the excitation introduced in the previous section. It is based on the difference between CIS and TDHF excitation energies to the excited singlet state (ΔE_{TDA}). Recalling that for a pure CT state with no spatial overlap between the involved orbitals $\mathbf{B} = \mathbf{0}$, and that in this limit, TDHF converges to CIS. Then, smaller values of ΔE_{TDA} mean that the role of the **B** terms is less important, indicating a significant CT character. The values in Table 1.7 show that ΔE_{TDA}, i.e. the role of **B**, decreases with the molecular length. Differences between those cases with similar donor–acceptor separation will be dictated by the overlap between occupied and virtual orbitals contributing to the transition. The D-Cn-A dyes present slightly larger ΔE_{TDA} energies compared to D-Tn-A dyes, pointing to more efficient overlaps for the Cn linkers, in agreement with the trend found for the computed Λ parameter.

Finally, the discrepancies between LRC and non-LRC functionals in the computation of excited states might be an indication of the CT nature of the electronic transitions. Stretching this idea, one could exploit these discrepancies and use the LRC effect as a quantitative measurement of CT by analyzing the relative excitation energies obtained with a designed variety of functionals. Here, we take advantage of the different physics in pure GGA, hybrid and LRC functionals based on PBE in order to explore the CT nature of the S_0 to S_1 transition in the D-Tn-A and D-Cn-A dyes. Table 1.8 summarizes the computed energies obtained with the purely GGA PBE functional, the PBEh hybrid functional (20% of HF) and the LRC forms LRC-ωPBE and LRC-ωPBEh (both with $\omega = 0.2$ bohr^{-1}).

The presence of non-local exchange systematically increases the computed transition energies in all dyes. The PBEh energies are systematically blue-shifted (0.5–0.8 eV) compared to PBE. The LRC scheme has a much larger impact in the computed energies than the homogeneous hybrid, which is a clear manifestation of the intramolecular CT. Differences between LRC-ωPBE and LRC-ωPBEh are much smaller (<0.2 eV). The increase in the computed excitation energies by the LRC functionals is larger in the D-Tn-A family, which correlates well with the differences in Λ overlaps (Table 1.7). In fact, the non-LRC flavors of PBE predict smaller transition energies for the D-Tn-A dyes, while LRC-ωPBE and LRC-ωPBEh results point to the opposite, in agreement to experimental data.[129]

Table 1.8 Excitation energies to the lowest singlet states (in eV) computed with several PBE-based functionals for the studied dyes optimized with LRC-ωPBEh/6-31G(d).

Dye	PBE	PBEh	LRC-ωPBE	LRC-ωPBEh
T1	1.84	2.38	3.12	3.32
T2	1.45	2.10	3.03	3.20
T3	1.21	1.95	2.97	3.12
T4	1.06	1.87	2.95	3.14
C2	1.59	2.22	3.00	2.94
C3	1.43	2.10	2.84	2.81
C4	1.31	2.01	2.71	3.09

5.9 Dependence of excitation energies on the ω parameter

In the previous section we have shown how it is possible by modifying the degree of HF exchange in TDDFT functionals to characterize the CT nature of electronic transitions. This approach can be extended to a meticulous analysis of the dependence of the computed excitation energies and the long-range parameter ω. Although in practice this is clearly not the simplest or computationally cheapest methodology to quantify the CT character, it is the proper way to exhaustively explore CT by means of the role of the long-range correction in TDDFT.

The plot in Figure 1.17 reflects a strong dependence of the excitation energies with the parameter ω, which controls the partition of the Coulomb operator into short (DFT) and long (HF) range components, a clear indication of the CT character of the S_0 to S_1 transition in D-Tn-A and D-Cn-A dyes. All curves present the same fundamental shape, which resemble a displaced error function, also observed previously in a study of CT transitions.[145]

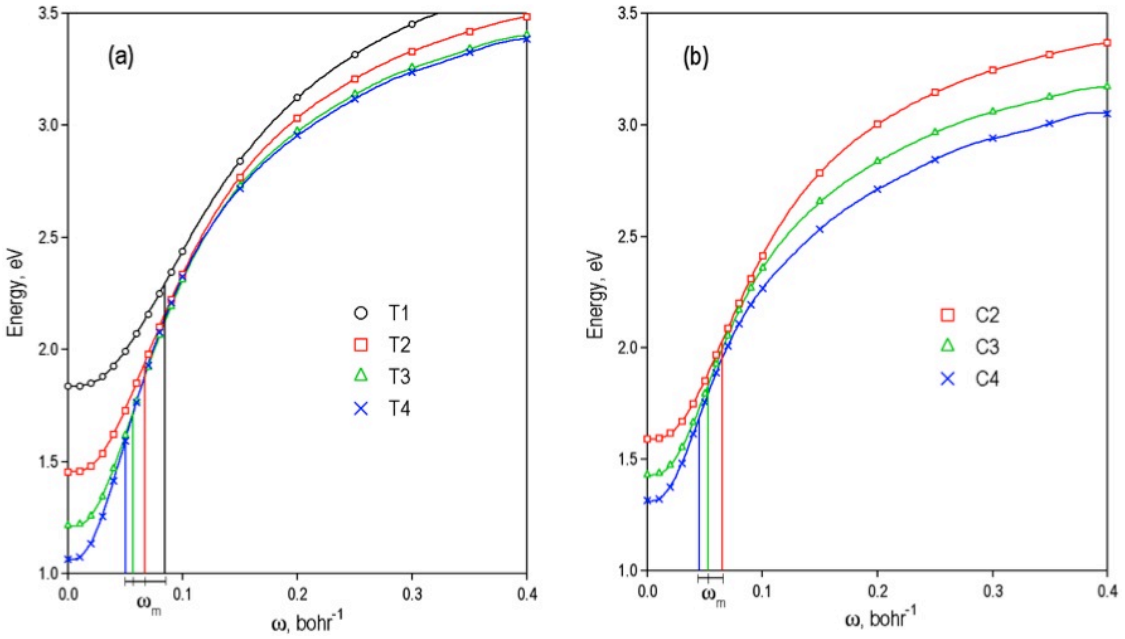

Figure 1.17 Excitation energies (eV) for the D-Tn-A (a) and D-Cn-A (b) dyes as a function of the range-separation parameter ω. The midpoint ω_m values (Table 1.9) are also indicated.

The energy profiles in Figure 1.17 can be characterized by two parameters: (i) the inflection point of the curve (ω_m in Equation 1.17) and (ii) the energy gap between the ω=0 and ω→∞ limits ($\Delta E_{0\infty}$), that is the difference between excitation energies computed with 100% and 0% of HF exchange, respectively. The midpoint ω_m is where the slope of the energy curve with respect to ω is maximal. In other words, differential variations of ω at ω_m ($\omega_m \pm \delta\omega$) produce the largest possible change of the computed excitation energy. It is directly related to a distance $1/\omega_m$, indicating an average interelectronic separation from where the non-local exchange starts to operate. Therefore, ω_m can be interpreted as a measure of the CT length. The $\Delta E_{0\infty}$ energy gap is an absolute measure of the global impact of the HF exchange on $E(S_1)$.

$$\left.\frac{\partial^2 E(S_1)}{\partial \omega^2}\right|_{\omega=\omega_m} = 0 \qquad (1.17)$$

Results in Table 1.9 corroborate that longer donor–acceptor distances imply lengthier CT processes and require the exact exchange to be incorporated at larger interelectronic separations (smaller ω). As a result, the $1/\omega_m$ parameter linearly correlates to the molecular length (Appendix, Figure A1.2). It can be seen that the ω_m value is systematically larger in the Tn family, in agreement with the previously discussed results, such as the Λ test, which point to slightly smaller S_0/S_1 overlaps for the D-Tn-A dyes.

Table 1.9 Characterization parameters of the excitation energy dependence on ω, computed by LRC-ωPBE. (ω_m in $bohr^{-1}$, $1/\omega_m$ in Å and $\Delta E_{0\infty}$ in eV)

Dye	ω_m	$1/\omega_m$	$\Delta E_{0\infty}$
T1	0.085	6.24	2.07
T2	0.067	7.86	2.20
T3	0.057	9.28	2.32
T4	0.050	10.55	2.43
C2	0.065	8.13	1.92
C3	0.053	10.01	1.82
C4	0.045	11.83	1.78

Finally, it is important to notice that the ω_m values obtained for the studied dyes are considerably smaller than the results that can be extracted from the computation of π,π* intermolecular CT excitation energies.[145] This is an indication that the study of intramolecular CT by means of LRC-TDDFT methods should be probably performed with smaller ω values than the ones typically established as default in standard quantum chemistry packages (ω=0.2-0.4 $bohr^{-1}$), which have been commonly optimized for intermolecular CT transitions, implying relatively short CT distances and small spatial overlaps between initial and final states compared to the usual situation in D-π-A organic dyes.

5.10 Ground and excited state oxidation potentials

The GSOP and the ESOP[126] are key parameters for the efficiency of molecular sensitizers in DSSCs. The relative GSOP and ESOP values with respect to the mediator's redox potential, typically I^-/I_3^-, and the TiO_2 CBE determine the driving force for the dye regeneration and the electron injection processes, respectively.

The computed values of GSOP and ESOP for all dyes (Figure 1.18) are compatible with the experimental requirements for an efficient electron transfer.[15,126] In both families of dyes, i.e. those with Tn or Cn linkers, the increase of the conjugation length reduces the GSOP. As discussed above, the geometrical restrictions imposed by the Cn linkers have a larger impact on the highest occupied orbitals (Figure 1.12). Therefore, the energy destabilization in D-Cn-A dyes is larger on the neutral ground state compared to the oxidized molecule. Consequently, the computed GSOP values are systematically lower in the D-Cn-A dyes with respect to the D-Tn-A ones.

Equation 1.16 indicates that ESOP is linked to the relative values of GSOP and $E_{0\text{-}0}$. Both quantities decrease with molecular conjugation. For dyes with n = 1, 2 and 3 the GSOP dictates the behavior of ESOP, that is, the longer the dye the smaller (less negative) the molecular ESOP. In n = 4 cases the trend is reverted and the ESOP is slightly more negative than for the shorter D-T3-A and D-C3-A cases (Figure 1.18).

Although experimentally these measurements are commonly performed in solution,[8] the solvation effect in solvents with low dielectric constants is expected to be rather small, as it has been the case in recent calculations of oxidation potentials for similar organic dyes.[127] Thus, we believe our calculations already capture the behavior of the oxidation potentials, and we would expect only small variations of the GSOP and ESOP values when introducing the effect of the solvent. It is also important to highlight that non-LRC functionals, such as B3LYP, yield ESOP values that are too low compared to the TiO_2 CBE. This is a direct consequence of the systematic underestimation of the computed transition energies to CT states by standard functionals. All the LRC-ωPBEh and B3LYP results of GSOP and ESOP for the D-Tn-A and D-Cn-A dyes can be found in the Appendix (Table A1.5) together with the structural parameters for the optimized geometries of the oxidized species of the Tn and Cn series (Table A1.6).

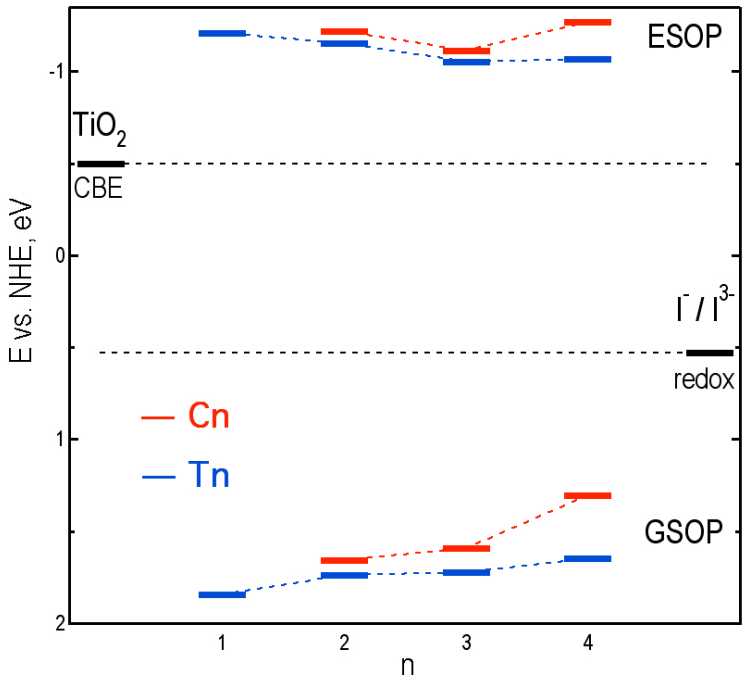

Figure 1.18 Representation of the computed GSOP and ESOP energy levels of D-Tn-A (blue) and D-Cn-A (red) dyes, and the experimental CBE of TiO_2 and the redox potential (black). Values are given in eV and with respect to the normal hydrogen electrode (NHE).

5.11 Conclusions

The present work takes advantage of simple computational tools to describe in detail the atomic and electronic structure intricacies of molecular sensitizers. This study goes beyond standard calculations on the vertical transition energies and the associated oscillator strengths, providing a new insight from electronic structure calculations to unravel and characterize the light-harvesting properties of organic dyes.

The obtained results highlight the effect that structural features, such as molecular planarity or linearity, can eventually have in the photophysical properties of organic dyes. Our calculations reveal that the rigid Cn linkers induce slightly lower transition energies and larger oscillator strengths compared to the more flexible Tn spacers. The extent of the electronic conjugation is a key element that can be used to tune the light-harvesting capacity of the dyes. Longer π-bridges reduce the ground to excited energy gap and increase the transition probability. The CT degree of the two families is rather similar and has a mild dependence on the donor–acceptor spatial separation.

We have shown how it is possible to use a variety of electronic structure tools in order to directly or indirectly predict and even quantify the CT nature of the transition. In addition to some standard measures, such as the Λ test, the variation on the Mulliken charges or the transition dipole moment, we have introduced and discussed other non-conventional measures: the CIS energy gap between the lowest excited singlet and triplet states, the relative CIS and TDHF energies, and the impact of the exact exchange in hybrid and LRC functionals. Application of these tools to our target molecules exemplifies how they can be used to unfold the details of electronic transitions. The study of the dependence of the excitation energies on the ω long-range parameter has driven us to conclude that the optimal ω values for the study of D-π-A dyes should be probably smaller than the standard values typically optimized for intermolecular processes. The ω parameter is clearly system dependent and further investigations are needed to adjust appropriate values to explore excitation energies in D-π-A molecules. The list of parameters for the quantification of CT upon electronic excitation discussed here does not pretend to be complete, and other appealing approaches can be found in the recent literature, such as CT indices based on the analysis of the electron density distribution at the ground and excited states.[146]

The GSOP and ESOP of molecular sensitizers have been computed with a LRC functional. The results indicate that both, Tn and Cn dyes, have appropriate oxidation potentials to sensitize the TiO_2 semiconductor with the I^-/I_3^- couple as the redox mediator. Differences between the studied dyes are relatively small, with the shorter molecules producing lower GSOP and higher ESOP values.

5.12 Computational details

The LRC-ωPBEh functional[79] in combination with the 6-31G(d) basis set has been chosen as the default computational model within the TDA.[68] All LRC-ωPBE and LRC-ωPBEh calculations have been done with ω = 0.2 a.u, except in the "Dependence of excitation energies on the ω parameter" section. Ground state optimized molecular geometries have also been compared to the B3LYP[90,91] and MP2 results. For the sake of comparison, all presented molecular orbital diagrams have been computed at the HF level and the computation of the Λ parameter,[118] transition Mulliken charges, transition dipole moments, singlet–triplet energy differences and the role of the TDA in the ''Charge transfer character'' section have all been performed within the CIS (and TDHF) methodology. Calculations of GSOP and ESOP include translational, rotational and vibrational enthalpies and entropies obtained within the harmonic approximation. In the computation of the adiabatic transition energy we assume equal zero-point energy corrections in the ground and excited states, thus its value is obtained as the energy gap between the two states in their equilibrium geometries. The 30 lowest singlet-to-singlet transitions of the D-Tn-A and D-Cn-A dyes were considered in the simulation of the UV/vis absorption spectra. The absorption and emission profiles were calculated by means of a Gaussian model with a full width at the half-maximum (fwhm) of 3000 cm^{-1}. The dependence of D-Tn-A and D-Cn-A computed excitation energies on the long-range parameter have been adjusted to a 20th order polynomial function. The roots of the second order partial derivative of the excitation energy with respect to ω (ω_m) have been obtained numerically with the Sage software.[147] All calculations have been done with the Q-Chem package.[135]

5.13 Appendix

Table A1.4 Vertical and adiabatic excitation energies (in eV) for the S_0 to S_1 transition computed at the LRC-ωPBEh/6-31G(d) level.

dye	ΔE_v	f	%H-L	$E_{0\text{-}0}$
T1	3.32	1.37	51	3.06
T2	3.20	1.87	37	2.89
T3	3.12	2.22	27	2.78
T4	3.09	2.66	19	2.72
C2	3.14	2.00	50	2.88
C3	2.94	2.44	55	2.70
C4	2.81	2.83	54	2.58

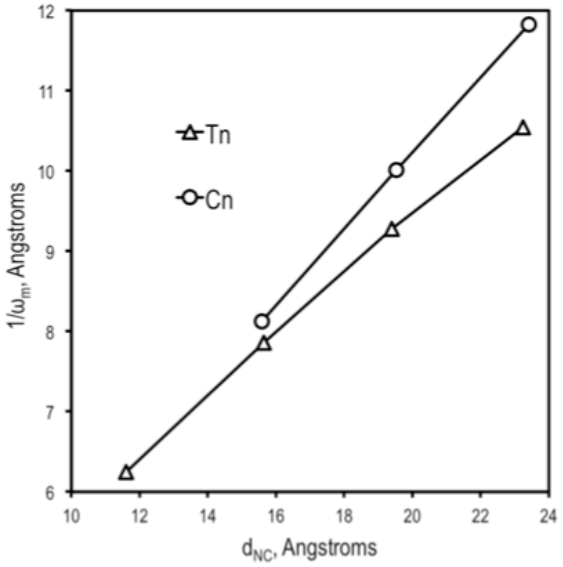

Figure A1.2 Correlation between molecular length (d_{NC}) and the $1/\omega_m$ parameter.

Table A1.5 B3LYP and LRC-ωPBEh computed GSOP and ESOP energies of D-Tn-A and D-Cn-A. Values are given in eV and with respect to the normal hydrogen electrode (NHE).

dye	GSOP		ESOP	
	B3LYP	ωPBEh	B3LYP	ωPBEh
T1	1.52	1.85	-0.14	-1.21
T2	1.41	1.74	-0.22	-1.15
T3	1.27	1.73	-0.33	-1.05
T4	1.16	1.65	-0.42	-1.07
C2	1.31	1.66	-0.42	-1.22
C3	1.12	1.59	-0.64	-1.11
C4	0.96	1.31	-0.80	-1.27

Table A1.6 Structural parameters for the optimized geometries of the oxidized species of the D-Tn-A and D-Cn-A dyes. Dihedral angles θ_{DD} and θ_{TT} (for n = 3, 4) correspond to average values.

linker	d_{NC}		θ_{DD}		θ_{DT}		θ_{TT}	
	B3LYP	ωPBEh	B3LYP	ωPBEh	B3LYP	ωPBEh	B3LYP	ωPBEh
T1	11.61	11.53	35.7	38.9	14.1	23.9	-	-
T2	15.70	15.60	31.2	34.9	9.8	17.9	1.0	17.3
T3	19.42	19.32	29.7	29.8	8.6	11.2	1.4	8.4
T4	23.45	23.21	27.6	24.7	8.6	6.8	0.9	15.3
C2	15.60	15.50	37.7	28.9	10.4	10.7	0.3	0.3
C3	19.52	19.39	26.0	18.9	9.5	4.6	0.2	0.1
C4	23.41	23.26	24.3	17.8	9.3	4.5	0.1	0.0

6. Heteroatom effect on the π-linker

6.1 Introduction

The work presented in this section was done in collaboration with the experimental groups of Prof. Emilio Palomares (*ICIQ*, Tarragona, Spain) and Prof. Peng Wang (*Chinese Academy of Sciences*, China). They synthesized and characterized[148] two new push-pull organic dyes, S-Se and Se-S (Figure 1.19). Both molecules contain the bis(4-hexyloxyphenylamino)styril unit as the donor group, the cyanoacrylate acid as the acceptor, and the selenophene–thiophene (Se-S) and thiophene–selenophene (S-Se) moieties as the conjugated linkers. DSSCs were fabricated employing these two photosensitizers and the cobalt(II/III) redox electrolyte. The devices exhibited good solar energy conversion efficiencies of ~6%, while lower efficiencies were obtained with the iodide/triiodide electrolyte. The performance of these two dyes was compared to three closely related sensitizers in which the π-bridge was changed. These linker units were thiophene-thiophene (S-S), selenophene-selenophene (Se-Se) and cyclopentadithiophene (CPDT). All the dyes in Figure 1.19 were compared paying special attention to the differences on their geometries, molecular dipoles and electron recombination lifetimes.

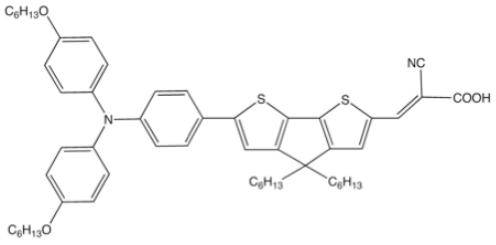

CPDT

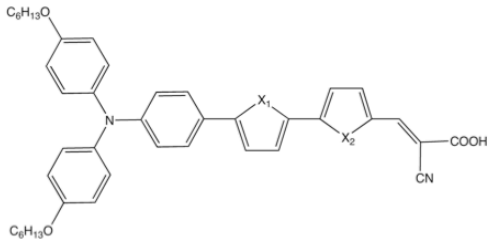

	X_1	X_2
S-S	S	S
S-Se	S	Se
Se-S	Se	S
Se-Se	Se	Se

Figure 1.19 Studied D-π-A dyes.

As it has been previously reported, the molecular sensitizer in DSSC plays a crucial role, not only on the photo-generation of the device electrical current, but in many cases, also minimizing the losses due to undesired back-electron transfer reactions. The role of the π-linker in D-π-A dyes on the back-electron transfer between the photo-injected electrons at the TiO_2 surface and the oxidized electrolyte is not yet fully understood and is still objective of many discussions.

Our goal herein was to understand the differences between these dyes and to rationalize the effects of varying the position of chemical moieties on the π-bridge over the final device performance. We aimed, finally, to determine whether the presence of molecular dipoles on the TiO_2 surface, the chemical nature of the π-bridge, or both factors are key to enhance the charge recombination reactions that ultimately limit the device efficiency under working conditions.

6.2 Discussion

The light-harvesting capacity of DSSCs is strongly dependent on the spectral response of the molecular sensitizer and the capability of the electrolyte to regenerate efficiently the oxidized dye.[2] Therefore, we initially evaluated the absorption spectra of the Se-S and S-Se dyes in chloroform solution (Figure 1.20). The absorption profiles for the two dyes are very similar, and the absorption maximum molar extinction coefficients of the lowest energy band are close to the values reported for the bithiophene (S-S) and biselenophene (Se-Se) analogues (Table 1.10). The absorption band at lower energies corresponds to the intramolecular CT transition between the donor and the acceptor units. The π–π* transition and the CT absorption bands for S-Se show a small shift, but it is unlikely that this variation can be due to different intermolecular π-π stacking interactions.

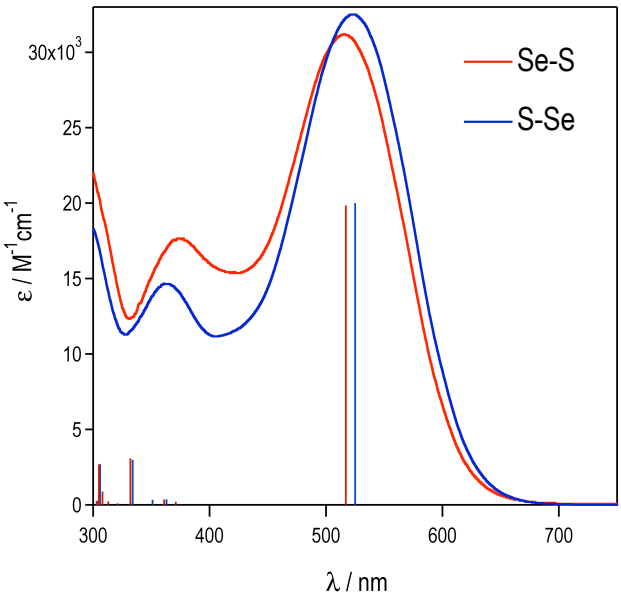

Figure 1.20 Electronic absorption spectra of the Se-S and S-Se sensitizers dissolved in chloroform. Vertical bars correspond to the lowest singlet-to-singlet computed electronic transitions and their strength (in arbitrary units). Computational values have been shifted to match the absorption maxima of the main peak.

Optical maximum absorption transitions of S-S, S-Se, Se-S and Se-Se dyes extend across a narrow energy range. Although computed vertical transition energies appear systematically blue shifted with respect to experimental absorption peaks, the computed relative values are in good agreement with the experiment (Table 1.10), as also seen in Figure 1.20. The energy ordering and the almost 10 nm of separation between the Se-S and S-Se maxima (~0.04 eV) is well recovered, and the oscillator strengths show a similar trend to the extinction coefficients.

As we have seen in the previous section and as also discussed by Wang and collaborators[130], the molecular rigidity imposed by the cyclopentadithiophene linker has a major impact on the absorption spectrum. As a result, CPDT presents a slightly lower transition energy and a much higher molecular extinction coefficient than the "non-CPDT" counterparts. Again, this behavior is also captured by computational results. Our DFT calculations predict a fairly noticeable loss of planarity at the conjugated bridge of the S-S, S-Se, Se-S and Se-Se dyes. The torsion angles of linkers with at least one selenium atom are of the order of 15° and a bit smaller (~8°) for the bithiophene unit. These results are very similar to the results from the preceding section and also to previous calculations performed for the bithophene and biselenophene cases.[134] It is also worth mentioning that steric hindrance prevents the coplanarity between the donor and π-bridge moieties. This effect is present in the entire set of conformations, with dihedral angles between the phenyl ring of the triarylamine group and the linker being practically the same in all cases (26–28°).

Table 1.10 Experimental maximum absorption wavelengths λ_{max} (in nm) and extinction coefficients ε_{max} (10^3 M^{-1} cm^{-1}) and computed vertical excitation energies E_v (in eV), oscillator strengths *f,* and ground state dipole moments μ (in Debye) of the studied dyes in chloroform. Photovoltaic parameters measured for the DSSC devices are also given, the short-circuit photocurrent density j_{sc} (in mA/cm^2) and the open-circuit photovoltage V_{oc} (in V).

Dye	λ_{max}	E_v	ε_{max}	*f*	μ	j_{sc}	V_{oc}
S-S	525[a], 523[b]	410	3.8[a], 30.5	1.83	7.80	10.03	0.873
S-Se	525	417	32.5	1.86	7.70	11.00	0.817
Se-S	516	413	31.2	1.85	7.63	10.17	0.813
Se-Se	549[b]	421	35.1[b]	1.87	7.89	10.72	0.832
CPDT	555[a]	417	62.7[a]	2.03	9.98	14.24	0.929

[a] Reference 129.

[b] Reference 134.

Decomposition of the TDDFT excitation indicates that the main contribution to the optical state corresponds to the HOMO-to-LUMO electronic promotion with sizable participation of HOMO-1 and LUMO+1 orbitals (Appendix, Table A1.7). In all cases, the HOMO is mostly localized over the triarylamine donor group, while the LUMO is centered at the anchoring moiety with some delocalization towards the π-linker, mainly over the closest conjugated ring of the π-bridge (Figure 1.21). This common D–π–A structure provides the proper hole and particle separation for a fast interfacial electron injection from the excited state to the titania conduction band and dye regeneration. The HOMOs of S-S, S-Se, Se-S and Se-Se are virtually degenerate. On the other hand, there are noticeable differences in the energies of the first unoccupied orbital (Appendix, Table A1.8). The selenophene ring has a larger stabilization effect on the LUMO of the cyanoacrylic acid, possibly due to its lower electronegativity compared to sulfur. As a result, S-Se and Se-Se present LUMOs with lower energies than Se-S and S-S dyes (Figure 1.22). The stabilization effect due to the second five-member conjugated ring (closer to the donor moiety) is less important. Thus, the small differences between excitation energies of these dyes (Table 1.10) are controlled by the energies of their LUMOs, i.e. S-S > Se-S > S-Se > Se-Se, which can be easily tuned and understood by the presence and disposition of thiophene and/or selenophene rings in the spacer.

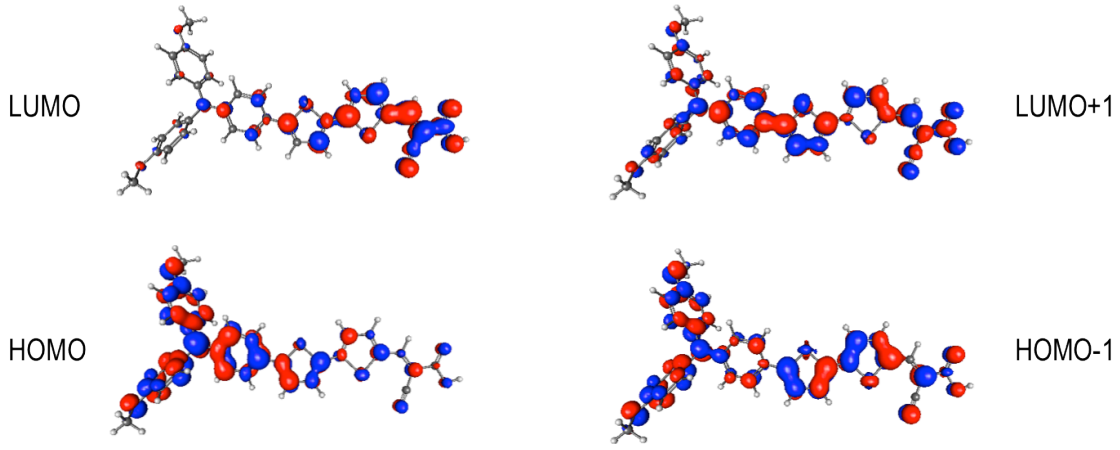

Figure 1.21 Isodensity representation of the frontier MOs of the S-Se dye involved in the S_0 to S_1 electronic transition. Orbitals for Se-S show very similar distributions.

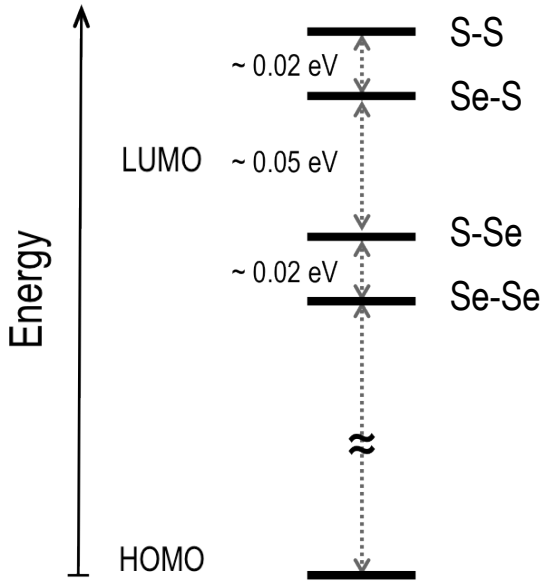

Figure 1.22 Schematic representation of the HOMO and LUMO energy diagram of the Se-S, S-Se, S-S, Se-Se dyes.

The short-circuit photocurrent density (j_{sc}), whose magnitude determines the performance of the solar cell,[2] is directly linked to the light harvesting ability of the molecular dyes, that is, the probability of the optical transition. This is reflected by the rather good correlation between the computed oscillator strengths and the measured j_{sc} values in Table 1.10. Moreover, effective electron injection occurs for all studied dyes as the LUMO energy level is well above the TiO_2 conduction band. Thus, the superior IPCE (Incident Photon to Current Efficiency conversion) reported[148] for DSSCs employing the CPDT dye with respect to the other dye can be attributed to a better packing of CPDT, which allows for a better TiO_2 surface coverage. This IPCE photovoltaic parameter is a measure of how efficiently the device converts the incident light into electrical energy at a given wavelength.

On the other hand, the open-circuit photovoltage (V_{oc}) in DSSC devices, which is also related to the efficiency of the cell,[2] is established by the quasi-Fermi level of the dye-coated titania film and the red/ox potential of the electrolyte. Hence, the V_{oc} is the result of two main contributions: (i) a thermodynamic factor determined by the position of the CBE, and (ii) a kinetic contribution linked to the density of conduction band electrons in the semiconductor that may recombine either with the oxidized dye or the oxidized electrolyte. Moreover, the dipole moment of the adsorbed sensitizer can induce a shift in the TiO_2 conduction band, and the high V_{oc} observed in several organic dyes has been attributed to a positive dipole moment orientation towards the surface.[149] In fact, it has been shown that,

for certain dyes, the V_{oc} of DSSCs linearly increases with the sensitizer's dipole moment component perpendicular to the semiconductor surface.[150]

Our results show a good correlation between the measured V_{oc} of the cell and the computed dipole moments of the organic dyes (Table 1.10). Noticeably, CPDT presents a much larger dipole moment than the rest of studied dyes, which can be attributed to structural factors, i.e. a larger molecular linearity and planarity. However, this variation by itself cannot explain the much larger V_{oc} measured for the CPDT linker compared to the more flexible bridges in S-S, S-Se, Se-S, and Se-Se. We would also like to emphasize that the very small differences between Se-S and S-Se are well reproduced by their dipole moments.

On the other hand, it is sometimes argued that the geometry of the sensitizer can have a crucial impact on the measured photovoltages.[151-154] The molecular planarity favors ordered close packing of adsorbed dyes onto the semiconductor surface. As discussed above, in the set of studied organic dyes there are basically no differences in the molecular planarity of S-S, S-Se, Se-S, and Se-Se dyes, thus, we do not expect major differences regarding their coverage of the semiconductor surface. The planarity at the CPDT linker however has effects on the surface coverage leading to higher photocurrent as measured by our experimental collaborators.[148]

Our collaborators carried out charge extraction and transient photovoltage decay measurements[148] to analyze if the different dipoles promoted by the dye surface coverage affect the position of the TiO_2 CBE and, furthermore, if this shift can be correlated to slower electron lifetimes. From their experiments they concluded that the different dyes, when absorbed onto the TiO_2 surface, induce mild variations on the energy level of the TiO_2 CBE, but that the relative shift cannot be responsible for the 100 mV difference in voltage observed for CPDT. The much larger value of V_{oc} measured for the CPDT dye is also a consequence of the slower recombination dynamics between the photo-injected electrons and the oxidized electrolyte (Cobalt(III)phen or iodide). From additional experiments, our collaborators found a larger electron lifetime value for the CPDT devices when compared with the other dyes. This is in agreement with a better molecular packing at the TiO_2 surface that blocks the back-electron transfer of the TiO_2 electrons to the electrolyte.

6.3 Conclusions

Two new organic D–π–A dyes with a π-bridge that combines the selenophene and the thiophene moieties have been compared with other paradigmatic organic dyes in their efficiencies in DSSCs. The measured photovoltaic parameters and efficiencies have been rationalized considering the formation of dipoles at the semiconductor surface, the dye's structural properties, and their effect on the TiO_2 CBE and the electron lifetime. We have discussed that the device photocurrent was higher for the dye that exhibited better molecular packing and that it was independent of the molecular dipole and its possible influence over charge injection from the excited state of the dye. The larger V_{oc} observed for CPDT can be explained not only by the TiO_2 CBE shift due to the molecular dipole, but also due to the better molecular packing that retards the back-electron transfer from the photo-injected electrons at the TiO_2 and the oxidized electrolyte.

6.4 Computational details

Molecular structures have been optimized within DFT employing the LRC-ωPBEh functional[79] with the 6-31+G(d) basis set. Transition energies were computed with TDDFT within the TDA[68] and the same functional and the larger 6-311+G(2d,2p) basis set. The effect of the solvent (chloroform) has been taken into consideration in all calculations with the polarizable continuum model (PCM).[104] All calculations were performed with the Q-Chem package.[135] Molecular structures of the studied dyes might present different conformations (Figure A1.3) regarding the relative orientation of the two five-member rings in the linker and the disposition of the π-bridge with the cyanoacrylic acid group. The computational results discussed in this section correspond to the ground state for the most stable forms represented in Scheme 1.19. The fused form of the linker in CPDT fixes the *cis* disposition of the two thiophene units, while in all other cases the two rings are preferably in the *trans* form. Comparison between different conformations can be found in the Appendix.

6.5 Appendix

Table A1.7 Vertical excitation energies, oscillator strengths *f*, and amplitude contributions (%) to the S_0 to S_1 transition for all conformers.

Dye	Conf.	ΔE / eV	*f*	H→L	H-1→L	H→L+1
S-S	CC	3.05	1.90	50	34	8
	CT	3.05	1.91	51	33	9
	TC	3.03	1.83	53	34	7
	TT	3.02	1.84	53	33	8
S-Se	CC	2.98	1.86	51	34	7
	CT	2.98	1.88	52	34	8
	TC	2.97	1.86	53	34	7
	TT	2.96	1.87	55	32	7
Se-S	CC	3.02	1.94	51	33	8
	CT	3.04	1.95	49	35	9
	TC	3.00	1.85	53	32	8
	TT	3.01	1.84	53	32	8
Se-Se	CC	2.95	1.90	52	34	7
	CT	2.97	1.91	50	35	8
	TC	2.95	1.87	54	33	7
	TT	2.93	1.88	54	32	7
CPDT	CC	2.98	2.17	57	30	6
	CT	2.99	2.19	57	30	7
	TC	2.98	2.03	57	30	6
	TT	2.99	2.03	57	30	7

Table A1.8 MO energies (eV) of the studied dyes (TC conformation).

dye	H-1	H	L	L+1
S-S	-7.79	-6.85	-1.46	0.14
S-Se	-7.78	-6.82	-1.51	0.10
Se-S	-7.80	-6.83	-1.47	0.06
Se-Se	-7.78	-6.83	-1.53	-0.06
CPDT	-7.63	-6.78	-1.36	0.31

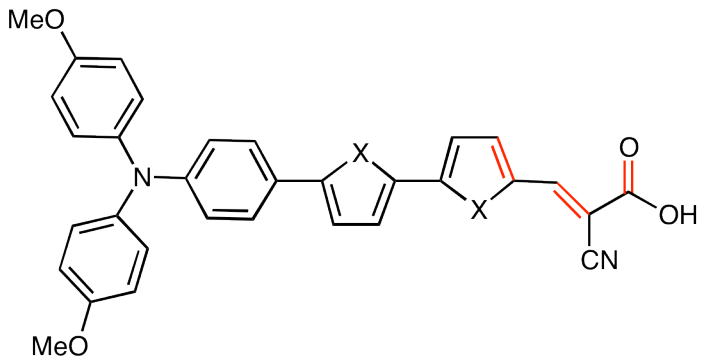

Figure A1.3 Nomenclature employed to distinguish between different conformations. Depending on the relative cis or trans disposition of the double bonds shown in red, one can have up to four different conformations. X corresponds either to S or Se. For instance, the dye shown herein would be the TC conformer, which is the most stable for all the optimized dyes.

7. Quinoidal thiophene π-bridge and solvent effects

7.1 Introduction

As mentioned previously, the first step towards finding dyes with optimal photophysical properties for DSSCs is to characterize their absorption in solution. In a recent paper,[155] the group of Prof. Segawa reported a D-π-A type organic dye, **QT** (Figure 1.23), with a quinoidal thiophene as π-bridge in order to efficiently extend the π-conjugation without a significant increase of the photosensitizer's molecular size, which may be sometimes detrimental for efficient photoconversion.[156-160] Their work was inspired by earlier reports in which efficient light harvesting of the visible spectrum was obtained using extended π-conjugated systems.[161-163] The photoelectric conversion efficiency of 5.2% obtained with the quinoidal thiophene dye demonstrated its beneficial photophysical properties.

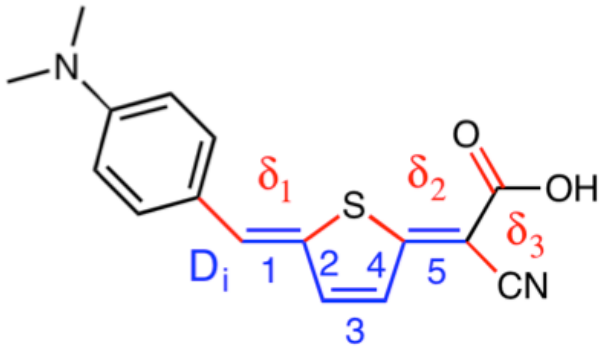

Figure 1.23 Most stable conformation of **QT** (CTT) with structural labels discussed in the text.

In their work, the solvent dependence of the absorption maxima of the quinoidal thiophene dye was also studied and they found a linear relationship with the solvents polarity (Figure 1.24). This trend however is not followed in alcohol solvents, for which a blue shift of the absorption maxima was observed compared to aprotic solvents of similar polarity (e.g. acetonitrile or dimethylsulfoxide (DMSO)). The authors pointed to hydrogen bonding interactions being responsible for such observations, but did not carry out further experiments to investigate this issue in deeper detail.

The aim of this section of the thesis was to investigate the origin of the blue-shift in the absorption maxima observed for **QT** in alcohol solvents. An initial approach was to study the absorption process of the **QT** dye in the different solvents explored in the original experimental paper by means of modeling the solvent as a continuum dielectric with the IEF-PCM method. With this approach, the experimental results could not be reproduced,

thus indicating that specific solute-solvent interactions not recovered by continuum solvation models must be responsible for the blue-shift in the absorption band with alcohol solvents, as already suggested in the original paper. Towards this end, models including explicit solvent molecules were considered to identify the interactions responsible for such shift, in particular, hydrogen-bonding interactions between solvent molecules and the quinoidal thiophene dye. Methanol was the solvent considered in the calculations, since it is the smallest of the three alcohols investigated in the experimental paper, thus simplifying the simulations and the election of cluster models for the calculation of the excited states. The identification of the principal hydrogen bonding interactions between methanol molecules and the quinoidal thiophene dye was one of the major goals of this work, and the experimental observations were rationalized on the basis of the performed calculations.

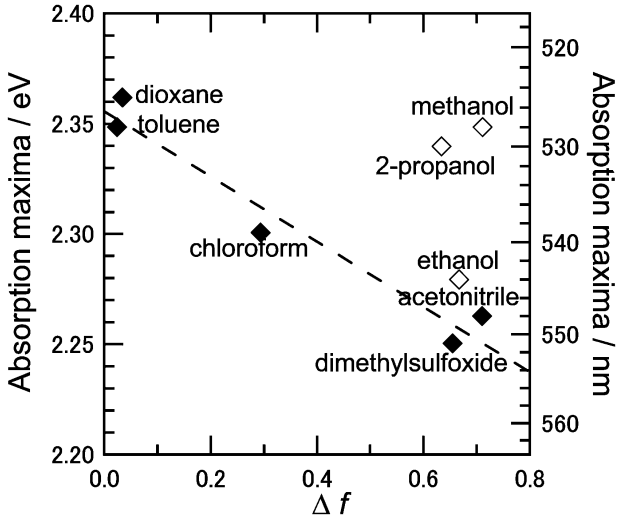

Figure 1.24 Solvent dependence of absorption maxima of the **QT** dye, plotted versus Δf (polarity function, see equation 1.18 in Appendix). The dashed line corresponds to a fitting for the 5 points shown in filled style. Taken from reference 155.

7.2 Molecular structure

In order to investigate the photophysical properties of **QT**, we first look at its ground state structure in solution. The **QT** molecule presents several structural conformers, each one of them corresponding to a local minimum on the ground state PES. These forms can be mostly described in terms of three dihedral angles corresponding to the relative disposition between the different moieties of the dye (Figure 1.23). Note that different dispositions of H atoms within the methyl and carboxylic acid groups also result in different conformations, but since they represent only slight variations of the structure with a very small effect on the photophysical properties of the molecule, they have not been considered in our study.

Electronic conjugation of the **QT** dye imposes molecular planarity along the entire molecule, only broken by the hydrogen atoms on the methyl groups of the dimethylaniline fragment. Energy profiles along each of the three dihedral angles defined in Figure 1.23 exhibit two energy minima corresponding to *cis* (δ~0º) and *trans* (δ~180º) conformations. The *cis* conformation is preferred for the δ_1 angle in order to avoid steric hindrance between hydrogen atoms in the two rings, while electronic interactions favor the *trans* disposition between sulfur and cyano groups (δ_2) and between the cyano and carbonyl groups (δ_3). Therefore, the energetically most stable conformer can be labeled in terms of δ_1, δ_2, and δ_3 as CTT (*cis*-*trans*-*trans*). The *cis*/*trans* energy differences in solution for δ_1, δ_2, and δ_3 obtained as the relative energies between the CTT form and the conformers TTT, CCT, and CTC respectively, averaged over all studied solvents, are computed as 2.4, 1.7 and 2.4 kcal/mol, respectively. These values dictate the relative stability between conformers (Figure 1.25 and Appendix, Table A1.9). It is worth noticing that molecular planarity is preserved in all conformers except for the ones with δ_1 in *trans* (TXX forms), which exhibit torsion angles of the order of δ_1~155º to minimize interactions between hydrogen atoms on the two rings. Potential energy profiles computed along the δ_1, δ_2, and δ_3 torsion angles can be found in the Appendix (Figure A1.4).

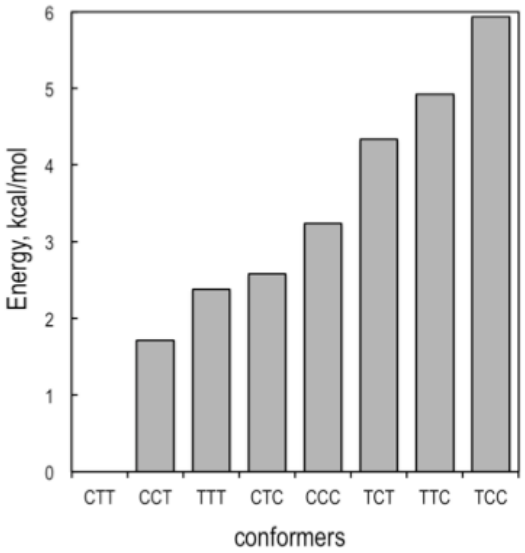

Figure 1.25 Computed relative stability of **QT** conformers with respect to the most stable conformer (CTT) in solution, averaged over all studied solvents.

Interatomic C-C distances confirm the quinoidal form of the thiophene unit in all conformations and solvents (Figure 1.26). The larger bond length obtained for D5 with respect to the D1 and D3 C-C bonds can be attributed to the electron withdrawing power of the cyanoacrylic acid group, which diminishes its double bond character.

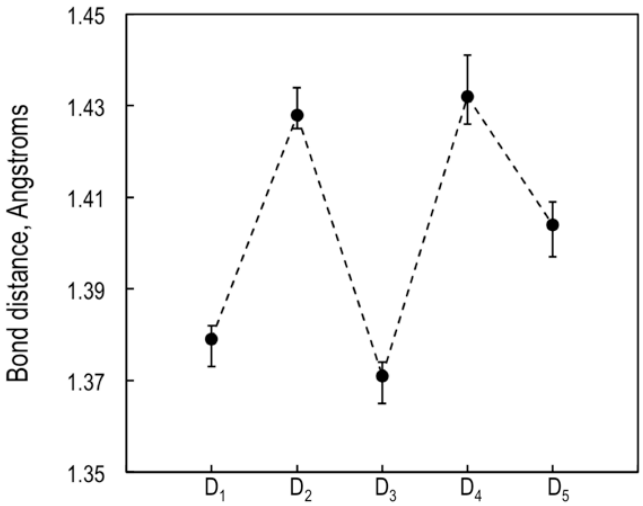

Figure 1.26 Average interatomic distances of **QT** for all conformers and solvents. Vertical bars indicate maximum and minimum values. Labels correspond to Figure 1.23.

7.3 Electronic structure

The HOMO and the LUMO of **QT** are π and π* orbitals mainly localized on the dimethylaniline fragment and cyanoacrylic acid group respectively, although both orbitals also exhibit considerable delocalization over the rest of the molecule (Figure 1.27). This picture already predicts a moderate donor-to-acceptor electron transfer character upon photoexcitation for this compound. The electron distribution of the two frontier orbitals almost does not change with the dielectric constant of the environment, and solvent polarity has a rather mild impact on the HOMO and LUMO energies (Appendix, Table A1.10). The most noticeable effect is the stabilization of the LUMO with the increase of the solvent polarity, resulting in a decrease of the HOMO/LUMO energy gap.

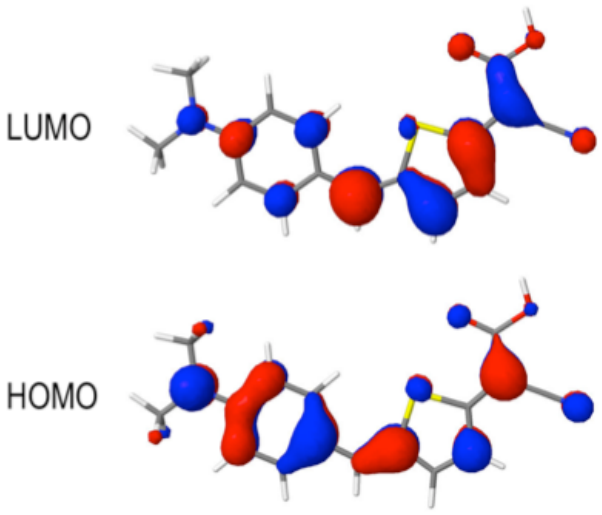

Figure 1.27 Representation of HOMO and LUMO for the **QT** (CTT) dye in chloroform solution.

The electronic transition to the lowest singlet state at the Frank-Condon region is described as an HOMO-to-LUMO (π,π^*) electron promotion. The excitation energies for the lowest energy conformer (CTT) and for the set of studied solvents are computed within the 2.49–2.54 eV range, just slightly larger (~0.2 eV) than the experimentally measured absorption maxima (Appendix, Table A1.11). The non-vanishing overlap between the two frontier orbitals and the CT character of the transition induce rather strong oscillator strengths, which is a requirement for a good sensitizer in DSSCs. Excitation energies and oscillator strengths computed for other conformers are very close to the values obtained for CTT, with differences in the transition energy no larger than 0.10 eV (Appendix, Table A1.12).

It is worth pointing out that electronic population of the LUMO upon photoexcitation is expected to reduce the quinoidal character of the linker. Indeed, relaxation of the quinoidal dye on the S_1 PES results in an increase of D1, D3, and D5 and a decrease of the D2 and D4 C-C bonds. This is the exact opposite effect observed in similar D-π-A non-quinoidal dyes, where the molecular structure at the conjugated bridge becomes closer to the quinoidal form (Appendix, Figure A1.5). A detailed comparison between optimized geometrical parameters for the S_0 and S_1 states of **QT** and a non-quinoidal counterpart can be found in the Appendix (Table A1.13).

7.4 Solvent effects

Due to the CT character of the transition to the lowest excited singlet state of **QT**, vertical transition energies decrease with the dielectric constant of the solvent. Computed energies using a polarizable continuum model exhibit a nearly linear relationship with respect to solvent polarity (Figure 1.28), quantified by the solvent polarity function Δf (see Appendix). The experimental absorption maxima also follow this linear relationship for the case of aprotic solvents.[155] On the other hand, alcohol solvents, i.e. methanol, ethanol and propanol, do not follow this trend and their experimental maxima are sensibly blue shifted with respect to the expected value taking its solvent polarity. Methanol is the solvent that induces the largest shift of the maximum absorption peak, in the order of 0.1 eV. These solvents present particular solute-solvent interactions modifying the photophysical properties of the molecule beyond the polarizable continuum and deserve special consideration.

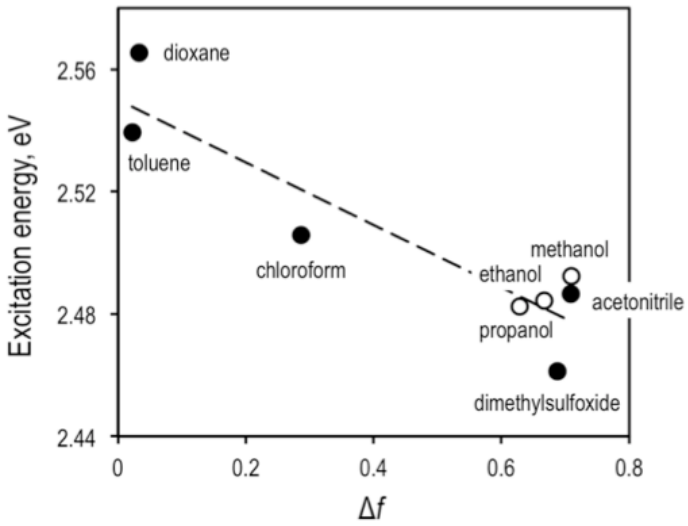

Figure 1.28 Solvent dependence (Δf) of computed vertical excitation energies of **QT**. Empty circles indicate polar protic solvents. Dashed line corresponds to a linear fitting.

As mentioned above, the different behavior of absorption energies in alcohol solvents was already experimentally noticed by Segawa et al.,[155] who suggested that hydrogen bonds between solvent molecules and the dye could be responsible for the observed blue shift of the absorption maxima. It is, however, difficult to experimentally confirm the role of these hydrogen bonds in the photophysical properties of the dye in solution. Moreover, it is not clear a priori how many of such solute-solvent interactions are responsible for the different behavior between protic and aprotic solvents. On the other hand, these and other questions can be tackled computationally by combining different techniques and calculations. In the following, we explore the nature of these potential interactions and how they modify the photophysical properties of the **QT** dye. Firstly, to give a qualitative understanding of the observed blue shift, we investigate the two extreme cases resulting from the interaction between the dye and protic solvents, that is the protonated and deprotonated forms of **QT**. Then we explore in more detail the $S_0 \rightarrow S_1$ transition in methanol by including explicitly some solvent molecules in our computational model.

The most acidic proton in **QT** is the one on the carboxylic group. Therefore, the deprotonated molecule contains the cyanoacrylate moiety as the electron acceptor group. The LUMO of the anionic species is largely destabilized with respect to the neutral form and the computed transition energy to S_1, also mainly described by the HOMO-LUMO transition, is approximately 0.3 eV blue shifted (in dioxane) with respect to the neutral case (Table 1.11). On the other hand, the most basic position of the dye corresponds to the nitrogen atom in the amine electron donor group. Protonation of the amine leads to a 0.5

eV blue shift of the vertical transition to S_1 in dioxane solution because the HOMO is further stabilized than the LUMO by ~0.6 eV. The computed blue shifts for the protonated and deprotonated dyes with respect to the neutral form are rather constant along the studied range of solvent polarities, i.e. 2.21 (dioxane) < ε < 35.7 (acetonitrile). Generalizing these results, we can predict that both types of dye-solvent interactions, that is weakening of the O-H bond in the carboxylic group and proton-amine contacts, will induce an increase of the absorption energy.

Table 1.11 HOMO-LUMO energy gap ΔE_{HL} (in eV), vertical excitation energies $\Delta E(S_1)$ (in eV), oscillator strengths (*f*), and HOMO→LUMO contribution (in %) of the transition to the lowest excited singlet state of neutral (**QT**), deprotonated (**QT**$^-$) and protonated (**HQT**) dyes computed in dioxane.

	Molecule		
	QT	**QT**$^-$	**HQT**
ΔE_{HL}	4.57	4.95	5.16
$\Delta E(S_1)$	2.57	2.91	3.05
f	1.40	1.43	1.24
H→L	97	97	98

In addition to the carboxylic and amine groups, the quinoidal dye contains several sites prone to interact with the hydroxyl group of the alcohol solvents, so it is important to identify which are these interactions and how many solvent molecules need to be explicitly considered in a computational model in order to reproduce the experimental findings correctly. In order to acquire a more realistic picture of **QT** in alcohol solution taking into account all these possible interactions between the dye and the solvent, we performed a computational analysis with explicit solvent molecules for the case of methanol. First, we performed molecular dynamics calculations in order to identify potential interaction modes between **QT** and methanol molecules. We would like to emphasize that we do not pretend to use classical molecular dynamics simulations to acquire the dynamical behavior of the dye in solution, but rather to get a structural insight of the dye-solvent system. Then, we took the most promising structural candidates to perform quantum chemistry calculations of the dye with the first solvation shell.

Analysis of the lowest energy configurations obtained along the force field molecular dynamics trajectory reveal that there are five potentially relevant solvent-dye interactions: hydrogen contact to the amine's nitrogen atom, hydrogen bond acceptor and donor interactions with COOH, hydrogen interaction with the CN group and the interaction of a

methanol molecule with the quinoidal thiophene unit. The refinement of the low-energy structures by quantum chemistry calculations with the dye and five explicit methanol molecules embedded in a polarizable continuum confirms the presence of these solute-solvent interactions, as indicated in Figure 1.29 with the (a)–(e) labels.

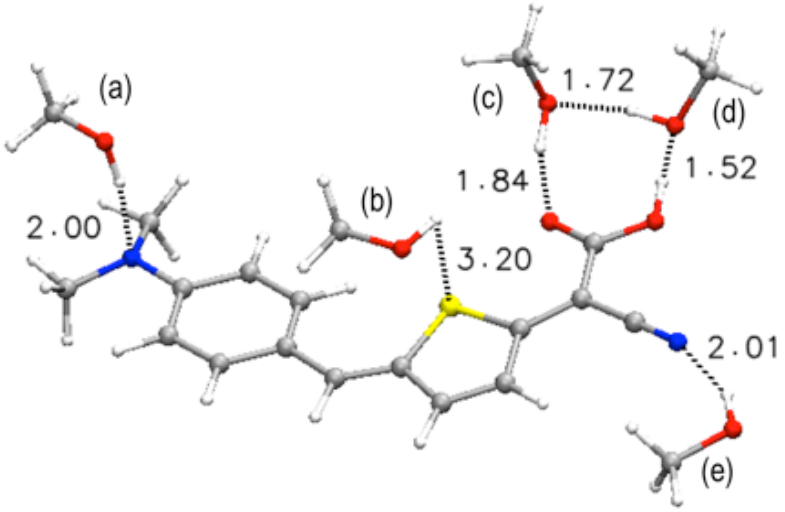

Figure 1.29 Lowest optimized geometry for the **QT** dye with five explicit methanol molecules computed at the M06-2X/6-31+G(d,p) level. Dotted lines indicate the shortest atomic distances (in Å) between methanol molecules and the molecular dye.

The most stable molecular geometry of **QT** obtained in methanol solution by explicitly considering five solvent molecules (Figure 1.29) also shows a quinoidal structure of the linker, but presents some structural modifications with respect to the optimized geometry obtained for the dye without explicit consideration of solvent molecules which are worth pointing out. The interaction of the aminic nitrogen atom with a methanol molecule (a) pyramidalizes the trigonal nitrogen and breaks the electronic conjugation with the benzene ring. As a consequence, there is a loss of stabilization energy due to planarity between benzene and thiophene rings, resulting in a slight torsion between the two planes (~10º). Therefore, there is a general loss of conjugation throughout the dye due to the solvent-solute interactions. Methanol-dye explicit interactions also induce changes in the bond distances, especially those within the cyanoacrylic moiety. The carbonyl C=O bond length decreases by ~0.04 Å while the O-H one increases by ~0.06 Å, in line with the presence of strong hydrogen bond interactions. The N-C (amine-phenyl) bond length also increases by ~0.03 Å due to the pyramidalization of the nitrogen.

When including explicitly methanol molecules in the electronic structure calculations there is a larger energetic stabilization for the HOMO than for the LUMO in comparison to the

results without explicit solvent. The fact that the most important change is found for the energy of the HOMO suggests that the methanol-**QT** hydrogen bond formation on the amine has a major role in the blue shift of excitation energies with respect to aprotic solvents. The vertical transition energy to S_1 for the optimized model of the dye including five methanol molecules is 2.78 eV, that is 0.29 eV higher than the energy computed for the optimized dye without explicit solvent molecules (2.49 eV). This is inline with the ~0.1 eV blue shift observed experimentally.[155] Comparison between these two values, i.e. computed and experimental shifts, has to be taken with precaution, because the computational results have been obtained for the frozen optimal ground state geometry, which cannot be directly compared with the experimental measures of absorption maxima.

In order to identify and rationalize the main factors responsible for the computed increase in the excitation energy, we compare the molecular orbital energy diagrams of the two types of approaches to the solvent effects (with and without explicit methanol molecules). In addition, we also consider molecular orbital energies obtained by taking the geometry optimized with explicit solvent molecules and performing a PCM calculation without solvent molecules, i.e. only considering geometrical changes (Figure 1.30). Comparison of these three computational models allows to distinguish between geometrical and electronic effects.

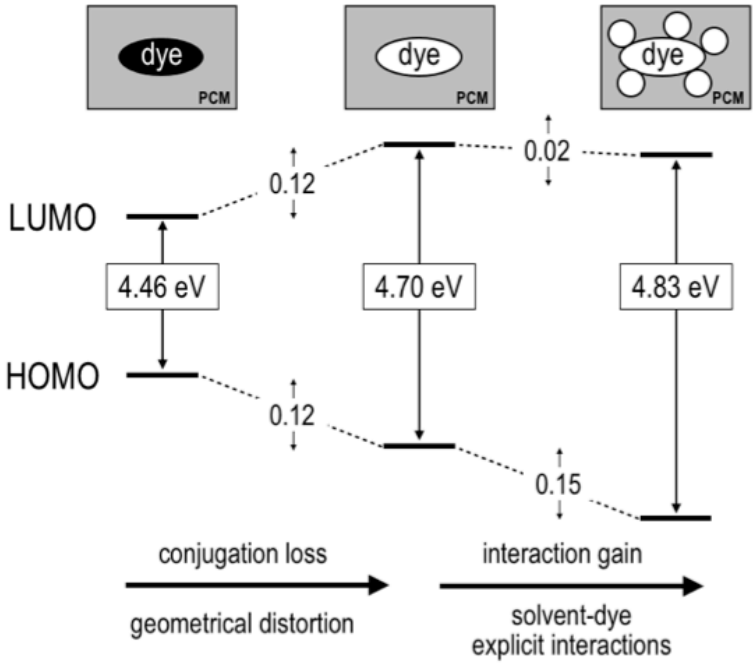

Figure 1.30 HOMO and LUMO energy diagram of **QT** in methanol solution computed within PCM (left), with PCM + five methanol molecules (right), and with PCM taking the geometry from PCM + five methanol molecules (middle). White and black representations of the dye indicate molecular geometries optimized with and without explicit methanol molecules, respectively.

As discussed above, geometrical distortions due to the presence of explicit solute-solvent interactions result in a loss of molecular planarity of the dye, which can be related to the loss of conjugation of the π-system. As a result, when plugging in the dye with the geometry optimized with explicit solvent in a PCM calculation there is a considerable (0.24 eV) increase of the HOMO-LUMO gap (from left to middle in Figure 1.30). The presence of explicit methanol-dye interactions results in an additional relaxation of the HOMO, while the energy of the LUMO remains almost unchanged (from middle to right in Figure 1.30), resulting in an additional 0.13 eV increase of the gap. Excitation energies to S_1 for these three situations follow the same behavior as the HOMO-LUMO gap (Table 1.12), with an estimated increase of 0.21 eV due to the geometrical change and of 0.08 eV due to electronic factors.

Table 1.12 HOMO/LUMO gap ΔE_{HL} (in eV), excitation energies $\Delta E(S_1)$ (in eV), oscillator strengths (*f*), and HOMO→LUMO contribution (in %) of the transition to the lowest excited singlet of **QT** in methanol solution computed in PCM with PCM and PCM + 5 methanol optimized structures of the dye, and in PCM + 5 methanol molecules.

System	Geometry	ΔE_{HL}	$\Delta E(S_1)$	*f*	H→L
QT	PCM	4.46	2.49	1.40	97
QT	PCM+5MeOH	4.70	2.70	1.31	96
QT+5MeOH	PCM+5MeOH	4.83	2.78	1.28	96

In order to weight the relative impact of each one of the five explicit solvent-dye interactions, we recomputed orbital and transition energies to the lowest singlet of **QT** for all possible models with four explicit methanol molecules by sequentially removing one of the molecules from the optimized structure with five methanol molecules. Energy changes with respect to the case with all five methanol molecules are shown in Table 1.13.

Our calculations indicate that the largest change in the S_1 excitation energy is related with the hydrogen bond interaction on the aminic nitrogen (a). This interaction is responsible for an important stabilization of the HOMO energy, which is ~0.11 eV larger than the related LUMO stabilization, causing an overall 0.07 eV blue shift in the transition energy. This behavior can be rationalized by the larger localization of the HOMO on the donor group. Other interactions have a minor impact on the orbital energies. Moreover, the HOMO/ LUMO relative changes are much smaller and they do not affect the excitation energies as much. The interaction of the methanol molecule (d) with the OH group on the cyanoacrylic acid destabilizes the HOMO and LUMO energies by 0.05 and 0.08 eV respectively. The

LUMO is further destabilized than the HOMO since it is more localized on the acceptor moiety. This translates into a blue shift of 0.025 eV of the transition energy. Methanol interactions with the CN and the CO groups have a very similar effect. The HOMO and LUMO are stabilized by a similar amount ~0.05 eV, leading to a very small decrease of the transition energy. The methanol molecule (b) lying above the quinoidal thiophene is the one with the smallest effect on the frontier MO energies and the excitation energy to S_1, due to the weak interaction with the dye. This explicit interaction induces a very small destabilization of the HOMO and LUMO, leading to an increase of only 0.01 eV in the transition energy. In summary, although several hydrogen bonds between methanol molecules and the donor and acceptor groups of the dye can be formed, the principal interaction causing a blue shift of the transition energy compared to aprotic solvents of similar polarity to methanol is the one with the amine group. Solvatochromic shifts on the absorption spectrum resulting from the interaction between the amine group and protic solvents have been identified and investigated in other organic compounds.[164-166]

Table 1.13 Relative energies of **QT** with four methanol molecules for the HOMO (ΔE_H), LUMO (ΔE_L) and lowest excited singlet ($\Delta\Delta E(S_1)$) with respect to the values with five methanol molecules. Geometries correspond to the case with five solvent molecules (a)–(e) and the removed methanol molecule is indicated by contact group of the dye (Figure 1.29). All values are given in meV.

Contact group	Label	ΔE_H	ΔE_L	$\Delta\Delta E(S_1)$
Amine	(a)	-159	-49	70
Thiophene	(b)	15	33	11
CO	(c)	-33	-49	-17
OH	(d)	54	80	25
CN	(e)	-33	-41	-9

7.5 Conclusions

In the present study, a quinoidal dye with potential interest as a D-π-A organic molecular sensitizer in DSSCs has been computationally explored in terms of its atomic and electronic structure, and the solvent dependency of its excitation energy to the lowest excited singlet state has been investigated in detail. As a general trend, the maximum of the absorption band linearly decreases with solvent polarity, which is a consequence of the CT character of the electronic transition. Polar protic solvents, however, do not follow this relationship and tend to blue shift transition energies with respect to aprotic solvents with the same dielectric constant. This behavior can be rationalized by dye-solvent interactions related to the presence of hydrogen bonds. We have decomposed the impact of the explicit

interactions of protic solvent molecules with **QT** into geometrical and electronic effects, and we have identified the interaction between a methanol molecule and the amine group of the dye as the main source of the difference with respect to the behavior in aprotic solvents. From the present results we can conclude that absorption maxima of these dyes in protic solvents cannot be properly predicted with polarizable continuum models and that explicit solvent molecules should be included in the computational model.

7.6 Computational details

Electronic structure calculations for ground and excited states were performed within the DFT and TDDFT frameworks, respectively. Ground state geometry optimizations of the molecular dye in solution with no explicit solvent molecules were carried out with the B3LYP functional.[90,91] Optimized structures with the M06-2X functional[167] are almost identical to the B3LYP geometries.[168] The stationary geometry for the lowest energy conformer (CTT as in Figure 1.23) was confirmed to be a true minimum by evaluation of the Hessian. Excited state calculations were performed with TDDFT and the CAM-B3LYP functional.[85] In all the calculations, the 6-31+G(d,p) basis set was used and the effects of the solvent were taken into account with IEF-PCM.[107,108] The solvents considered in our calculations with the corresponding dielectric constants are: dioxane ($\varepsilon = 2.21$), toluene ($\varepsilon = 2.37$), chloroform ($\varepsilon = 4.71$), propanol ($\varepsilon = 19.26$), ethanol ($\varepsilon = 24.85$), methanol ($\varepsilon = 32.61$), acetonitrile ($\varepsilon = 35.69$), and dimethylsulfoxide ($\varepsilon = 46.83$). Geometry optimizations in methanol solution of model systems containing explicit solvent molecules were performed with the M06-2X functional, as it has been recommended in the presence of non-covalent interactions.[167] All electronic structure calculations were performed with the Gaussian 09 package.[169] In order to systematically scan over potentially relevant solvent-dye interactions, classical molecular dynamics simulations (Appendix, Figure A1.6) were performed for the most stable isomer (CTT) with 950 methanol molecules in a 40 Å cubic box, in accordance with the density of methanol in the experimental conditions, that is 0.792 g/cm^3. The OPLS-AA force field[170] was used and reparametrized in order to reproduce DFT calculations (see below). A 100 ps simulation with 1 fs time step was run in the canonical (NVT) ensemble at 298 K using periodic boundary conditions with the Tinker program.[171] The principal solute-solvent interactions were identified from the molecular dynamics simulations and low energy structures were used as initial guesses in DFT geometry optimizations. From this procedure we identified up to five solvent molecules with significant interaction with the dye.

When certain angle bending and torsional parameters where not available in the OPLS-AA force field, those corresponding to similar atom types were used. In addition, some torsion parameters involving dihedral angles of thiophene and the CN and COOH units had to be modified to prevent the dye from excessively loosing its planarity during the molecular dynamics simulation. The force field parameters for the dye may be found in reference 168. It should be noted that snapshots from this simulation served solely to identify potential solute-solvent interactions and as starting points for further DFT optimizations. Excited states with explicit solvent molecules were then calculated from a representative DFT optimized geometry.

7.7 Appendix

Polarity function

The solvents polarity was quantified via the polarity function Δf just like Segawa and coworkers did in their original paper.[155] This function is defined as:

$$\Delta f = \frac{\varepsilon - 1}{\varepsilon + 2} - \frac{n^2 - 1}{n^2 + 2} \tag{1.18}$$

where ε and n are the relative permittivity and the refractive index of the solvent.

Table A1.9 Relative ground state conformer stability ΔE (in kcal/mol) of the **QT** dye in different solvents.

Conf.	ACN	chloroform	dioxane	DMSO	ethanol	methanol	toluene	vacuum
CTT	0.00	0.00	0.00	0.00	0.00	0.00	0.00	0.00
CCT	1.79	1.73	1.66	1.79	1.78	1.79	1.66	1.53
TTT	2.26	2.40	2.51	2.26	2.27	2.26	2.50	2.58
CTC	2.13	2.60	3.00	2.11	2.17	2.14	2.96	3.50
CCC	2.86	3.27	3.60	2.84	2.89	2.87	3.57	3.98
TCT	4.28	4.37	4.41	4.28	4.29	4.28	4.41	4.36
TTC	4.43	4.97	5.40	4.41	4.48	4.44	5.36	5.88
TCC	5.39	6.01	6.47	5.36	5.44	5.40	6.42	6.97

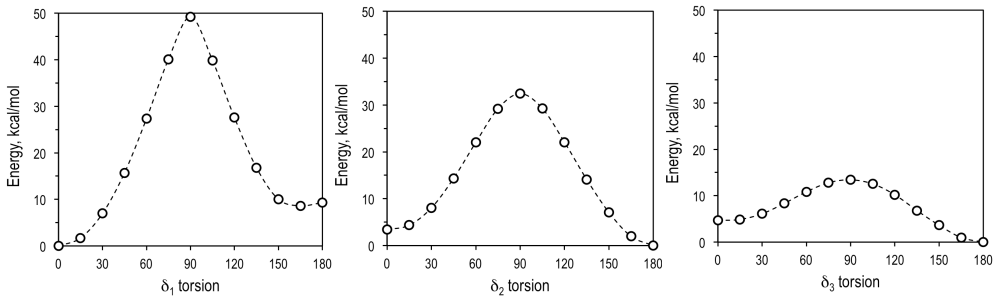

Figure A1.4 Potential energy profiles computed along the δ_1 (left), δ_2 (middle) and δ_3 (right) torsion angles computed at the M06-2X/6-31+G(d,p) level in chloroform from the CTT optimized conformer, i.e. δ_1=0°, δ_2=180°, and δ_3=180°.

Table A1.10 HOMO, LUMO and HOMO-LUMO gap of **QT** computed in different solvents with the PCM model.

Solvent	Δf	H / eV	L / eV	ΔH,L / eV
vacuum	0.00	-6.63	-1.97	4.66
toluene	0.02	-6.58	-2.02	4.56
dioxane	0.03	-6.58	-2.01	4.57
chloroform	0.29	-6.57	-2.06	4.51
DMSO	0.69	-6.56	-2.11	4.46
ACN	0.71	-6.56	-2.10	4.46
propanol	0.63	-6.56	-2.10	4.47
ethanol	0.67	-6.56	-2.10	4.46
methanol	0.71	-6.56	-2.10	4.46

Table A1.11 Polarity function (Δf), experimental absorption maxima (taken from reference 155), and calculated vertical excitation energies to S_1 of **QT** in different solvents.

Solvent	Δf	ΔE_{exp} / eV	ΔE / eV
toluene	0.02	2.35	2.54
dioxane	0.03	2.36	2.57
chloroform	0.29	2.30	2.51
DMSO	0.69	2.25	2.46
ACN	0.71	2.26	2.49
propanol	0.63	2.34	2.48
ethanol	0.67	2.28	2.48
methanol	0.71	2.35	2.49

Table A1.12 Vertical S_1 transition energies and corresponding oscillator strengths for all **QT** conformers in different solvents.

Conf.	dioxane		ACN		methanol	
	ΔE / eV	f	ΔE / eV	f	ΔE / eV	f
CCC	2.54	1.41	2.46	1.42	2.46	1.41
CCT	2.54	1.40	2.46	1.40	2.46	1.40
CTC	2.57	1.47	2.48	1.47	2.49	1.46
CTT	2.57	1.40	2.49	1.40	2.49	1.40
TCC	2.50	1.49	2.39	1.54	2.39	1.54
TCT	2.49	1.45	2.39	1.51	2.39	1.50
TTC	2.52	1.50	2.41	1.56	2.42	1.55
TTT	2.53	1.45	2.43	1.51	2.43	1.50

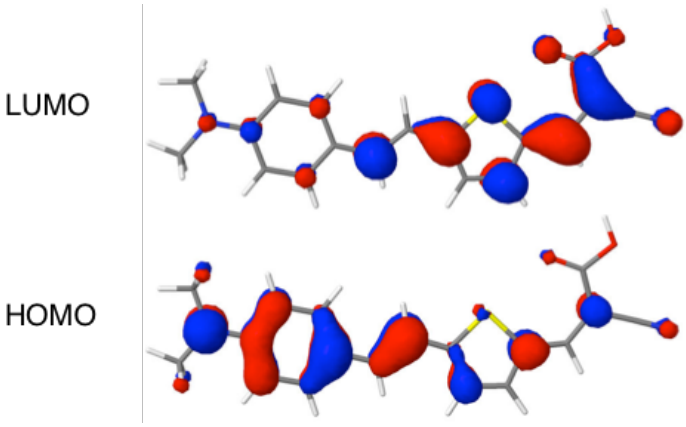

Figure A1.5 HOMO and LUMO representation of the non-quinoidal counterpart of the **QT** dye in chloroform solution.

Table A1.13 Interatomic distances (in Å) of the thiophene unit for the optimized S_0 and S_1 states of **QT** dye and the non-quinoidal counterpart in chloroform solution.

		D1	D2	D3	D4	D5
quinoidal (**QT**)	S_0	1.378	1.430	1.369	1.431	1.401
	S_1	1.410	1.413	1.387	1.406	1.415
	$\Delta(S_1-S_0)$	0.03	-0.02	0.02	-0.03	0.01
non-quinoidal	S_0	1.437	1.404	1.391	1.409	1.413
	S_1	1.395	1.421	1.369	1.428	1.398
	$\Delta(S_1-S_0)$	-0.04	0.02	-0.02	0.02	-0.02

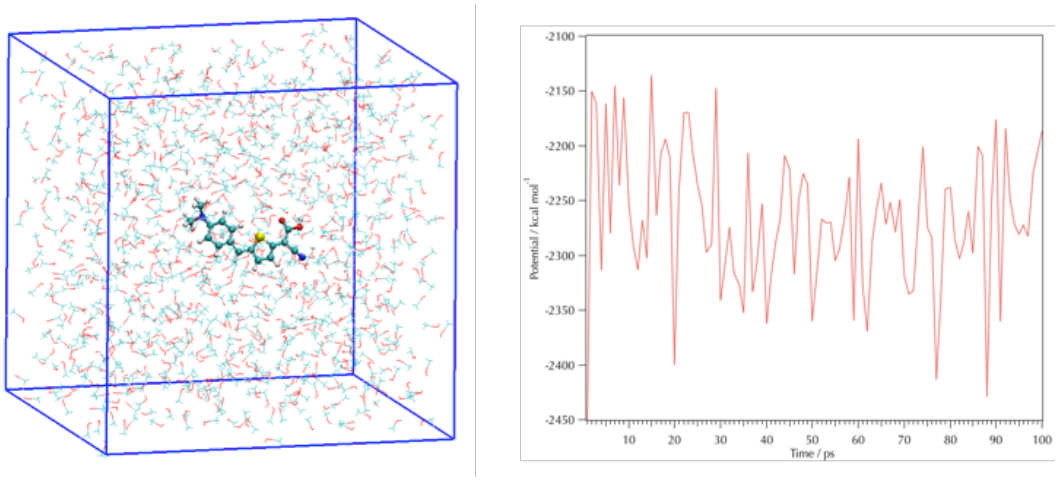

Figure A1.6 Cubic box with one **QT** molecule and 950 methanol molecules and plot of the system's potential energy throughout the molecular dynamics simulation.

8. General conclusions

The main conclusions from this chapter can be summarized as following.

The photoabsorption properties of D-π-A dyes are influenced by the choice of the π-linker. The geometrical characteristics of the linkers tune the excitation energies and oscillator strengths of CT state of the dyes. The good performance of DSSC devices employing a cyclopentadithiophene π-linker can be attributed to its planarity and linearity, inducing larger oscillator strengths.

Longer π-bridges based on thiophene and cyclopentadithiophene units reduce the excitation energy and also increase the transition probability to S_1. The CT nature of the optical state can be quantified by several techniques. Our results indicate that the optimal ω values for the study of D-π-A dyes with the LRC-ωPBEh functional should be probably smaller than the standard values used. The GSOP and ESOP values of the Tn and Cn dyes indicate that they both have appropriate oxidation potentials to sensitize the TiO_2 semiconductor with the I^-/I_3^- couple as the redox mediator.

The selenium heteroatom substitution in a bithiophene linker does not have a great influence on the photophysical properties of the dyes. The larger V_{oc} value of DSSCs operating with dyes containing the cyclopentadithiophene linker compared to related linkers based on sulfur and selenium can be attributed to the shift of the CBE of TiO_2 due to the molecular dipole as well as the better molecular packing that retards the back-electron transfer from the photo-injected electrons at the TiO_2 and the oxidized electrolytes.

The shift of the CT absorption band in different solvents of a D-π-A dye based on a quinoidal thiophene linker has been rationalized by explicit dye-solvent interactions related to the presence of hydrogen bonds in methanol solution. The interaction between a methanol molecule and the amine group of the dye has been identified as the main source for the different absorption energy with respect to the behavior in aprotic solvents.

9. References

(1)O'Regan, B.; Grätzel, M. *Nature* **1991**, *353*, 737.
(2)Hagfeldt, A.; Boschloo, G.; Sun, L.; Kloo, L.; Pettersson, H. *Chem. Rev.* **2010**, *110*, 6595.
(3)Odobel, F.; Le Pleux, L.; Pellegrin, Y.; Blart, E. *Acc. Chem. Res.* **2010**, *43*, 1063.
(4)Qin, P.; Zhu, H.; Edvinsson, T.; Boschloo, G.; Hagfeldt, A.; Sun, L. *J. Am. Chem. Soc.* **2008**, *130*, 8570.
(5)Shockley, W.; Queisser, H. J. *J. Appl. Phys.* **1961**, *32*, 510.
(6)Gong, J.; Sumathy, K.; Qiao, Q.; Zhou, Z. *Renewable Sustainable Energy Rev.* **2017**, *68, Part 1*, 234.
(7)Kim, S.; Lee, J. K.; Kang, S. O.; Ko, J.; Yum, J. H.; Fantacci, S.; De Angelis, F.; Di Censo, D.; Nazeeruddin, M. K.; Grätzel, M. *J. Am. Chem. Soc.* **2006**, *128*, 16701.
(8)Hagberg, D. P.; Marinado, T.; Karlsson, K. M.; Nonomura, K.; Qin, P.; Boschloo, G.; Brinck, T.; Hagfeldt, A.; Sun, L. *J. Org. Chem.* **2007**, *72*, 9550.
(9)Hagberg, D. P.; Yum, J.-H.; Lee, H.; De Angelis, F.; Marinado, T.; Karlsson, K. M.; Humphry-Baker, R.; Sun, L.; Hagfeldt, A.; Grätzel, M.; Nazeeruddin, M. K. *J. Am. Chem. Soc.* **2008**, *130*, 6259.
(10)Moon, S.-J.; Yum, J.-H.; Humphry-Baker, R.; Karlsson, K. M.; Hagberg, D. P.; Marinado, T.; Hagfeldt, A.; Sun, L.; Grätzel, M.; Nazeeruddin, M. K. *J. Phys. Chem. C* **2009**, *113*, 16816.
(11)Casanova, D.; Rotzinger, F. P.; Grätzel, M. *J. Chem. Theory Comput.* **2010**, *6*, 1219.
(12)Pastore, M.; Mosconi, E.; De Angelis, F.; Grätzel, M. *J. Phys. Chem. C* **2010**, *114*, 7205.
(13)Clifford, J. N.; Martinez-Ferrero, E.; Viterisi, A.; Palomares, E. *Chem. Soc. Rev.* **2011**, *40*, 1635.
(14)Yum, J.-H.; Baranoff, E.; Wenger, S.; Nazeeruddin, M. K.; Grätzel, M. *Energy Environ. Sci.* **2011**, *4*, 842.
(15)Kalyanasundaram, K.; Grätzel, M. *Coord. Chem. Rev.* **1998**, *177*, 347.
(16)Nazeeruddin, M. K.; Kay, A.; Rodicio, I.; Humphry-Baker, R.; Mueller, E.; Liska, P.; Vlachopoulos, N.; Graetzel, M. *J. Am. Chem. Soc.* **1993**, *115*, 6382.
(17)K. Nazeeruddin, M.; Pechy, P.; Gratzel, M. *Chem. Commun.* **1997**, 1705.
(18)Maestri, M.; Armaroli, N.; Balzani, V.; Constable, E. C.; Thompson, A. M. W. C. *Inorg. Chem.* **1995**, *34*, 2759.
(19)Swetha, T.; Reddy, K. R.; Singh, S. P. *Chem. Rec.* **2015**, *15*, 457.
(20)Li, L.-L.; Diau, E. W.-G. *Chem. Soc. Rev.* **2013**, *42*, 291.
(21)Higashino, T.; Imahori, H. *Dalton Trans.* **2015**, *44*, 448.
(22)Walter, M. G.; Rudine, A. B.; Wamser, C. C. *J. Porphyrins Phthalocyanines* **2010**, *14*, 759.
(23)Martin-Gomis, L.; Fernandez-Lazaro, F.; Sastre-Santos, A. *J. Mater. Chem. A* **2014**, *2*, 15672.
(24)Wang, C.-L.; Shiu, J.-W.; Hsiao, Y.-N.; Chao, P.-S.; Wei-Guang Diau, E.; Lin, C.-Y. *J. Phys. Chem. C* **2014**, *118*, 27801.
(25)Mann, J. R.; Gannon, M. K.; Fitzgibbons, T. C.; Detty, M. R.; Watson, D. F. *J. Phys. Chem. C* **2008**, *112*, 13057.
(26)Mishra, A.; Fischer, M. K. R.; Bäuerle, P. *Angew. Chem., Int. Ed.* **2009**, *48*, 2474.
(27)Ooyama, Y.; Harima, Y. *ChemPhysChem* **2012**, *13*, 4032.
(28)Zhang, L.; Cole, J. M. *ACS Appl. Mater. Interfaces* **2015**, *7*, 3427.
(29)Clifford, J. N.; Palomares, E.; Nazeeruddin, M. K.; Thampi, R.; Grätzel, M.; Durrant, J. R. *J. Am. Chem. Soc.* **2004**, *126*, 5670.
(30)Zhang, F.; Luo, Y.-h.; Song, J.-s.; Guo, X.-z.; Liu, W.-l.; Ma, C.-p.; Huang, Y.; Ge, M.-f.; Bo, Z.; Meng, Q.-B. *Dyes Pigm.* **2009**, *81*, 224.
(31)Liang, M.; Chen, J. *Chem. Soc. Rev.* **2013**, *42*, 3453.
(32)De Angelis, F. *Chem. Phys. Lett.* **2010**, *493*, 323.
(33)Sánchez-de-Armas, R.; Oviedo, J.; San Miguel, M. Á.; Sanz, J. F. *J. Phys. Chem. C* **2011**, *115*, 11293.
(34)Ooyama, Y.; Kanda, M.; Uenaka, K.; Ohshita, J. *ChemPhysChem* **2015**, *16*, 3049.
(35)Duncan, W. R.; Prezhdo, O. V. *Annu. Rev. Phys. Chem.* **2007**, *58*, 143.
(36)Ooyama, Y.; Furue, K.; Enoki, T.; Kanda, M.; Adachi, Y.; Ohshita, J. *Phys. Chem. Chem. Phys.* **2016**, *18*, 30662.
(37)Helgaker, T.; Jorgensen, P.; Olsen, J. *Molecular Electronic-Structure Theory*; Wiley & Sons Ltd.: West Sussex, England, 2014.
(38)Foresman, J. B.; Head-Gordon, M.; Pople, J. A.; Frisch, M. J. *J. Phys. Chem.* **1992**, *96*, 135.
(39)Dreuw, A.; Head-Gordon, M. *Chem. Rev.* **2005**, *105*, 4009.

(40)Head-Gordon, M.; Rico, R. J.; Oumi, M.; Lee, T. J. *Chem. Phys. Lett.* **1994**, *219*, 21.
(41)Head-Gordon, M.; Maurice, D.; Oumi, M. *Chem. Phys. Lett.* **1995**, *246*, 114.
(42)Christof, H.; Florian, W. *J. Chem. Phys.* **2000**, *113*, 5154.
(43)Hattig, C.; Hald, K. *Phys. Chem. Chem. Phys.* **2002**, *4*, 2111.
(44)Rhee, Y. M.; Head-Gordon, M. *J. Phys. Chem. A* **2007**, *111*, 5314.
(45)Rowe, D. J. *Rev. Mod. Phys.* **1968**, *40*, 153.
(46)Emrich, K. *Nucl. Phys. A* **1981**, *351*, 379.
(47)Geertsen, J.; Rittby, M.; Bartlett, R. J. *Chem. Phys. Lett.* **1989**, *164*, 57.
(48)John, F. S.; Rodney, J. B. *J. Chem. Phys.* **1993**, *98*, 7029.
(49)Sergey, V. L.; Anna, I. K. *J. Chem. Phys.* **2004**, *120*, 175.
(50)Wormit, M.; Rehn, D. R.; Harbach, P. H. P.; Wenzel, J.; Krauter, C. M.; Epifanovsky, E.; Dreuw, A. *Mol. Phys.* **2014**, *112*, 774.
(51)Krauter, C. M.; Pernpointner, M.; Dreuw, A. *J. Chem. Phys.* **2013**, *138*, 044107.
(52)Roos, B. O. In *Advances in Chemical Physics*; John Wiley & Sons, Inc.: 2007, p 399.
(53)Roos, B. O.; Andersson, K.; F¸lscher, M. P. *Chem. Phys. Lett.* **1992**, *192*, 5.
(54)Siegbahn, P. E. M. In *Methods in Computational Molecular Physics*; Diercksen, G. H. F., Ed.; Reidel: Dordrecht, 1983, p 189.
(55)Mukherjee, D.; Pal, S.; Per-Olov, L. In *Adv. Quantum Chem.*; Academic Press: 1989; Vol. Volume 20, p 291.
(56)*Recent Advances in Multi-reference Methods*; World Scientific: Singapore, 1999.
(57)Marques, M. A. L.; Ullrich, C.; Nogueira, F.; Rubio, A.; Burke, K.; Gross, E. K. U. *Time-Dependent Density Functional Theory*; Springer-Verlag: Berlin, Heidelberg, 2006.
(58)Maitra, N. T. *J. Chem. Phys.* **2016**, *144*, 220901.
(59)Ullrich, C. A. *Time-Dependent Density-Functional Theory: Concepts and Applications*; Oxford University Press: Oxford, 2012.
(60)Ullrich, C. A.; Yang, Z.-h. *Braz. J. Phys.* **2014**, *44*, 154.
(61)Casida, M. E.; Huix-Rotllant, M. *Annu. Rev. Phys. Chem.* **2012**, *63*, 287.
(62)Runge, E.; Gross, E. K. U. *Phys. Rev. Lett.* **1984**, *52*, 997.
(63)Hohenberg, P.; Kohn, W. *Phys. Rev.* **1964**, *136*.
(64)Kohn, W.; Sham, L. J. *Phys. Rev.* **1965**, *140*, A1133.
(65)Gross, E. K. U.; Kohn, W. *Phys. Rev. Lett.* **1985**, *55*, 2850.
(66)Casida, M. E. In *Recent Advances in Computational Chemistry Vol 1, Recent Advances in Density Functional Methods, Part I*; World Scientific: Singapore, 1995.
(67)Dreuw, A.; Head-Gordon, M. *J. Am. Chem. Soc.* **2004**, *126*, 4007.
(68)Hirata, S.; Head-Gordon, M. *Chem. Phys. Lett.* **1999**, *314*, 291.
(69)Fetter, A. L.; Walecka, J. D. *Quatum Theory of Many-Particle Systems*; McGraw-Hill: New York, 1971.
(70)Ring, P.; Schuck, P. *The nuclear many-body problem*; Springer-Verlag: Heidelberg, 1980.
(71)Dreuw, A.; Weisman, J. L.; Head-Gordon, M. *J. Chem. Phys.* **2003**, *119*, 2943.
(72)Dreuw, A.; Fleming, G. R.; Head-Gordon, M. *Phys. Chem. Chem. Phys.* **2003**, *5*, 3247.
(73)Sobolewski, A. L.; Domcke, W. *Chemi. Phys.* **2003**, *294*, 73.
(74)Zhao, Y.; Truhlar, D. G. *Acc. Chem. Res.* **2008**, *41*, 157.
(75)Perdew, J. P.; Zunger, A. *Phys. Rev. B* **1981**, *23*, 5048.
(76)Iikura, H.; Tsuneda, T.; Yanai, T.; Hirao, K. *J. Chem. Phys.* **2001**, *115*, 3540.
(77)Vydrov, O. A.; Scuseria, G. E. *J. Chem. Phys.* **2006**, *125*, 234109.
(78)Chai, J.-D.; Head-Gordon, M. *J. Chem. Phys.* **2008**, *128*, 084106.
(79)Rohrdanz, M. A.; Martins, K. M.; Herbert, J. M. *J. Chem. Phys.* **2009**, *130*, 054112.
(80)Heyd, J.; Scuseria, G. E.; Ernzerhof, M. *J. Chem. Phys.* **2003**, *118*, 8207.
(81)Henderson, T. M.; Janesko, B. G.; Scuseria, G. E. *J. Chem. Phys.* **2008**, *128*, 194105.
(82)Casanova, D. *ChemPhysChem* **2011**, *12*, 2979.
(83)Jacquemin, D.; Perpete, E. A.; Scuseria, G. E.; Ciofini, I.; Adamo, C. *J. Chem. Theory Comput.* **2008**, *4*, 123.
(84)Lange, A. W.; Herbert, J. M. *J. Am. Chem. Soc.* **2009**, *131*, 3913.
(85)Yanai, T.; Tew, D. P.; Handy, N. C. *Chem. Phys. Lett.* **2004**, *393*, 51.
(86)Hehre, W. J.; Ditchfield, R.; Pople, J. A. *J. Chem. Phys.* **1972**, *56*, 2257.

(87)Hariharan, P. C.; Pople, J. A. *Mol. Phys.* **1974**, *27*, 209.
(88)Francl, M. M.; Pietro, W. J.; Hehre, W. J.; Binkley, J. S.; Gordon, M. S.; DeFrees, D. J.; Pople, J. A. *J. Chem. Phys.* **1982**, *77*, 3654.
(89)Clark, T.; Chandrasekhar, J.; Spitznagel, G. W.; Schleyer, P. V. R. *J. Comput. Chem.* **1983**, *4*, 294.
(90)Lee, C.; Yang, W.; Parr, R. G. *Phys. Rev. B* **1988**, *37*, 785.
(91)Becke, A. D. *J. Chem. Phys.* **1993**, *98*, 5648.
(92)Neugebauer, J.; Jacob, C. R.; Wesolowski, T. A.; Baerends, E. J. *J. Phys. Chem. A* **2005**, *109*, 7805.
(93)De Angelis, F.; Fantacci, S.; Gebauer, R. *J. Phys. Chem. Lett.* **2011**, *2*, 813.
(94)Douma, D. H.; M'Passi-Mabiala, B.; Gebauer, R. *J. Chem. Phys.* **2012**, *137*, 154314.
(95)Kollman, P. A.; Massova, I.; Reyes, C.; Kuhn, B.; Huo, S.; Chong, L.; Lee, M.; Lee, T.; Duan, Y.; Wang, W.; Donini, O.; Cieplak, P.; Srinivasan, J.; Case, D. A.; Cheatham, T. E. *Acc. Chem. Res.* **2000**, *33*, 889.
(96)Jacquemin, D.; Mennucci, B.; Adamo, C. *Phys. Chem. Chem. Phys.* **2011**, *13*, 16987.
(97)Mennucci, B. *Phys. Chem. Chem. Phys.* **2013**, *15*, 6583.
(98)Mennucci, B.; Caprasecca, S.; Guido, C. A. In *Advances in Physical Organic Chemistry*; Ian, H. W., Nicholas, H. W., Eds.; Academic Press: 2016; Vol. Volume 50, p 203.
(99)Loco, D.; Polack, É.; Caprasecca, S.; Lagardère, L.; Lipparini, F.; Piquemal, J.-P.; Mennucci, B. *J. Chem. Theory Comput.* **2016**, *12*, 3654.
(100)Cramer, C. J.; Truhlar, D. G. *Chem. Rev.* **1999**, *99*, 2161.
(101)Tomasi, J.; Mennucci, B.; Cammi, R. *Chem. Rev.* **2005**, *105*, 2999.
(102)Mennucci, B. *Wiley Interdiscip. Rev.: Comput. Mol. Sci.* **2012**, *2*, 386.
(103)Herbert, J. M.; Lange, A. W. In *Many-Body Effects and Electrostatics in Multi-Scale Computations of Biomolecules* Pan Stanford: 2015, p 1.
(104)Truong, T. N.; Stefanovich, E. V. *Chem. Phys. Lett.* **1995**, *240*, 253.
(105)Barone, V.; Cossi, M. *J. Phys. Chem. A* **1998**, *102*, 1995.
(106)Cossi, M.; Rega, N.; Scalmani, G.; Barone, V. *J. Comput. Chem.* **2003**, *24*, 669.
(107)Mennucci, B.; Cancès, E.; Tomasi, J. *J. Chem. Phys. B* **1997**, *101*, 10506.
(108)Cancès, E.; Mennucci, B.; Tomasi, J. *J. Chem. Phys.* **1997**, *107*, 3032.
(109)Daniel, M. C. *J. Chem. Phys.* **2000**, *112*, 5558.
(110)Cossi, M.; Barone, V. *J. Phys. Chem. A* **2000**, *104*, 10614.
(111)Cammi, R.; Mennucci, B. *J. Chem. Phys.* **1999**, *110*, 9877.
(112)Cossi, M.; Barone, V. *J. Chem. Phys.* **2001**, *115*, 4708.
(113)Tomasi, J.; Persico, M. *Chem. Rev.* **1994**, *94*, 2027.
(114)Cammi, R.; Tomasi, J. *Int. J. Quantum Chem.* **1995**, *56*, 465.
(115)Improta, R.; Barone, V.; Scalmani, G.; Frisch, M. J. *J. Chem. Phys.* **2006**, *125*, 054103.
(116)You, Z.-Q.; Mewes, J.-M.; Dreuw, A.; Herbert, J. M. *J. Chem. Phys.* **2015**, *143*, 204104.
(117)Mulliken, R. S. *J. Chem. Phys.* **1955**, *23*, 1833.
(118)Peach, M. J. G.; Benfield, P.; Helgaker, T.; Tozer, D. J. *J. Chem. Phys.* **2008**, *128*, 044118.
(119)Ratner, M. A.; Schatz, G. C. *Introduction to Quantum Mechanics in Chemistry*; Prentice Hall: Upper Saddle River, NJ, 2001.
(120)Klessinger, M.; Michl, J. *Excited States and Photochemistry of Organic Molecules*; VCH: New York, 1995.
(121)Szabo, A.; Ostlund, N. S. *Modern Quantum Chemistry: Introduction to Advanced Electronic Structure Theory*; Dover Publications Inc.: New York, 1996.
(122)McGlynn, S. P.; Azumi, T.; Kinoshita, M. *Molecular Spectroscopy of the Triplet State*; Pretince-Hall: Englewood Cliffs, New Jersey, 1969.
(123)Turro, N. J. *Modern Molecular Photochemistry*; University Science Books: Sausalito, CA, 1991.
(124)Barltrop, J. A. *Excited States in Organic Chemistry*; Wiley: London, 1975.
(125)Sobolewski, A. L.; Domcke, W. *Chem. Phys.* **2003**, *294*, 73.
(126)De Angelis, F.; Fantacci, S.; Selloni, A. *Nannotechnology* **2008**, *19*, 424002.
(127)Pastore, M.; Fantacci, S.; De Angelis, F. *J. Chem. Phys. C* **2010**, *114*, 22742.
(128)Perepichka, I. F.; Perepichka, D. F. *Handbook of Thiophene-Based Materials: Applications in Organic Electronics and Photonics*; John Wiley & Sons Ltd.: New York, 2009; Vol. 2.
(129)Li, R.; Liu, J.; Cai, N.; Zhang, M.; Wang, P. *J. Phys. Chem. B* **2010**, *114*, 4461.
(130)Xu, M.; Zhang, M.; Pastore, M.; Li, R.; De Angelis, F.; Wang, P. *Chem. Sci.* **2012**, *3*, 976.

(131)Tsao , H. N.; Yi , C.; Moehl, T.; Yum, J.-H.; Zakeeruddin, S. M.; Nazeeruddin, M. K.; Grätzel, M. *ChemSusChem* **2011**, *4*, 591.
(132)Xu, M.; Wenger, S.; Bala, H.; Shi, D.; Li, R.; Zhou, Y.; Zakeeruddin, S. M.; Grätzel, M.; Wang, P. *J. Phys. Chem. C* **2009**, *113*, 2966.
(133)Wang, M.; Xu, M.; Shi, D.; Li, R.; Gao, F.; Zhang, G.; Yi, Z.; Humphry-Baker, R.; Wang, P.; Zakeeruddin, S. M.; Grätzel, M. *Adv. Mater.* **2008**, *20*, 4460.
(134)Li, R.; Lv, X.; Shi, D.; Zhou, D.; Cheng, Y.; Zhang, G.; Wang, P. *J. Phys. Chem. C* **2009**, *113*, 7469.
(135)Shao, Y.; Molnar, L. F.; Jung, Y.; Kussmann, J.; Ochsenfeld, C.; Brown, S. T.; Gilbert, A. T. B.; Slipchenko, L. V.; Levchenko, S. V.; O'Neill, D. P.; DiStasio Jr, R. A.; Lochan, R. C.; Wang, T.; Beran, G. J. O.; Besley, N. A.; Herbert, J. M.; Lin, C. Y.; Voorhis, T. V.; Chien, S. H.; Sodt, A.; Steele, R. P.; Rassolov, V. A.; Maslen, P. E.; Korambath, P. P.; Adamson, R. D.; Austin, B.; Baker, J.; Byrd, E. F. C.; Dachsel, H.; Doerksen, R. J.; Dreuw, A.; Dunietz, B. D.; Dutoi, A. D.; Furlani, T. R.; Gwaltney, S. R.; Heyden, A.; Hirata, S.; Hsu, C.-P.; Kedziora, G.; Khalliulin, R. Z.; Klunzinger, P.; Lee, A. M.; Lee, M. S.; Liang, W.; Lotan, I.; Nair, N.; Peters, B.; Proynov, E. I.; Pieniazek, P. A.; Rhee, Y. M.; Ritchie, J.; Rosta, E.; Sherrill, C. D.; Simmonett, A. C.; Subotnik, J. E.; Iii, H. L. W.; Zhang, W.; Bell, A. T.; Chakraborty, A. K. *Phys. Chem. Chem. Phys.* **2006**, *8*, 3172.
(136)Sobolev, A. N.; Belsky, V. K.; Romm, I. P.; Chernikova, N. Y.; Guryanova, E. N. *Acta Cryst. C* **1985**, *41*, 967.
(137)Alibabaei, L.; Kim, J. H.; Wang, M.; Pootrakulchote, N.; Teuscher, J.; Di Censo, D.; Humphry-Baker, R.; Moser, J. E.; Yu, Y. J.; Kay, K. Y.; Zakeeruddin, S. M.; Gratzel, M. *Energy Environ. Sci.* **2010**, *3*, 1757.
(138)Sun, M.; Ding, Y.; Xu, H. *J. Phys. Chem. B* **2007**, *111*, 13266.
(139)Li, Y.; Li, H.; Zhao, X.; Chen, M. *J. Phys. Chem. A* **2010**, *114*, 6972.
(140)Mazur, G.; Petelenz, P.; Slawik, M. Ç. *Chem. Phys.* **2012**, *397*, 92.
(141)Kurashige, Y.; Nakano, H.; Nakao, Y.; Hirao, K. *Chem. Phys. Lett.* **2004**, *400*, 425.
(142)Gao, Y.; Liu, C.-G.; Jiang, Y.-S. *J. Phys. Chem. A* **2002**, *106*, 2592.
(143)Bendikov, M.; Duong, H. M.; Starkey, K.; Houk, K. N.; Carter, E. A.; Wudl, F. *J. Am. Chem. Soc.* **2004**, *126*, 7416.
(144)Hsu, C.-P.; Hirata, S.; Head-Gordon, M. *J. Phys. Chem. A* **2001**, *105*, 451.
(145)Lange, A. W.; Rohrdanz, M. A.; Herbert, J. M. *J. Phys. Chem. B* **2008**, *112*, 6304.
(146)Le Bahers, T.; Adamo, C.; Ciofini, I. *J. Chem. Theory Comput.* **2011**, *7*, 2498.
(147)Stein, W.; et al.; 4.5.3 ed.; Sage Development Team: 2010.
(148)Climent, C.; Cabau, L.; Casanova, D.; Wang, P.; Palomares, E. *Org. Electron.* **2014**, *15*, 3162.
(149)Chen, P.; Yum, J. H.; Angelis, F. D.; Mosconi, E.; Fantacci, S.; Moon, S.-J.; Baker, R. H.; Ko, J.; Nazeeruddin, M. K.; Grätzel, M. *Nano Lett.* **2009**, *9*, 2487.
(150)Rühle, S.; Greenshtein, M.; Chen, S.-G.; Merson, A.; Pizem, H.; Sukenik, C. S.; Cahen, D.; Zaban, A. *J. Phys. Chem. B* **2005**, *109*, 18907.
(151)Haid, S.; Marszalek, M.; Mishra, A.; Wielopolski, M.; Teuscher, J.; Moser, J.-E.; Humphry-Baker, R.; Zakeeruddin, S. M.; Grätzel, M.; Bäuerle, P. *Adv. Funct. Mater.* **2012**, *22*, 1291.
(152)El-Shafei, A.; Hussain, M.; Islam, A.; Han, L. *J. Mater. Chem. A* **2013**, *1*, 13679.
(153)Chai, Q.; Li, W.; Zhu, S.; Zhang, Q.; Zhu, W. *ACS Sustainable Chem. Eng.* **2014**, *2*, 239.
(154)Xu, M.; Li, R.; Pootrakulchote, N.; Shi, D.; Guo, J.; Yi, Z.; Zakeeruddin, S. M.; Grätzel, M. *J. Phys. Chem. C* **2008**, *112*, 19770.
(155)Komatsu, M.; Nakazaki, J.; Uchida, S.; Kubo, T.; Segawa, H. *Phys. Chem. Chem. Phys.* **2013**, *15*, 3227.
(156)Wang, Z.-S.; Cui, Y.; Dan-oh, Y.; Kasada, C.; Shinpo, A.; Hara, K. *J. Phys. Chem. C* **2007**, *111*, 7224.
(157)Ehret, A.; Stuhl, L.; Spitler, M. T. *J. Phys. Chem. B* **2001**, *105*, 9960.
(158)Tatay, S.; Haque, S. A.; O'Regan, B.; Durrant, J. R.; Verhees, W. J. H.; Kroon, J. M.; Vidal-Ferran, A.; Gavina, P.; Palomares, E. *J. Mater. Chem.* **2007**, *17*, 3037.
(159)Liu, B.; Wang, B.; Wang, R.; Gao, L.; Huo, S.; Liu, Q.; Li, X.; Zhu, W. *J. Mater. Chem. A* **2014**, *2*, 804.
(160)Pastore, M.; De Angelis, F. *ACS Nano* **2010**, *4*, 556.
(161)Dentani, T.; Kubota, Y.; Funabiki, K.; Jin, J.; Yoshida, T.; Minoura, H.; Miura, H.; Matsui, M. *New J. Chem.* **2009**, *33*, 93.
(162)Liu, J.; Zhou, D.; Wang, F.; Fabregat-Santiago, F.; Miralles, S. G.; Jing, X.; Bisquert, J.; Wang, P. *J. Phys. Chem. C* **2011**, *115*, 14425.

(163)Choi, H.; Baik, C.; Kang, S. O.; Ko, J.; Kang, M.-S.; Nazeeruddin, M. K.; Grätzel, M. *Angew. Chem., Int. Ed.* **2008**, *47*, 327.
(164)Ho, T. I.; Lee, T. C.; Ho, J. H.; Wang, S. L. *Tamkang J. Sci. Eng.* **2003**, *6*, 37.
(165)Fdez. Galván, I.; Elena Martín, M.; Muñoz-Losa, A.; Aguilar, M. A. *J. Chem. Theory Comput.* **2009**, *5*, 341.
(166)De Meyer, T.; Hemelsoet, K.; Van der Schueren, L.; Pauwels, E.; De Clerck, K.; Van Speybroeck, V. *Chem. - Eur. J.* **2012**, *18*, 8120.
(167)Zhao, Y.; Truhlar, D. G. *Theor. Chem. Acc.* **2008**, *120*, 215.
(168)Climent, C.; Carreras, A.; Alemany, P.; Casanova, D. *Chem. Phys. Lett.* **2016**, *663*, 45.
(169)Frisch, M. J.; Trucks, G. W.; Schlegel, H. B.; Scuseria, G. E.; Robb, M. A.; Cheeseman, J. R.; Scalmani, G.; Barone, V.; Petersson, G. A.; Nakatsuji, H.; Li, X.; Caricato, M.; Marenich, A. V.; Bloino, J.; Janesko, B. G.; Gomperts, R.; Mennucci, B.; Hratchian, H. P.; Ortiz, J. V.; Izmaylov, A. F.; Sonnenberg, J. L.; Williams; Ding, F.; Lipparini, F.; Egidi, F.; Goings, J.; Peng, B.; Petrone, A.; Henderson, T.; Ranasinghe, D.; Zakrzewski, V. G.; Gao, J.; Rega, N.; Zheng, G.; Liang, W.; Hada, M.; Ehara, M.; Toyota, K.; Fukuda, R.; Hasegawa, J.; Ishida, M.; Nakajima, T.; Honda, Y.; Kitao, O.; Nakai, H.; Vreven, T.; Throssell, K.; Montgomery Jr., J. A.; Peralta, J. E.; Ogliaro, F.; Bearpark, M. J.; Heyd, J. J.; Brothers, E. N.; Kudin, K. N.; Staroverov, V. N.; Keith, T. A.; Kobayashi, R.; Normand, J.; Raghavachari, K.; Rendell, A. P.; Burant, J. C.; Iyengar, S. S.; Tomasi, J.; Cossi, M.; Millam, J. M.; Klene, M.; Adamo, C.; Cammi, R.; Ochterski, J. W.; Martin, R. L.; Morokuma, K.; Farkas, O.; Foresman, J. B.; Fox, D. J. In *Gaussian 09, Revisions B.01 and D. 01*; Gaussian, Inc.: Wallingford, CT, 2009.
(170)Jorgensen, W. L.; Maxwell, D. S.; Tirado-Rives, J. *J. Am. Chem. Soc.* **1996**, *118*, 11225.
(171)Ponder, J. W.; Richards, F. M. *J. Comput. Chem.* **1987**, *8*, 1016.